CARBON MONOXIDE ABSORPTION IN K AND M GIANTS AND THE C^{12}/C^{13} ABUNDANCE RATIO

by

Wayne Lewis Bailey

A Dissertation Submitted to the Faculty of the

DEPARTMENT OF ASTRONOMY

In Partial Fulfillment of the Requirements
For the Degree of

DOCTOR OF PHILOSOPHY

In the Graduate College

THE UNIVERSITY OF ARIZONA

1 9 7 1

THE UNIVERSITY OF ARIZONA

GRADUATE COLLEGE

I hereby recommend that this dissertation prepared under my direction by Wayne Lewis Bailey

entitled Carbon Monoxide Absorption in K and M Giants and the C^{12}/C^{13} Abundance Ratio

be accepted as fulfilling the dissertation requirement of the degree of Doctor of Philosophy

Rodger I. Thompson — Dissertation Director — April 20, 1971 — Date

After inspection of the final copy of the dissertation, the following members of the Final Examination Committee concur in its approval and recommend its acceptance:*

R. E. Williams	19 April 1971
T. L. Swihart	April 20, 1971
Ray D. Kaplan	April 20, 1971
D. L. Lee	26 April 1971

*This approval and acceptance is contingent on the candidate's adequate performance and defense of this dissertation at the final oral examination. The inclusion of this sheet bound into the library copy of the dissertation is evidence of satisfactory performance at the final examination.

STATEMENT BY AUTHOR

This dissertation has been submitted in partial fulfillment of requirements for an advanced degree at The University of Arizona and is deposited in the University Library to be made available to borrowers under rules of the Library.

Brief quotations from this dissertation are allowable without special permission, provided that accurate acknowledgment of source is made. Requests for permission for extended quotation from or reproduction of this manuscript in whole or in part may be granted by the head of the major department or the Dean of the Graduate College when in his judgment the proposed use of the material is in the interests of scholarship. In all other instances, however, permission must be obtained from the author.

SIGNED: Wayne Bonley

ACKNOWLEDGMENTS

The author would like to express his gratitude to the following people who have provided assistance in the completion of this dissertation:

The staff of the University of Arizona Computer Center and particularly Mr. Steve Jay for their assistance with the computation of the synthetic spectra;

Mr. Richard I. Mitchell for his assistance in preparing the stellar spectra for analysis;

Dr. Thomas L. Swihart for supplying advice and encouragement while the work was being carried out and for critically reading the manuscript and offering many useful suggestions for its improvement;

Dr. Harold L. Johnson for supplying the stellar spectra as well as his advice and encouragement throughout all phases of the work;

Dr. Rodger I. Thompson, the dissertation director, for his enthusiasm and advice while the work was in progress as well as offering many suggestions for improvement of the manuscript;

and my wife, Deborah, for her assistance with the tedious, mechanical details involved in the completion of this dissertation and for cheerfully tolerating the disruptions to a normal existence that are a part of any PhD program.

TABLE OF CONTENTS

TABLE OF CONTENTS--Continued

LIST OF ILLUSTRATIONS

LIST OF ILLUSTRATIONS--Continued

LIST OF ILLUSTRATIONS--Continued

LIST OF TABLES

ABSTRACT

The second overtone vibration-rotation bands of carbon monoxide are used to determine the C^{12}/C^{13} abundance ratio in fifteen stars of spectral types K2 through M6, luminosity classes III through Ia. The relation of the results to theoretical studies of the structure of evolved stars is discussed. Twenty three spectra of the fifteen stars, covering the wavenumber region 3900-8200 cm^{-1} or 2400-8200 cm^{-1} with a resolution of 8 cm^{-1} are analyzed.

A grid of synthetic carbon monoxide spectra is calculated using a Milne-Eddington curve of growth, for various values of C^{12}/C^{13} ratio, temperature, microturbulent velocity and damping parameter. These synthetic spectra are used to construct curves of growth for the band heads which are used to determine the C^{12}/C^{13} ratio from the stellar spectra.

The C^{12}/C^{13} ratio is significantly lower than the terrestrial value in all stars studied. This is interpreted as an indication that material, which has been processed through the CNO bi-cycle, has been transported from the interiors to the surfaces of the stars. This agrees with the theoretical models of the interiors of red giants which predict a convective zone extending from the surface to the CNO burning shell.

The ratio of carbon monoxide line to continuum opacity is determined. No attempt is made to interpret this ratio as a CO/H abundance ratio due to uncertainties in the continuous opacity.

INTRODUCTION

The stars of spectral types K and M, luminosity classes III through I, referred to as late type giants and supergiants, have been more difficult to interpret, both observationally and theoretically, than the hotter main sequence stars. Some of the reasons for this difficulty will be discussed below along with the advances we may expect due to the availability of infra-red spectra.

On the observational side, progress has been delayed due to the problems associated with the analysis of late type giant and supergiant spectra. The low temperatures of these stars cause them to be intrinsically faint in the photographic region of the spectrum. This region is also crowded with overlapping lines which makes quantitative analysis of the spectra difficult. When these problems have been overcome, the formation of molecules makes interpretation of atomic abundances difficult, since a significant fraction of many elements is in molecules. Some important molecules, among them carbon monoxide, have no spectral features in the photographic region, thus have been unobservable until the recent development of efficient infra-red spectroscopic techniques. Effective temperatures have been difficult to obtain because most of the stars' energy is radiated in the infra-red where observational difficulties have existed (Johnson 1966).

Theoretical understanding of the interior structure of cool giants and supergiants had to await the construction of good evolutionary models in the post-main sequence stages, since these are probably evolved stars. These models are now becoming available (Iben 1967) although they are not yet refined to the same extent as the main sequence models. Newly formed stars also pass through this region of the temperature luminosity plane as they contract to the main sequence, but this is a very short phase of their evolution. We are not likely to observe more than a few stars at this evolutionary stage.

The atmospheric models for these stars have not been thoroughly developed due to the importance of convection throughout the atmosphere as well as the necessity of including molecules in the opacity and equation of state. Model atmospheres have been calculated by several workers (Gingerich and Kumar 1964, Kumar 1964, Auman 1966, 1969, Tsuji 1966, Gingerich 1967, Gingerich et al. 1967, Carbon and Gingerich 1969); among the most sophisticated are those by Auman, who has included H_2O opacity and convection in the calculations. The calculated emergent spectra, however, do not fit the stellar spectra. The models predict more H_2O absorption than is seen in non-variable stars, only Mira variables do show strong H_2O absorption.

The Carbon Isotope Abundances

Shortly after its discovery in the laboratory, Sanford (1929) recognized the isotope C^{13} in the Swan bands of C_2 in the spectra of what are now referred to as carbon stars. Later, isotopic CN violet bands were also recognized. It was immediately apparent that the strength of the C^{13} bands in many carbon stars exceeded their laboratory strengths by a large factor. Several workers (Sanford 1932, 1940, Menzel 1930, Wurm 1932, McKellar 1936, 1948, 1949a, 1949b, Shajn 1942, Herzberg 1946, Daudin and Fehrenbach 1946, Shajn and Gaze 1948, 1950, 1954, Schopp 1954, Phillips 1957, 1966, Wyller 1957, 1959, 1960, 1966, Climenhaga 1960, 1966, Utsumai 1963, 1967, Cohen and Grandalen 1968, Hirai 1969, Fujita 1970, Greene 1970, Querci and Querci 1970, Thompson, Schnopper and Rose 1971, Spinrad et al. 1971) have contributed to answering the question of whether this implies a C^{12}/C^{13} ratio less than the terrestrial value of 89.

The Swan bands of C_2 occur in an easily observed region of the spectrum and are well suited to analysis of the C^{12}/C^{13} ratio. Other molecules involving carbon, such as CN, CH or CO, are less easily observed. Because the Swan bands are only strong in carbon stars, most of the analyses have been of carbon stars. These form two groups with respect to the C^{12}/C^{13} ratio. The larger group has a C^{12}/C^{13} ratio less than the terrestrial value. Individual stars have quoted values which range from 2 - 50. Analyses of the CN red system of bands sometimes

indicates a C^{12}/C^{13} ratio that is higher than that indicated by the Swan bands or CN violet system, both of which occur at shorter wavelengths. The second and smaller group has a C^{12}/C^{13} ratio that is greater than 100.

Prior to the availability and use of infra-red spectra at 1 and 2 microns, the only analysis of the C^{12}/C^{13} ratio in oxygen stars was by Schopp (1954). He found no evidence for an enhancement of the C^{12}/C^{13} ratio over the terrestrial value that could not be explained by the difficulty of detecting isotopic features in weak bands. At this point it seemed obvious that carbon stars were those stars that had mixed material, which had been processed through the CNO bi-cycle, to the surface thus producing a low C^{12}/C^{13} ratio. Oxygen stars either had not mixed interior material to the surface, or were not operating on the CNO bi-cycle.

Infra-red spectra of stars have recently become available covering the 1-2μ region (Kuiper 1962, 1964a, 1964b, Sinton 1962, 1966, Boyce and Sinton 1964, 1965, Woolf, Schwarzschild and Rose 1964, Danielson, Woolf, and Gaustad 1965, Mertz 1965, Moroz 1966, McCammon, Munch and Neugebauer 1967, Johnson et al. 1968, Sinton and Boyce (in press), Thompson et al. 1969, Johnson and Mendez 1970, Thompson and Schnopper 1970). As Kuiper first indicated, the most conspicuous feature of non-variable, oxygen stars is the $\Delta v = 2$ vibration-rotation band sequence of carbon monoxide at 2.3μ. Surprisingly, there were also strong

features present which Meinel (Kuiper 1962) suggested were due to $C^{13}O^{16}$. Because the CO bands were not resolved into rotational lines with the resolution used, it could be argued that the $C^{13}O^{16}$ features were misidentified. It would, however, be unlikely that the entire sequence of bands could be a coincidence, especially since $C^{13}O^{16}$ features also appeared in the $\Delta v=3$ sequence at 1.6μ. The identification problem was solved when Pierre Connes succeeded in producing high resolution spectra of the CO bands in Arcturus (Connes et al. 1968, Montgomery et al. 1969), which unambiguously showed that the features in question were due to $C^{13}O^{16}$.

The next step was to determine the value of the C^{12}/C^{13} ratio for the oxygen stars. Greene (1970) used the CO $\Delta v=2$ sequence in Connes' spectrum of Arcturus to determine $C^{12}/C^{13}\approx 3\text{-}4$. He also used the CN red system in the Photometric Atlas of the Spectrum of Arcturus (Griffin 1968) to determine $C^{12}/C^{13}\geqq 10$. Spinrad et al. (1971) has analyzed the CO bands in Connes' spectrum of Alpha Orionis with similar results. The carbon monoxide bands indicate a C^{12}/C^{13} ratio of about 3. Other bands show no C^{13}, implying $C^{12}/C^{13}>>3$. This disagreement between bands of different molecules in different spectral regions is extremely disturbing, but not surprising in view of the results from bands in different spectral regions in carbon stars mentioned above. The difficulty apparently is in the interpretation of the observations, not in the observations themselves.

The CNO Bi-cycle

The importance of the C^{12}/C^{13} ratio arises from its relation to the generation of energy in the interior of the star. According to Iben (1967), stars in the red giant phase are burning hydrogen in their interiors by means of the CNO bi-cycle. At equilibrium, the CNO bi-cycle produces $C^{12}/C^{13} \approx 4$ in the energy generating regions. This value is not very sensitive to temperature.

According to Iben's model for a 5 solar mass, population I star, the convective envelope begins to mix interior material to the surface at $T_{eff} \approx 4500$ K, prior to the star's reaching the tip of the red giant branch. This decreases both the carbon abundance and the C^{12}/C^{13} ratio as well as increases the nitrogen abundance and decreases the oxygen abundance. The total abundance of C, N and O remains constant. The carbon and oxygen are converted to nitrogen. These abundance changes occur at different rates. The C^{12}/C^{13} ratio and the carbon abundance reach their equilibrium values in only a few tens of thousands of years. The carbon is primarily converted to nitrogen, therefore the nitrogen abundance increases on this time scale. The oxygen abundance takes considerably longer to reach equilibrium. It does not begin to decrease noticably until tens of millions of years have elapsed and only reaches equilibrium after a few hundreds of millions of years. Clayton (1968) discusses energy generation in stars and its effect on the abundances of the elements in more detail than is necessary for our present purposes. We

will return to the subject of abundance changes due to energy generation in the stars in Chapter 4 where we will discuss the relation of our results to the interior of the stars.

At the red giant tip, Iben's model shows the triple alpha process being ignited which converts He^4 into C^{12}. If the products of this burning stage can be mixed to the surface, the carbon abundance and C^{12}/C^{13} ratio will again rise. Iben, however, states that convection will decrease after the red giant tip is passed and triple alpha products will not be mixed to the surface.

Carbon Monoxide

Carbon monoxide was recognized as an important factor in the molecular dissociation equilibrium in stellar atmospheres in the pioneer study by Russell (1934). These studies have been refined by several workers up to the present time (Fujita 1935, 1939, 1940, 1941, 1950, Bouigue 1954, 1957, de Jager and Neven 1957, Tsuji 1964) by including more molecules, better laboratory data and improved estimates of atomic abundances. At temperatures below 4500 K, the formation of CO proceeds until either carbon or oxygen is essentially exhausted. Because carbon monoxide remains abundant at temperatures as high as 5500 K, CO is a major constituent throughout the observable layers of cool stars and can even be detected in the sun. Carbon monoxide is also an

important source of opacity in the infra-red in spite of the low transition probability of its infra-red vibration-rotation transitions.

All electronic transitions from the ground state of CO occur in the vacuum ultraviolet, so in spite of its high abundance and importance to model atmospheres, it was not observable in stellar spectra until the infra-red spectra mentioned above became available. These showed the Δv-2,3 vibration-rotation band sequences.

Statistical methods for including line blanketing in model atmosphere calculations have now been developed (Strom and Kurucz 1966, Mihalas 1967). Determination of the CO abundance is necessary to include CO opacity in the model atmospheres. Molecular dissociation equilibrium calculations can be used for this purpose, but a direct determination is preferable. Also the carbon and oxygen abundances can not be determined unless the carbon monoxide abundance is determined, since a large fraction of the carbon and oxygen is tied up in CO.

To perform abundance analyses of the stellar CO bands, we need laboratory information on the energy levels, line positions and transition probabilities of the vibration-rotation lines. Extensive laboratory investigations of the spectrum of carbon monoxide have been carried out (Krupenie 1966). The data necessary to analyze the stellar bands has been published by Kunde (1967, 1968). Lists of integrated absorption coefficients and positions for the rotational lines of the

$\Delta v=1,2,3$, vibration-rotation band sequences are given for $C^{12}/C^{13}=89$, $O^{16}/O^{18}=493$ and temperatures of 500 K, 1000 K, 2000 K, 2500 K, 3000 K and 3500 K. A method of converting the data to other temperatures and C^{12}/C^{13} ratios is given in Appendix A.

The Present Investigation

In the past, observations of the C^{12}/C^{13} ratio seemed to show that CNO products were only visible on the surfaces of carbon stars. The more recent infra-red observations indicate a low C^{12}/C^{13} ratio for all K and M giants and supergiants, with the possible exception of χ Cygni (Johnson and Mendez 1970). This result is based on the assumption of a linear curve of growth for the CO bands. Because the C^{12}/C^{13} ratio is related to the operation of the CNO bi-cycle in the stellar interior and the mixing of interior material to the observable surface layers of the star, it is desirable to eliminate the assumption of a linear curve of growth and to determine the region of the temperature-luminosity plane where CNO bi-cycle products are visible.

Johnson has published (Johnson et al. 1968, Johnson and Mendez 1970) 23 infra-red spectra of 15 K and M stars suitable for analysis of the CO bands. This excludes all Mira variables for which spectra have been published since they have strong stellar H_2O absorption that overlaps the CO bands and makes analysis impossible. These are medium resolution spectra ($\frac{\nu}{\Delta\nu}\approx 500$) in which the rotational structure

of the CO bands is not resolved. They must be analyzed by means of synthetic spectra because the line by line techniques normally employed are not possible. This is the most extensive set of observations yet available, extending from K2 to M6 and including luminosity classes III through Ia, so an attempt at quantitative analysis seems definitely worthwhile.

Both the first and second overtone ($\Delta v=2,3$) vibration-rotation band sequences are available in these spectra. With the atmospheric correction applied by Johnson, at least six, first overtone $C^{12}O^{16}$ band heads are always available in the spectra. Depending on the quality of the terrestrial atmosphere during the observation, as many as eight band heads can be visible. The positions of the band heads and origins are listed in Appendix C for the $\Delta v=2$ bands of $C^{12}O^{16}$, $C^{13}O^{16}$, and $C^{12}O^{18}$, and the $\Delta v=3$ bands of $C^{12}O^{16}$ and $C^{13}O^{16}$.

We intend to use the CO first overtone vibration-rotation bands in Johnson's spectra of K and M stars to determine the carbon monoxide abundance and C^{12}/C^{13} abundance ratio. Since most of the carbon and oxygen are expected to be in the form of carbon monoxide, the CO abundance must be known in order to determine the carbon and oxygen abundances. We will not attempt to determine the carbon and oxygen abundances, since this would involve also determining the atomic abundances of C and O as well as all molecules involving them. We will, however, discuss the C and O abundances on the basis of

molecular dissociation equilibria in Chapter 4. This approach, while not as accurate as determining the abundance of all species of carbon and oxygen compounds, should be more accurate than using measured atomic abundances and molecular dissociation equilibrium calculations to determine the abundances of carbon and oxygen. Knowledge of the carbon monoxide abundance is also necessary to include CO opacity in model atmospheres. The CO abundances can be used directly for this purpose.

The C^{12}/C^{13} abundance ratio is sensitive to the energy generation mechanism in the stellar interior and to the efficiency of mixing from the interior to the surface of the star. The results from the stellar spectra will be used to compare to the theoretical predictions.

THE SYNTHETIC SPECTRA

Analysis of spectra in which individual lines are not resolved requires a grid of synthetic spectra. The line formation theory used to construct this grid is a curve of growth tabulated by Swihart and Brown (1967). This is a Milne-Eddington curve of growth, which implies that both the line and continuum are formed throughout the entire atmosphere of the star. The other extreme is the Schuster-Schwarzschild curve of growth which assumes that a pure continuum is produced below a layer that only contributes line absorption.

The Milne-Eddington model was chosen because CO is abundant throughout the entire atmosphere of cool stars. However, supergiants, and to a lesser degree, giants have extended atmospheres which may be an argument in favor of the Schuster-Schwarzschild model. Spinrad et al. (1971) claim the low central intensity of the CO lines in Alpha Orionis indicate the Schuster-Schwarzschild model is preferable, however a steep temperature gradient in the atmosphere could produce the same effect in the Milne-Eddington model. The curves of growth for both models are quite similar except for a vertical displacement, therefore the turbulent velocity should be the only parameter significantly affected cy the choice of model.

The line absorption coefficients published by Kunde (1967) were kindly provided by him on magnetic tape. These are integrated absorption coefficients for $C^{12}O^{16}$, $C^{13}O^{16}$ and $C^{12}O^{18}$, calculated for $C^{12}/C^{13}=89$, $O^{16}/O^{18}=493$ and temperatures of 500 K, 1000 K, 2000 K, 2500 K, 3000 K and 3500 K. The method used to convert these to other temperatures and isotope ratios is described in Appendix A.

Theory of the Curve of Growth

The Milne-Eddington Curve of Growth has been discussed several times (Aller 1960, 1963, Greenstein 1970, Wrubel 1949). The review given here follows closely that of Swihart and Brown (1967).

The source function in both line and continuum is assumed to be the Planck Function, $B_\nu(T)$. From now on, the explicit reference to temperature, T, will be dropped.

For a plane parallel atmosphere, the emergent intensity I_ν at angle $\theta = \cos^{-1}\mu$ from the normal to the surface is given by

$$(1)\quad I_\nu(\mu) = I_0 e^{-\tau_0} + \int_0^\infty B_\nu e^{-\tau_\nu/\mu} \frac{d\tau_\nu}{\mu}$$

where optical depth, τ_ν, is defined by

$$d\tau_\nu = \mathbf{K} dl$$

l=geometrical depth

For a semi infinite atmosphere,

$$\tau_0 = \infty$$

and

$$(2)\ I_\nu(\mu)=\int_0^\infty B_\nu e^{-\tau_\nu/\mu}\frac{d\tau_\nu}{\mu}$$

Using the subscripts ν or c to designate quantities that depend, respectively, on line and continuum parameters or continuum parameters only, the residual intensity, $r_\nu(\mu)$, at any frequency in an absorption line is

$$(3)\ r_\nu(\mu)=1-\frac{I_\nu(\mu)}{I_c(\mu)}=1-\frac{\int_0^\infty B_\nu e^{-\tau_\nu/\mu}\, d\,\tau_\nu/\mu}{\int_0^\infty B_\nu e^{-\tau_\epsilon/\mu}\, d\,\tau_\epsilon/\mu}$$

using subscript 1 to indicate dependence on line parameters only,

$$(4)\ d\tau_\nu = d\tau_c + d\tau_1 = (K_c + K_1)\rho dh = K_c(1+\eta)\rho dh = (1+\eta)d\tau_c$$

where the K's are mass absorption coefficients, ρ is the mass density, h is geometrical distance into the star and η is the ratio of line to continuous absorption coefficient at frequency ν.

The equivalent width, $W_\nu(\mu)$, is given by

$$(5)\ W_\nu(\mu)=\int_0^\infty r_\nu(\mu)\,d\tau_\nu$$

For stars it is necessary to integrate this over direction to convert from intensity to flux, but this will be postponed until later.

The evaluation of equation (5) requires a model atmosphere to specify the frequency and depth dependence of η, τ_c and B_ν. The Milne-Eddington model uses a very simple model atmosphere to simplify the analysis. The basic assumption of the Milne-Eddington model is that η is independent of h.

$$(6)\ \eta=\frac{K_1}{K_c}\neq f(h)$$

Two further assumptions will be made,

(a) The frequency dependence of η is given by the Voight function

(7) $\eta_\nu = \eta\ H(a,u)$

where $H(a,u)=\frac{a}{\pi}\int_{-\infty}^{\infty}\frac{e^{-x^2}}{(u-x)^2+a^2}\,dx$

and a is the ratio of the Lorentzian to Gaussian line widths.

(b) The source function is a linear function of the continuum optical depth

(8) $B = B_0 + B_1\tau_c$

Combining equations 3, 6 and 8 yields

(9) $r_\nu(\mu)=\frac{\mu}{\mu + B_0/B_1}\ \frac{\eta}{1+\eta}$

Using (5) and changing to the dimensionless frequency variable

$$u=\frac{\nu-\nu_0}{\Delta\nu_D}$$

where

$$\Delta\nu_D=\frac{\nu_o}{c}\left(\frac{2KT}{m}+\xi_T^2\right)^{1/2}$$

yields

(10) $\frac{W_\nu(\mu)}{\nu_0}=\frac{\mu}{\mu+B_0/B_1}\ \frac{\Delta\nu_D}{\nu_0}\ \int_{-\infty}^{\infty}\frac{\eta}{1+\eta}\,du$

We have taken B_0/B_1 outside the integral since it is a slowly varying function of frequency, and may be considered constant over the width of a line.

From 8 and 2

$$I_c(\mu)=B_0 + B_1 \mu$$

The observable quantity is flux, not intensity, for stars.

$$F_c=\int_{-1}^{+1} I_c(\mu)\mu\, d\mu$$

$$=B_0 + B_1(2/3)$$

$$=I_c(2/3)$$

Therefore, in (10) we will use

(11) $\mu = 2/3$

to yield

$$(12)\ \frac{W_\nu}{\nu_o}=\frac{2/3}{2/3 + B_0/B_1}\,\frac{\Delta\nu_D}{\nu_o}\int_{-\infty}^{\infty}\frac{\eta}{1+\eta}\,du$$

Using (7), the integral in (12) can be tabulated as a function of η and damping parameter, a. Defining

$$(13)\ D(\eta)=\int_{-\infty}^{\infty}\frac{\eta}{1+\eta}\,du$$

The plot of log C versus log η is the theoretical curve of growth. The curve of growth used was taken from Swihart and Brown (1967), Table 6.. For calculation, the polynomial approximations listed in Table 1 were used.

The curves of growth as given by Swihart and Brown, and as calculated by the polynominals are plotted in Figure 1. The polynomials

Table 1. Polynomial Approximations to the Curves of Growth

Log $\eta \leq -2$

$$\log D = 0.25 + \log \eta$$

Log a = -1

$-2 < \log \eta < 2.5$

$$\log D = 0.06 + 0.6650 \log \eta - 0.1550(\log \eta)^2 + 0.00127(\log \eta)^3 + 0.00938(\log \eta)^4$$

$2.5 \leq \log \eta$

$$\log D = -0.11 + 1/2 \log \eta$$

Log a = -2

$-2 \leq \log \eta < 3.5$

$$\log D = 0.0278 + 0.6172 \log \eta - 0.2011(\log \eta)^2 + 0.00534(\log \eta)^3 + 0.015089(\log \eta)^4 - 0.0020351(\log \eta)^5$$

$3.5 \leq \log \eta$

$$\log D = -0.60 + 1/2 \log \eta$$

Log a = -3

$-2 < \log \eta < 2.0$

$$\log D = 0.019 + 0.6204 \log \eta - 0.1888(\log \eta)^2 - 0.00142(\log \eta)^3 + 0.01027(\log \eta)^4 - 0.00122(\log \eta)^5$$

$2.0 \leq \log \eta < 4.4$

$$\log D = -0.048 + 0.6031 \log \eta - 0.15068(\log \eta)^2 + 0.002758(\log \eta)^3 + 0.0032315(\log \eta)^4$$

$4.4 \leq \log \eta$

$$\log D = -1.09 + 1/2 \log \eta$$

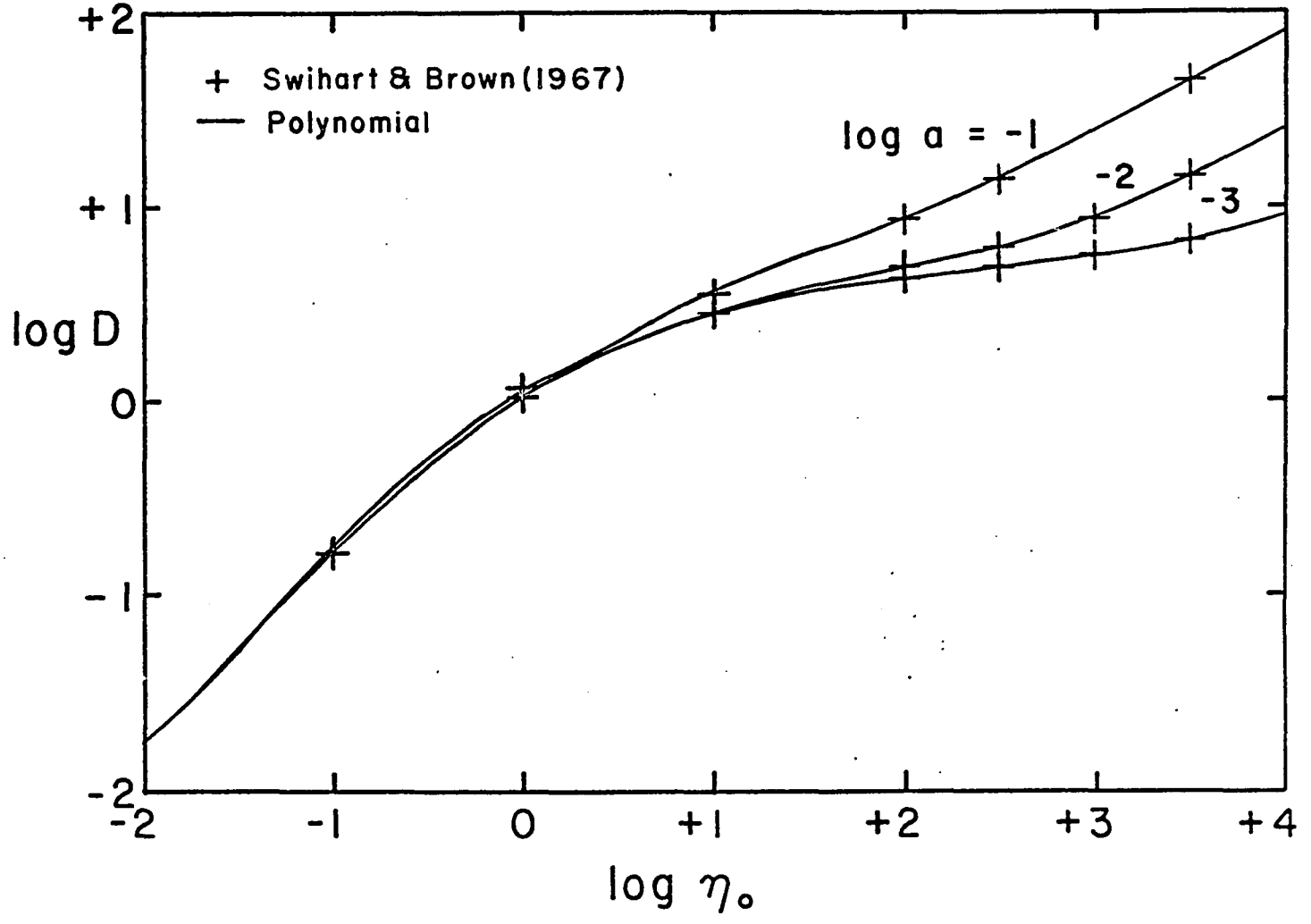

Fig. 1. Milne-Eddington Curves of Growth.

reproduce the calculated curves to much better than 10% accuracy in W_ν over almost their entire length.

Procedure

To calculate the equivalent width of a line, we need to know log a, η, $\Delta\nu_D$, B_0/B_1 and ν_o. We assume ν_o is known for the line. A value is assumed for log a. The value of B_0/B_1 can be obtained from a model atmosphere and is assumed constant over the entire band. The assumption of constant B_0/B_1 is not necessarily good, since the width of the usable section of the band sequence is about 10% of its central frequency, so the Planck function changes appreciably over the bands. This assumption, as well as the value of B_0/B_1, can be changed later without recalculating the entire band sequence, however, so it is a useful first approximation.

The value of η depends on the abundance and state of excitation of the carbon monoxide and on the continuous opacity. However, if a value of η is chosen for one line of the band sequence and the frequency dependence of the continuous opacity is known, the η values for all lines of the band are fixed (see below: Interpretation of η).

The choice of temperature and turbulent velocity determines $\Delta\nu_D$.

Given the above information, it is possible to calculate W_ν for each line. The total equivalent width between any two frequencies ν_1 and ν_2 is then the sum of the equivalent widths of all lines within the interval. This assumes that blending is negligible. The treatment of blending will be discussed below.

The average residual intensity in any frequency interval $\Delta\nu = \nu_2 - \nu_1$ is

$$(14)\quad R_\nu = 1 - \frac{\sum_{\nu=\nu_1}^{\nu_2} W_\nu}{\Delta\nu}$$

The band profile can be calculated by setting $\Delta\nu$ equal to the resolution of the observed spectra and calculating R_ν for successive resolution elements. In the vicinity of the band heads, the value of R_ν is sensitive to the choice of central frequency of the resolution elements. To alleviate this problem, the spectra are actually calculated with twice the number of resolution points that is necessary (i.e., for resolution of $\Delta\nu = 8\ \mathrm{cm}^{-1}$, R_ν was calculated at intervals of $4\ \mathrm{cm}^{-1}$) and the frequencies of the calculated points were chosen to coincide as closely as possible with the observed frequencies.

From (12), we see that

$$W_\nu = \frac{2/3}{2/3 + B_0/B_1} F$$

where $F = \Delta\nu_D \int_{-\infty}^{\infty} \frac{\eta}{1+\eta}\, du$

Equation (14) then becomes

$$R_\nu = 1 - \frac{\frac{2/3}{2/3 + B_0/B_1} \sum_{\nu=\nu_1}^{\nu_2} F}{\Delta\nu}$$

The value of B_0/B_1, therefore, does not affect the band profile. It is a scale factor that only affects the equivalent width.

Blended Lines

The calculation of the equivalent width of blended lines is a very difficult problem. A very simple approach to the problem is taken here, namely, if two lines occur closer than a specified frequency interval, $\Delta\nu_{bl}$, they are treated as totally blended, their η values are added together, and the sum is used to calculate their combined equivalent width. Otherwise, they are treated separately. The blending width, $\Delta\nu_{bl}$, was arbitrarily chosen as the larger of the two quantities $\Delta\nu_b$ or $\frac{W_\nu \text{ (unblended)}}{4}$. The second condition was inserted to allow for lines with strong wings that are significantly wider than their doppler cores, but the results are extremely insensitive to its inclusion. Ignoring blending entirely makes only a few percent change in the equivalent width of the band sequence.

Interpretation of η

Kunde (1967) has calculated values of the integrated absorption coefficients, S^m, for individual lines in the $\Delta v = 1, 2, 3$ vibration-rotation

bands of $C^{12}O^{16}$, $C^{13}O^{16}$ and $C^{12}O^{18}$. These are related to the line absorption coefficient, K_l, by

$$K_l = S^m M_{CO} N_{CO}$$

where M_{CO} = mass of a CO molecule

N_{CO} = number of density of CO

The continuous opacity is given by

$$K_c = a_\nu N_H$$

where a_ν = opacity per hydrogen atom

N_H = number density of hydrogen

We then have

$$(15)\quad \eta = \frac{K_l}{K_c}$$

$$= \frac{S^m M_{CO} N_{CO}}{a_\nu N_H}$$

A model atmosphere is necessary to provide a_ν. M_{CO} is known.

Whenever we refer to log η in reference to the synthetic spectra or the analysis of the stars, we mean the value of log η corresponding to $S^m = 5.07$ cm/gm. This value was chosen for the standard value of S^m simply because it is the S^m value of the highest frequency line in the $\Delta v = 2$ sequence at $T = 3500$ K. The values of η for all lines can be determined from

$$\eta = \frac{S^m}{5.07}\,\eta_{std}$$

From Equation (15), we have

$$(16)\quad \frac{N_{CO}}{N_H} = \eta\,\frac{a_\nu}{S^m\,M_{CO}}$$

The Grid of Synthetic Spectra

A grid of synthetic spectra was calculated with the following parameters.

$T = 2500$ K, 3500 K, 4500 K

$\xi_t = 0$, 10 km/s

$\log a = -1, -2, -3$

$C^{12}/C^{13} = 89, 20, 4$

The $\log \eta$ values were chosen to produce total equivalent widths for the first 6 bands that were in the range observed in stars (30 - 120 cm^{-1}). In addition, spectra were also calculated with parameters other than those listed above to provide more closely spaced sequences in one parameter or to determine the qualitative effect of exceeding the ranges specified above. Some of the synthetic spectra are presented in Figures 2-9. These are only meant to illustrate the appearance of typical spectra under various conditions. The actual analysis is carried out using the curves of growth presented in the next section. The continuum in the synthetic spectra is flat and coincides with the flat region

Fig. 2. Synthetic Spectra; Temperature Sequence with Log a = -3

$C^{12}/C^{13} = 89$, log η = 2.5, $\xi_t = 10$ km/s.

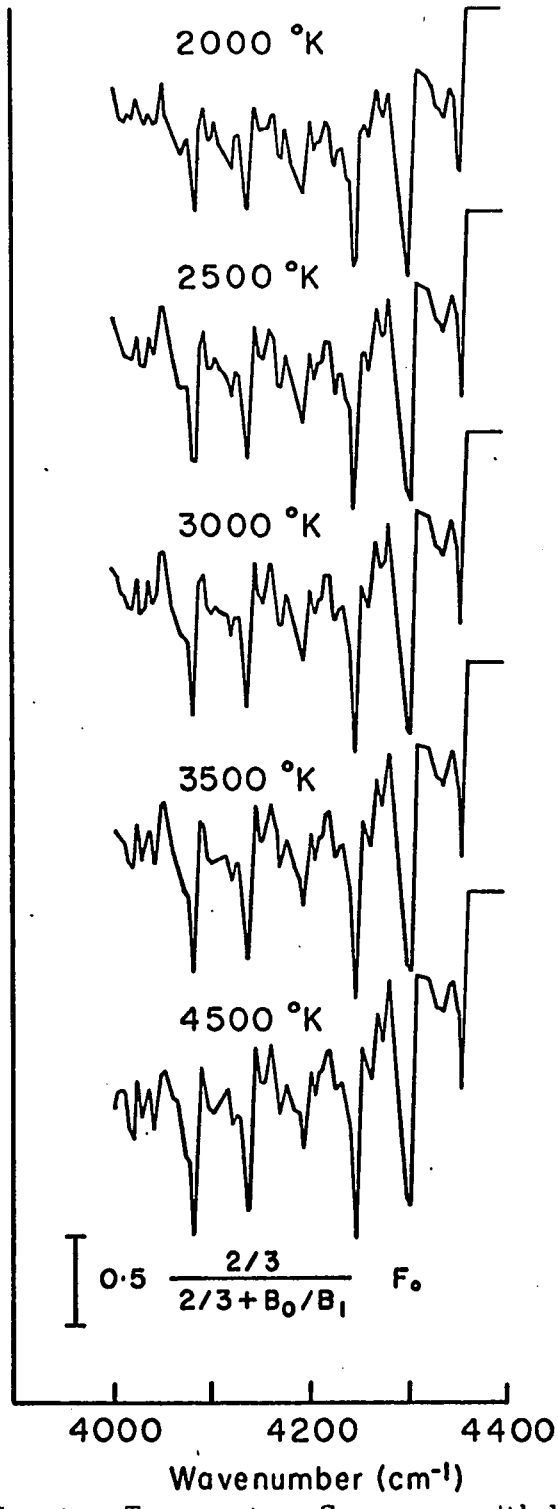

Fig. 2. Synthetic Spectra; Temperature Sequence with log a = -3

Fig. 3. Synthetic Spectra; Temperature Sequence with Log a = -1

$C^{12}/C^{13} = 89$, log $\eta = 1.5$, $\xi_t = 10$ km/s.

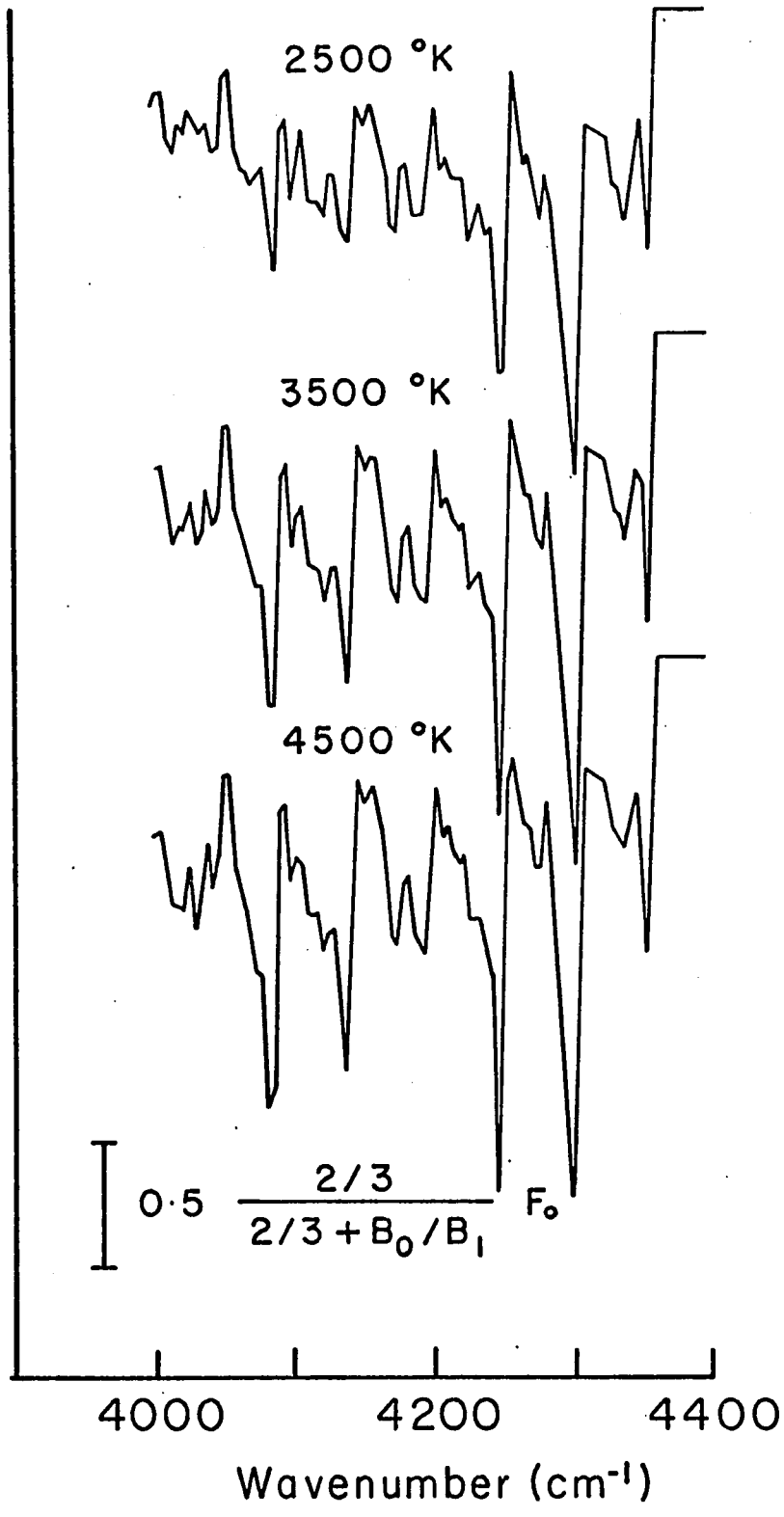

Fig. 3. Synthetic Spectra; Temperature Sequence with log a = -1

Fig. 4. Synthetic Spectra; Damping Parameter Sequence

$T = 3500$ K, log η 1.5, $\xi_t = 10$ km/s, $C^{12}/C^{13} = 4$

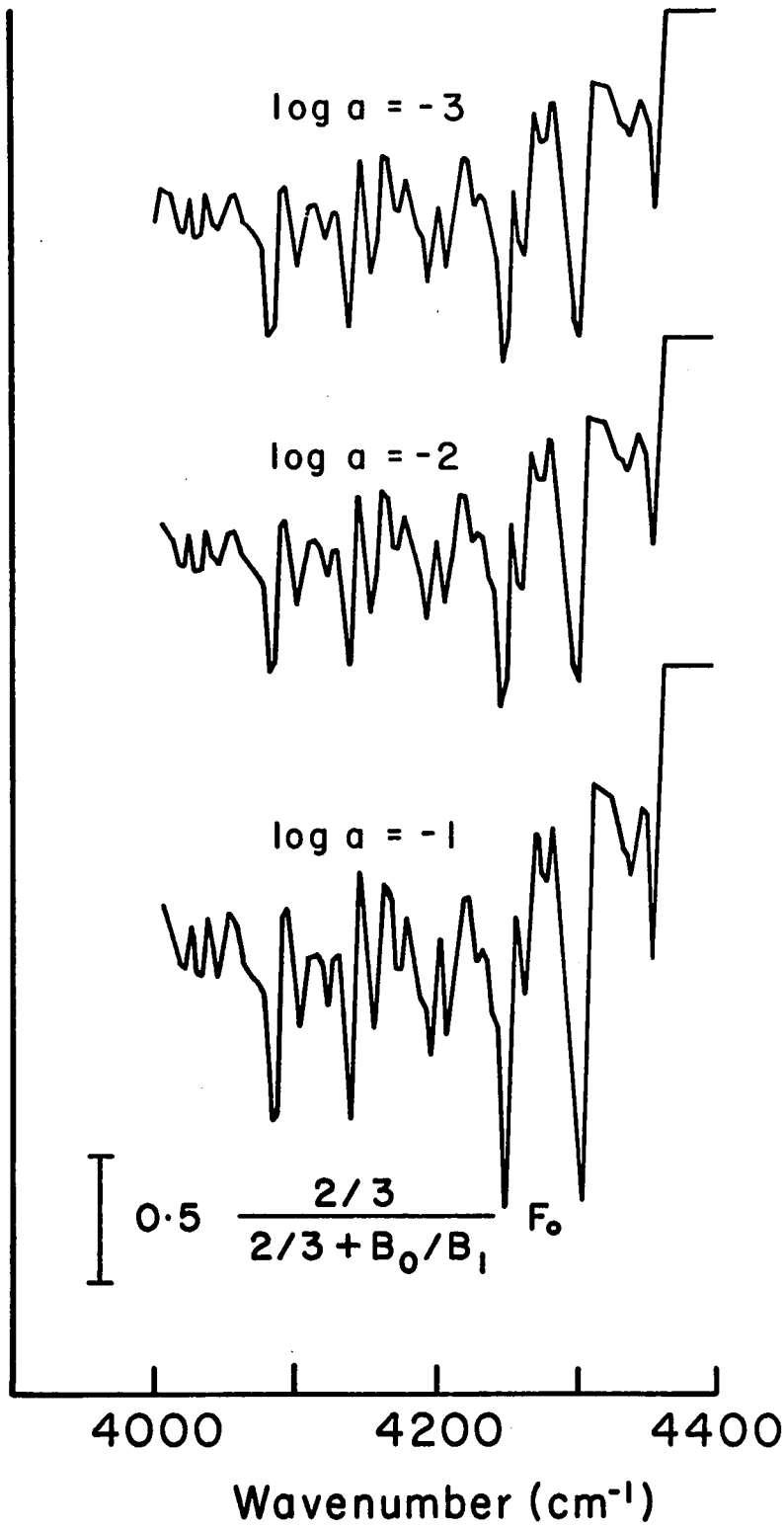

Fig. 4. Synthetic Spectra; Damping Parameter Sequence

Fig. 5. Synthetic Spectra; Microturbulent Velocity Sequence

$T = 3500$ K, $\log \eta = 3.5$, $\log a = -3$, $C^{12}/C^{13} = 20$

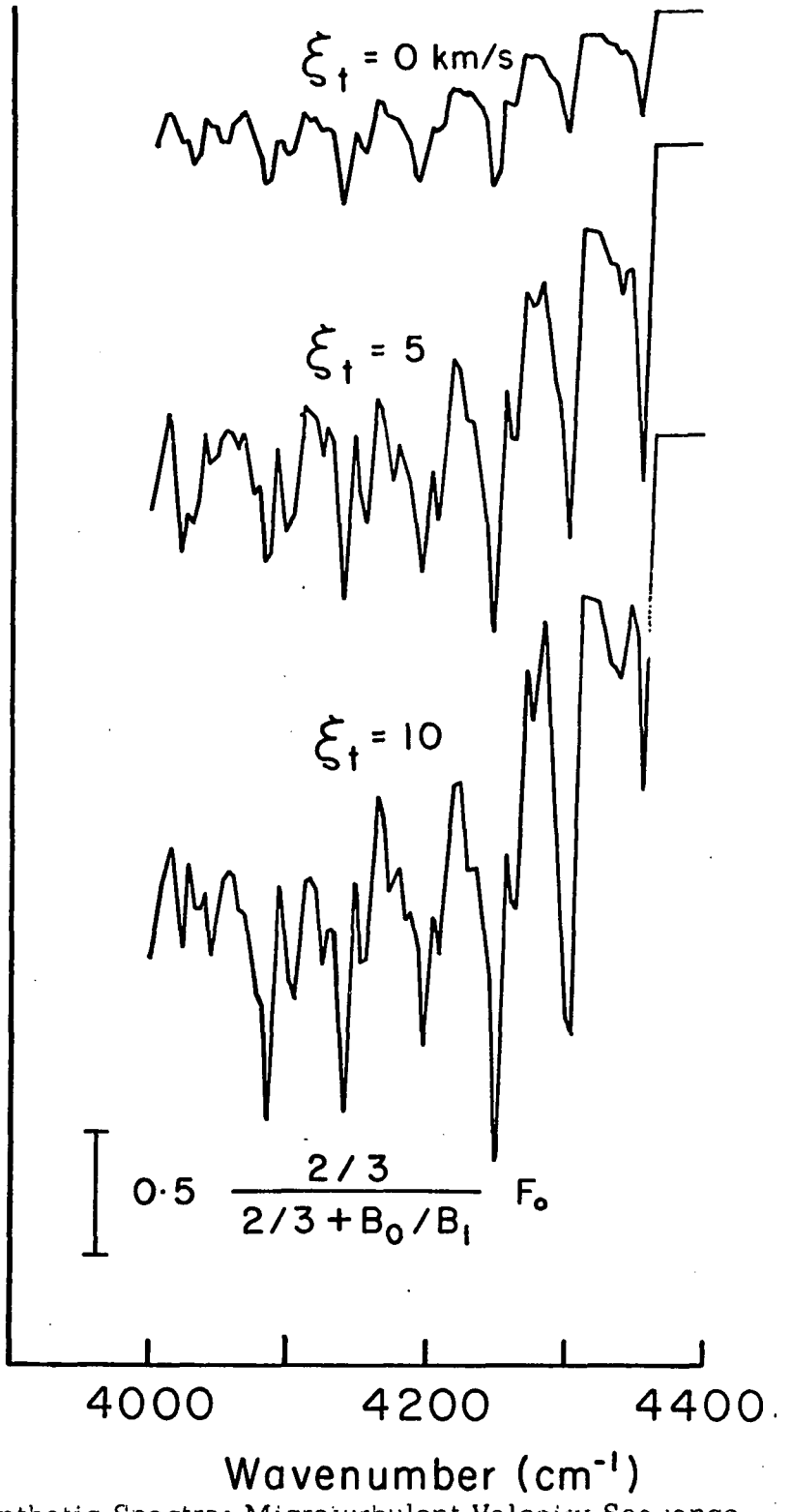

Fig. 5. Synthetic Spectra; Microturbulent Velocity Sequence

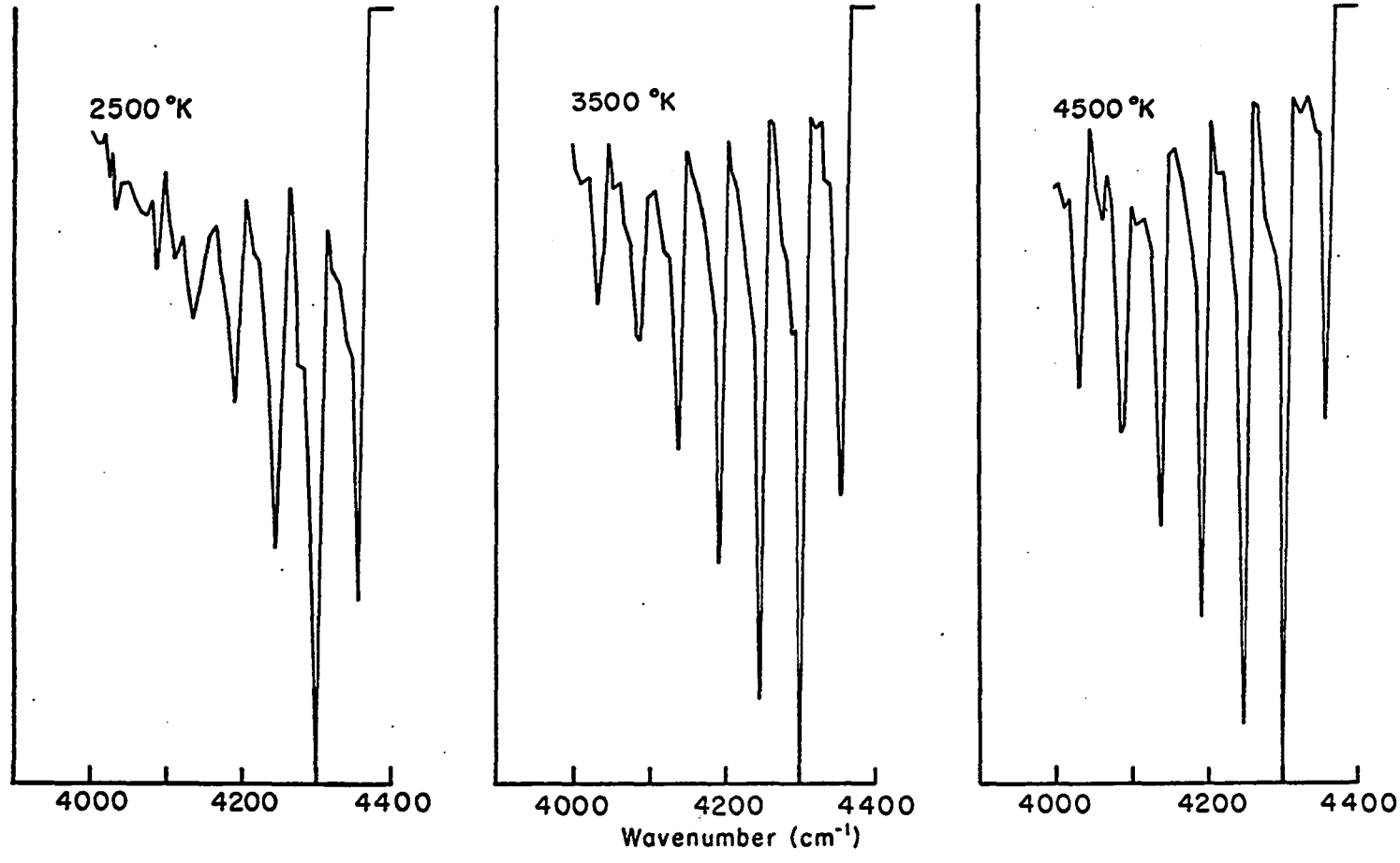

Fig. 6. Synthetic Spectra; Temperature Sequence with Linear Curve of Growth

$C^{12}/C^{13} = 89$

Fig. 7. Synthetic Spectra; Abundance Sequence with $T = 2500$ K

$\log a = -3$, $\xi_t = 10$ km/s, $C^{12}/C^{13} = 89$

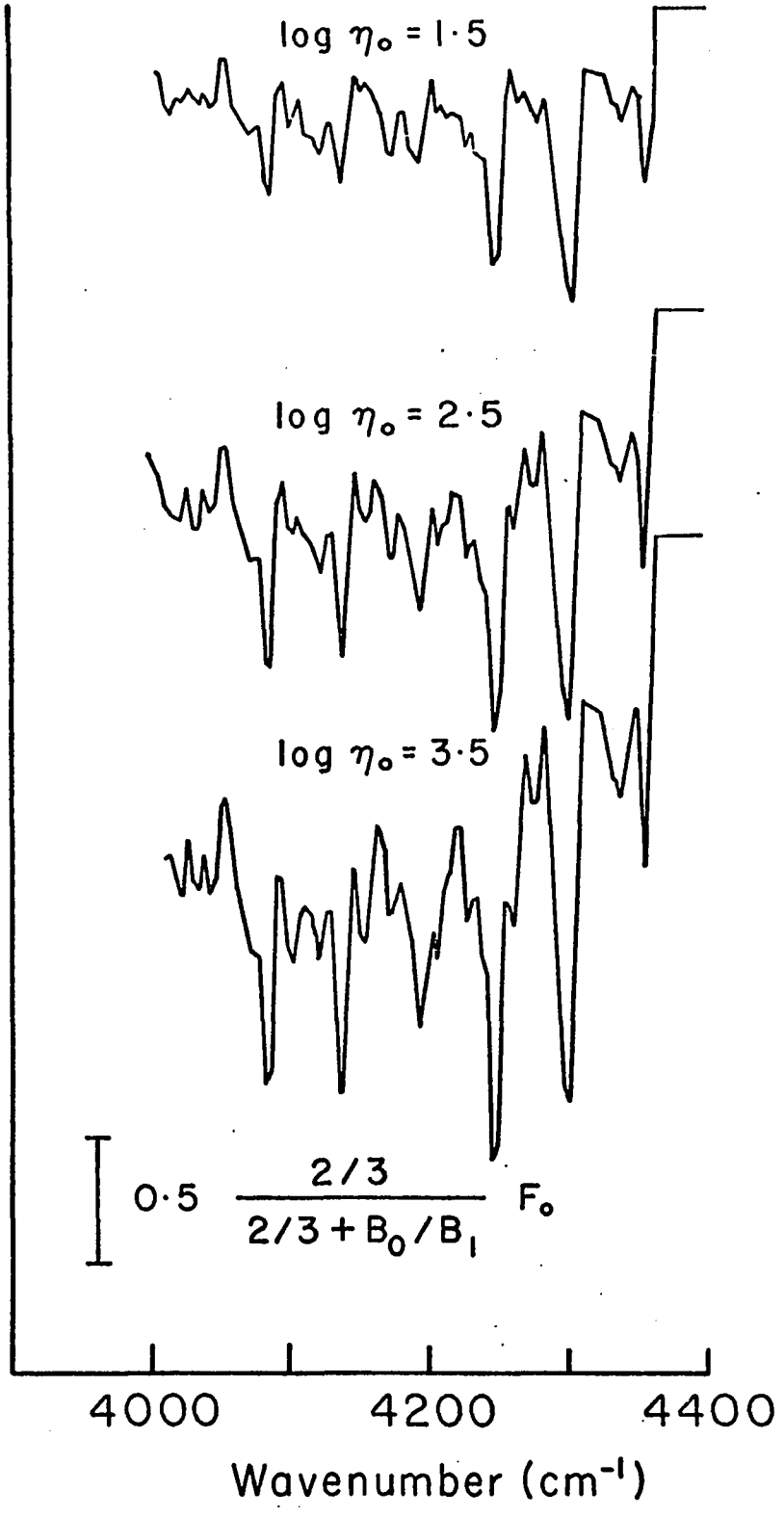

Fig. 7. Synthetic Spectra; Abundance Sequence with T = 2500 K

Fig. 8. Synthetic Spectra; Abundance Sequence with $T = 4500$ K

$\log a = -3$, $\xi_t = 10$ km/s, $C^{12}/C^{13} = 89$

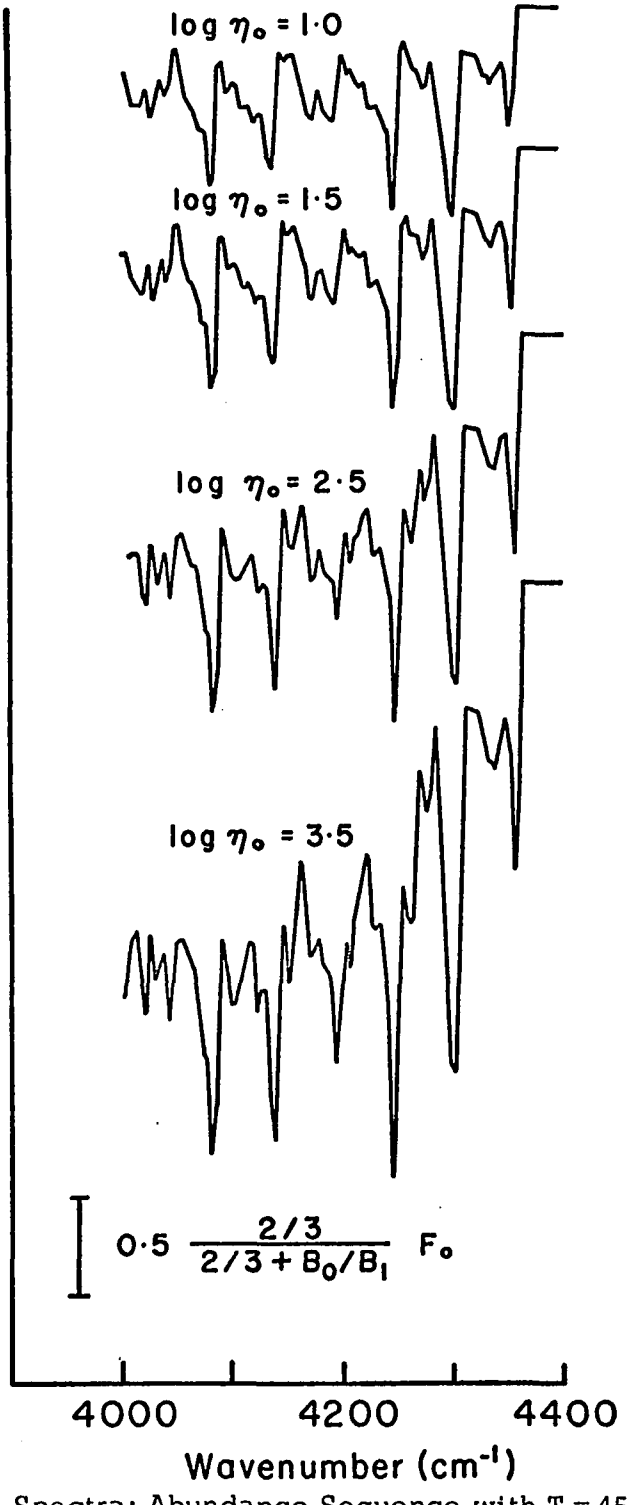

Fig. 8. Synthetic Spectra; Abundance Sequence with T = 4500 K

Fig. 9. Synthetic Spectra; Isotope Ratio Sequence

$T = 3500$ K, $\log a = -3$, $\log \eta = 2.5$, $\xi_t = 10$ km/s

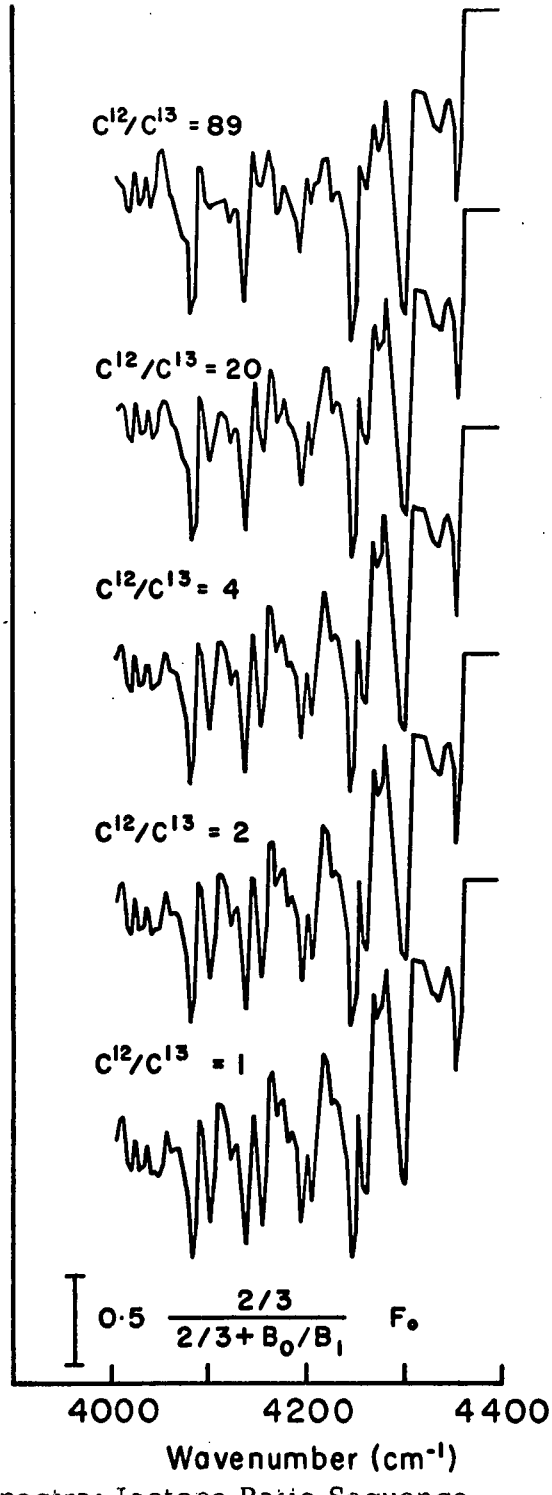

Fig. 3. Synthetic Spectra; Isotope Ratio Sequence

between 4360 cm^{-1} and 4400 cm^{-1}. The vertical axis is proportional to flux. The actual scale is indicated by the vertical bar which represents $0.5\left[(2/3/(2/3 + B_0/B_1)\right]$ of the continuum flux. Since B_0/B_1 only enters the equivalent width as a multiplicative factor, it only affects the flux scale, not the band profile.

Figures 2 and 3 are both temperature sequences, all other parameters held constant. Figure 2 has a small damping constant, log a = -3, Figure 3 has a larger damping constant, log a = -1. The long, flat portion of the curve of growth for log a = -3 tends to equalize the strength of the band heads compared to log a = -1. This effect only occurs, of course, if the lines are far enough up on the curve of growth to place a significant number of band head lines on the flat portion. Increased temperature also makes more band heads visible by increasing the population of the higher vibrational levels. There is no noticable effect on the shape of the individual band heads due to changes in the rotational excitation as the temperature changes. Temperature is most effective at producing more visible band heads when the lines are on the linear part of the curve of growth and least effective when they are on the flat portion.

Figure 4 is a sequence of spectra with varying log a. Small values of log a tend to equalize the band head strengths and produce a smaller total equivalent width for the band sequence. Both effects are

due to the longer flat section of the curve of growth for smaller "a" values.

A turbulent velocity sequence is shown in Figure 5. The turbulent velocity effects the spectrum in two ways. The most conspicuous is through the factor $\frac{\Delta \nu_D}{\nu_o}$ in the equivalent width. This produces the rapid increase in equivalent width with increasing $\Delta \nu_D$. The other effect is due to line blending. This has a small effect on the equivalent width; ignoring blending entirely increases the equivalent width by only a few percent. The details of the band profile, however, are sensitive to turbulent velocity through the blending. The appearance of the (2-0) band head at 4360 cm^{-1} with $\xi_t = 10$ km/s never occurs in stellar spectra. This may be a result of inaccurate line positions. The line positions were calculated using polynomial approximations to the energy levels. In some cases, the difference between calculated and measured line positions is as large as 0.5 cm^{-1}. The doppler width, $\Delta \nu_D$, is on the order of 0.02 cm^{-1}, therefore errors of this size can make significant changes in the blending. For this reason, this band head has been given lower weight than the others in the analysis.

The profiles of the band sequence when all lines are on the linear part of the curve of growth are shown in Figure 6 for several temperatures. Sequences of spectra with increasing carbon monoxide abundance are shown in Figures 7 and 8 for temperatures of 2500 K and 4500 K respectively. The effect of the non-linear curve of growth is

obvious. The contrast of the band heads becomes less sensitive to temperature as abundance increases but the general depression of the region from 4000 cm^{-1} to 4300 cm^{-1} still retains some temperature sensitivity through the higher level rotational transitions which occur all through this region. This is not an unambiguous temperature indicator however.

The effect of changing the C^{12}/C^{13} abundance ratio is shown in Figure 9. The relative strengths of the C^{13} and C^{12} band heads are a strong function of log a, abundance and temperature in addition to C^{12}/C^{13} ratio, but this illustrates the general trend. As mentioned previously, the spectra are useful primarily for qualitative comparisons with stellar spectra. For quantitative analysis of stars, the curves of growth discussed in the next section are more appropriate. We have, therefore, only included a representative sample of the spectra to illustrate the type of spectral changes caused by varying different parameters.

The Curves of Growth

For the analysis of the stellar carbon monoxide abundance, the synthetic spectra of the previous section were used to produce curves of growth for the first six band heads (4036-4360 cm^{-1}) of the $\Delta v = 2$ sequence. These are presented in Figures 10-12 as curves of log F versus log η where

$$\log F = \log W_\nu - \log \left[(2/3)/(2/3 + B_0/B_1) \right].$$

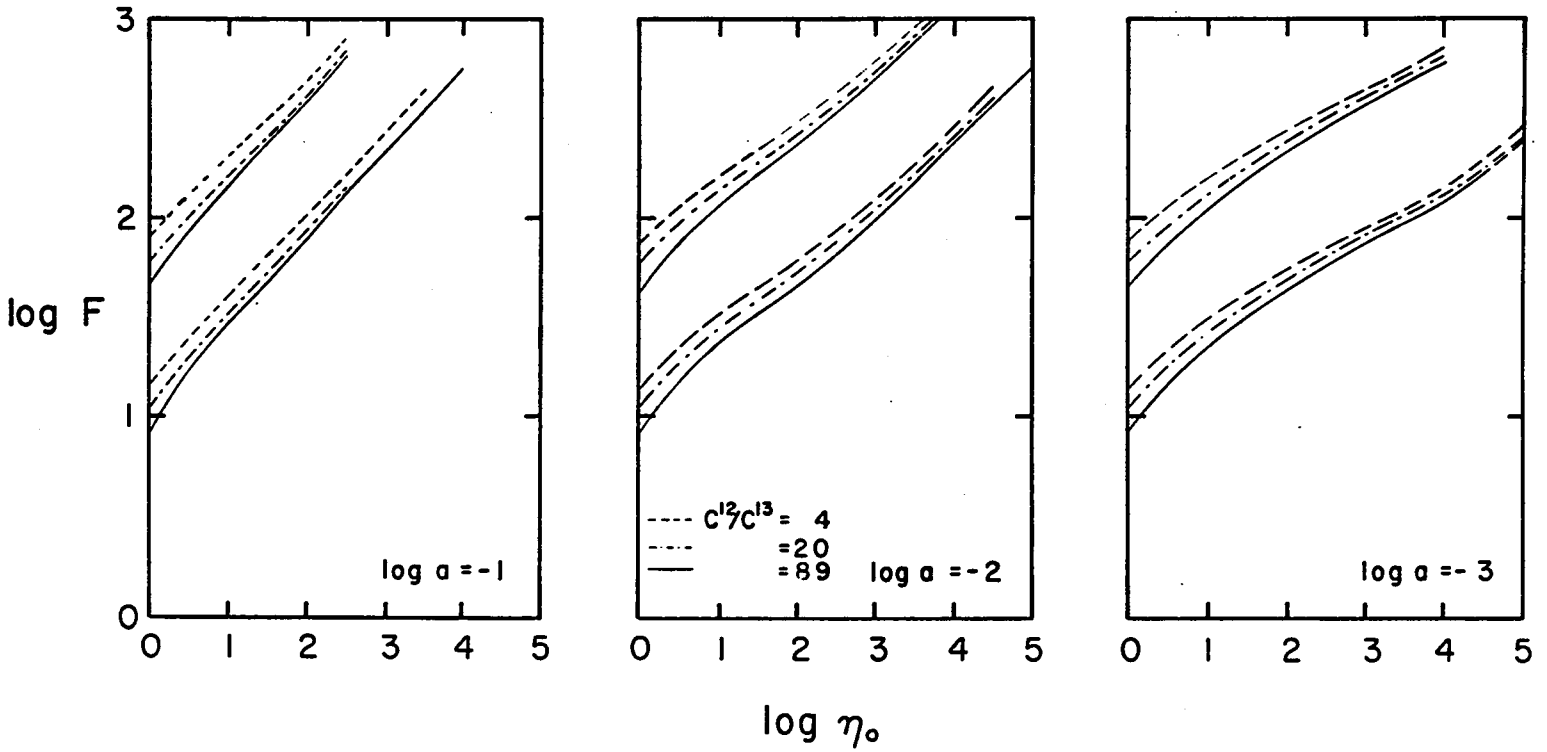

Fig. 10. Curve of Growth for the Region 4036-4360 cm^{-1} with T = 2500 K

The upper group of curves is for ξ_t = 10 km/s, the lower group is for ξ_t = 0 km/s

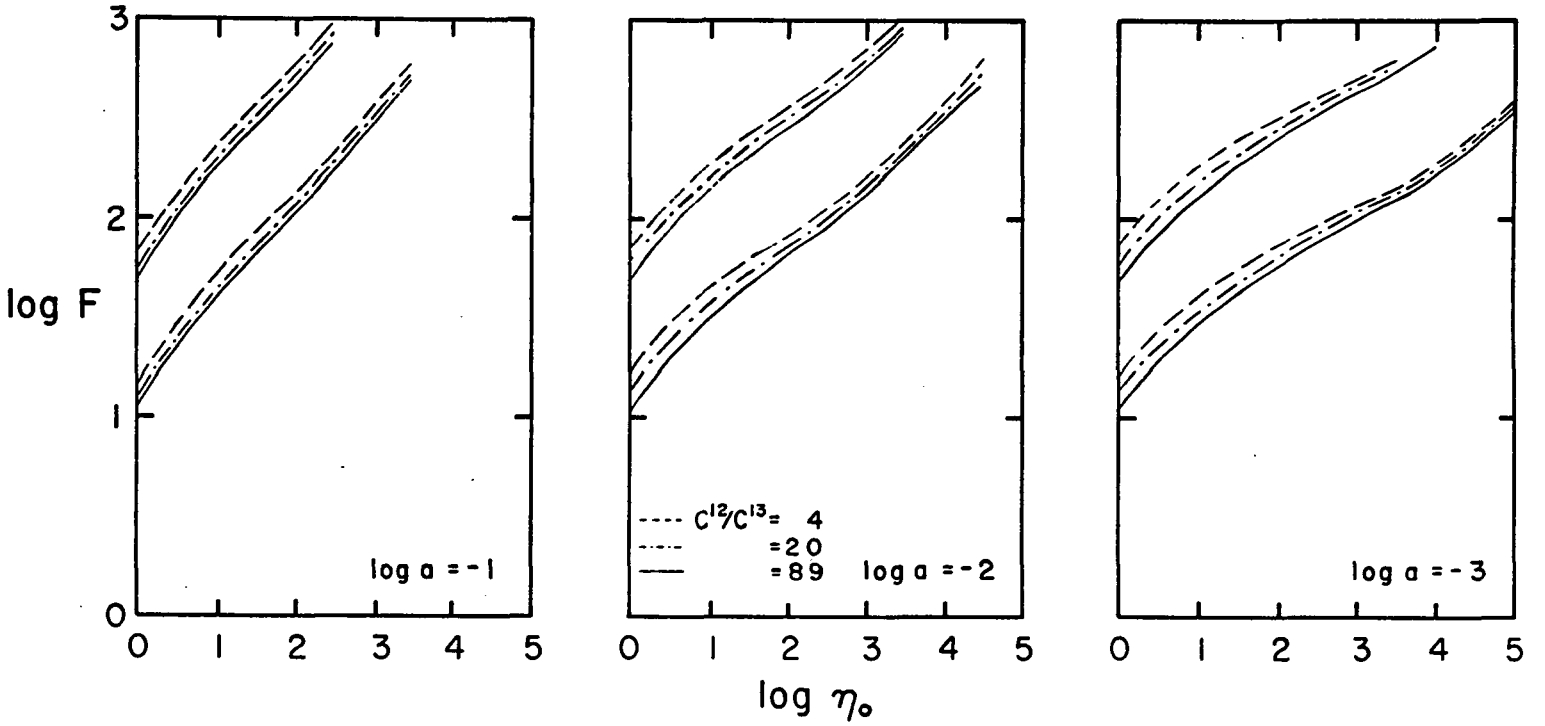

Fig. 11. Curve of Growth for the Region 4036-4360 cm^{-1} with T = 3500 K

See Fig. 10 for explanation of symbols.

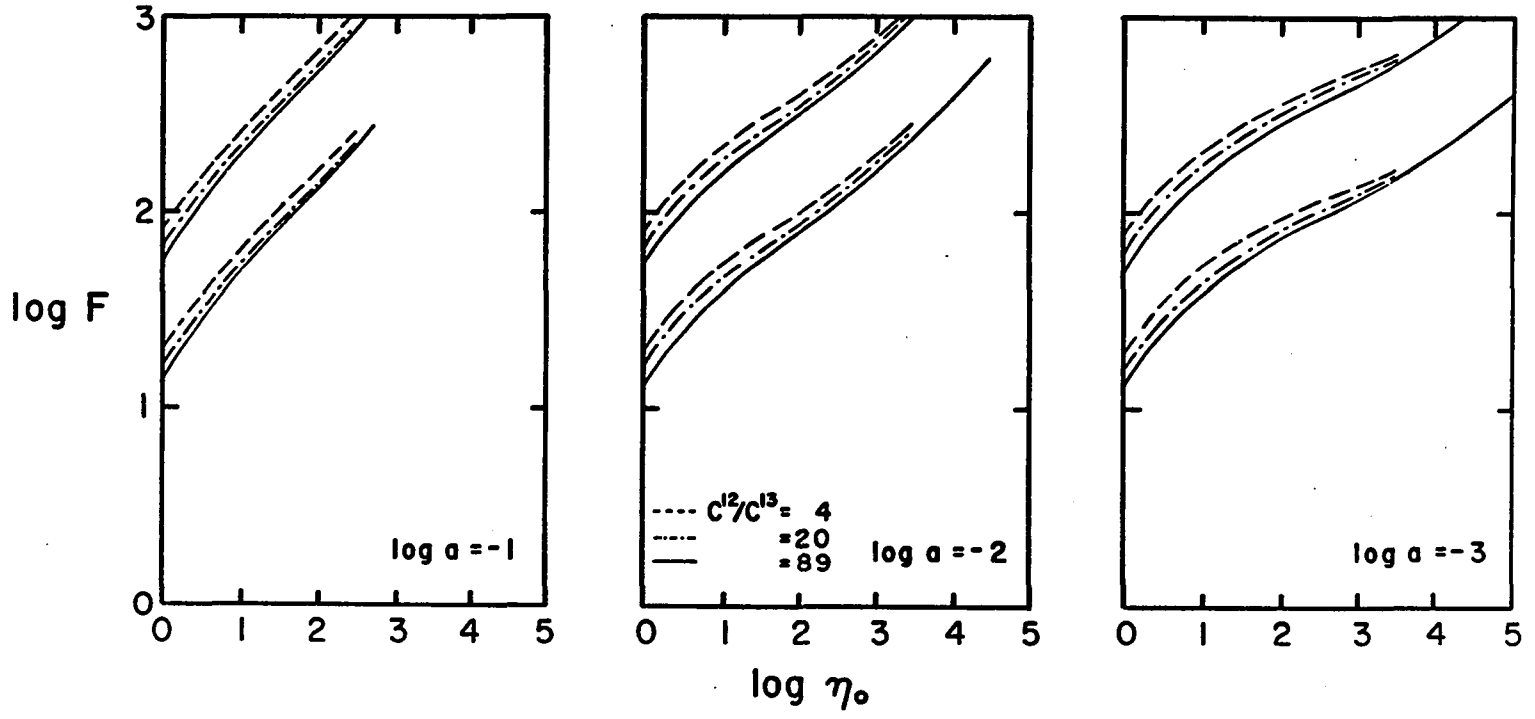

Fig. 12. Curve of Growth for the Region 4036-4360 cm^{-1} with T = 4500 K

See Fig. 10 for explanation of symbols.

To determine the C^{12}/C^{13} abundance ratio, it is necessary to measure at lease two features, one of which is sensitive to C^{13} abundance. The $C^{12}O^{16}$ (2-0) and (3-1) band heads have no $C^{13}O^{16}$ lines superimposed on them so either could serve as a C^{12} indicator. The region of the $C^{13}O^{16}$ (2-0) band head (4252-4264 cm^{-1}) is the best choice for a C^{13} indicator since it has the smallest number of superimposed $C^{12}O^{16}$ lines. It is also the furthest $C^{13}O^{16}$ band from the terrestrial H_2O band at 2.7μ so is the least affected by the correction for terrestrial atmospheric absorption. The final choice for a C^{12}/C^{13} indicator was the ratio of the equivalent widths of the $C^{13}O^{16}$ (2-0) band head (4252-4264 cm^{-1}) to the $C^{12}O^{16}$ (3-1) band head (4284-4308 cm^{-1}), indicated by W^{13}/W^{12}. The $C^{12}O^{16}$ (3-1) head was chosen instead of the (2-0) head for two reasons: (1) it is closer to the $C^{13}O^{16}$ (2-0) head, so questions of changing continuous opacity or B_0/B_1 are minimized and (2) as mentioned above, there is some question about reliability of the calculated $C^{12}O^{16}$ (2-0) heads at high ξ_t. The primary disadvantage of this choice is that we are comparing different vibrational levels in the two isotopes. If LTE applies, this has no effect, but any error in the relative populations of the first and second vibrational levels will appear directly in the C^{12}/C^{13} ratio. Understanding the population of the $v=1$ level will lead to a C^{12}/C^{13} ratio that is too large and overestimating the population of the $v=1$ level will lead to a C^{12}/C^{13} ratio that is too small. There is some evidence that the higher

vibrational levels are underpopulated in stars (Spinrad et al. 1971). If so, the C^{12}/C^{13} ratios derived here are lower limits.

The curves of growth for the $C^{12}O^{16}$ (3-1) and $C^{13}O^{16}$ (2-0) heads are presented in Figures 13-15 and 16-18 respectively. These are mainly useful for producing curves of W^{13}/W^{12} versus C^{12}/C^{13} abundance ratio, such as those in Figures 19-22. Figure 19 shows the curves of W^{13}/W^{12} versus C^{12}/C^{13} abundance ratio for those cases where all the lines in the two band heads are on the linear part of the curve of growth. In this case, log a and ξ_t are irrelevant. Figures 20, 21, and 22 show the same curves with $\xi_t = 10$ km/s and with T, log a, and log n as parameters. Curves like those of Figures 20-22 can easily be constructed for any values of ξ_t and log n using Figures 13-18.

These curves give the carbon monoxide abundance and C^{12}/C^{13} abundance ratio as a function of B_0/B_1, ξ_t, T, and log a. Some other means must be available to fix the value of these four parameters. For instance, B_0/B_1 can be taken from a model atmosphere. Any method available can then be used to pick a best guess for the values of the other three parameters. The combination of parameters yielding the best fit to the observed profile of the band sequence can be determined, or other analyses of the star, such as photometry or photographic spectra, can be used to fix one or more of the parameters. The means used to fix these three parameters will be discussed more fully for the individual stars in Chapter 3.

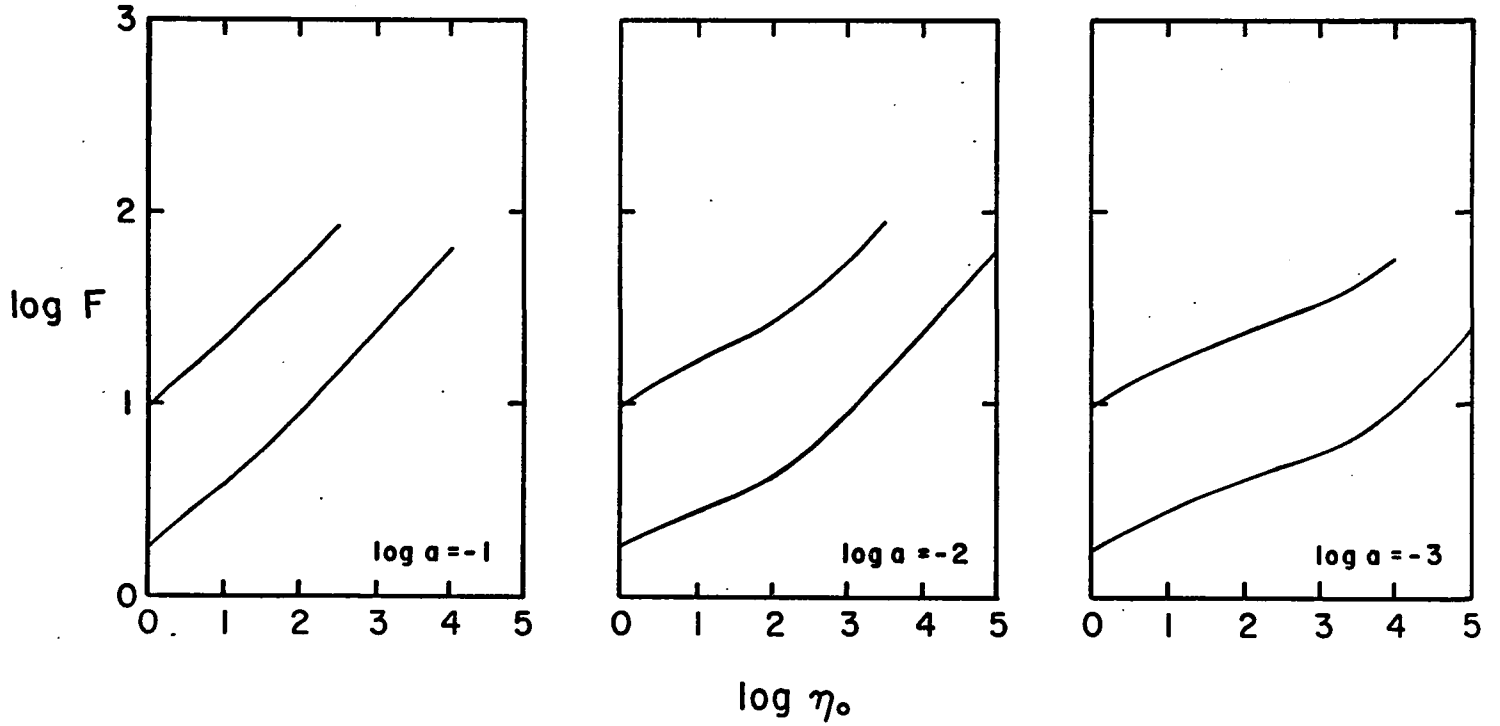

Fig. 13. Curve of Growth for the $C^{12}O^{16}$ (3-1) Band Head with T = 2500 K

The upper curve is for $\xi_t = 10$ km/s, the lower curve is for $\xi_t = 0$ km/s.

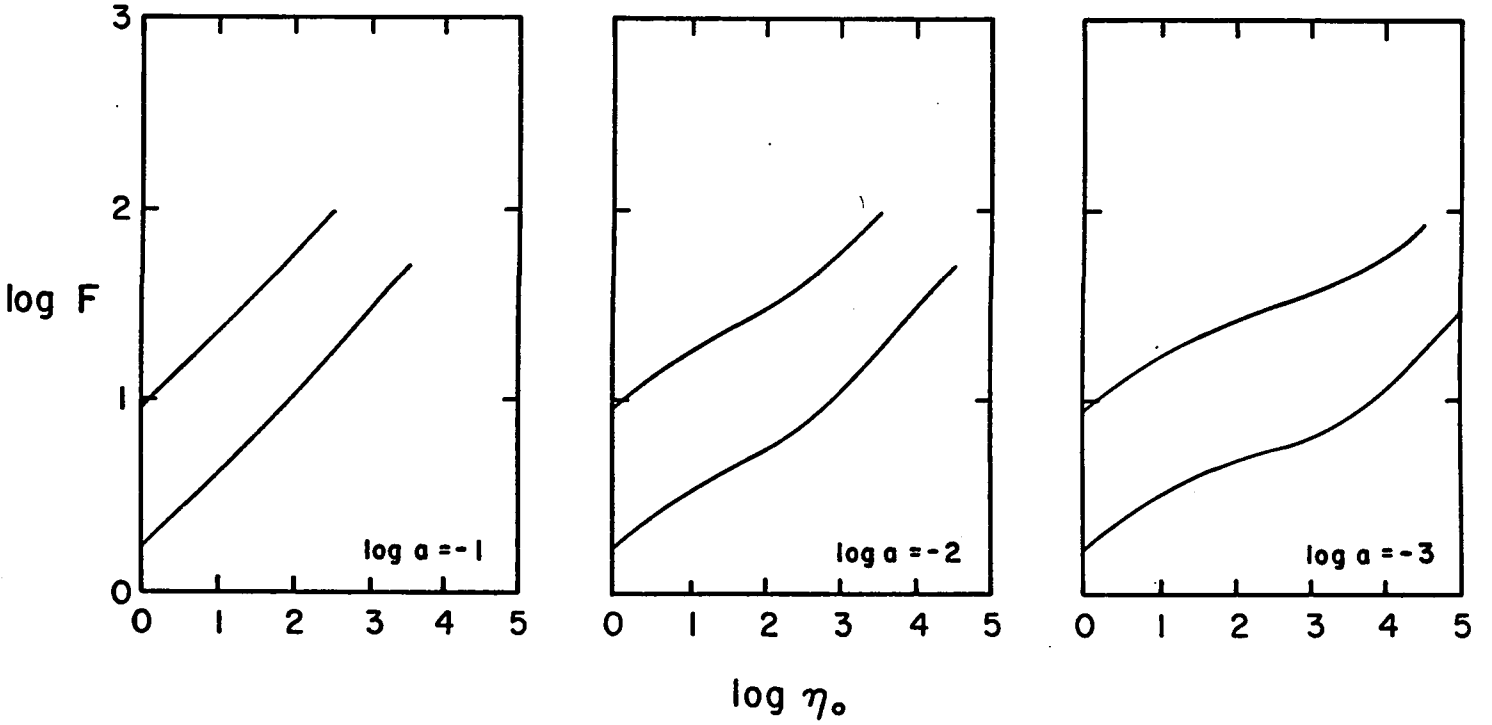

Fig. 14. Curve of Growth for the $C^{12}O^{16}$ (3-1) Band Head with T = 3500 K

The upper curve is for $\xi_t = 10$ km/s, the lower curve is for $\xi_t = 0$ km/s.

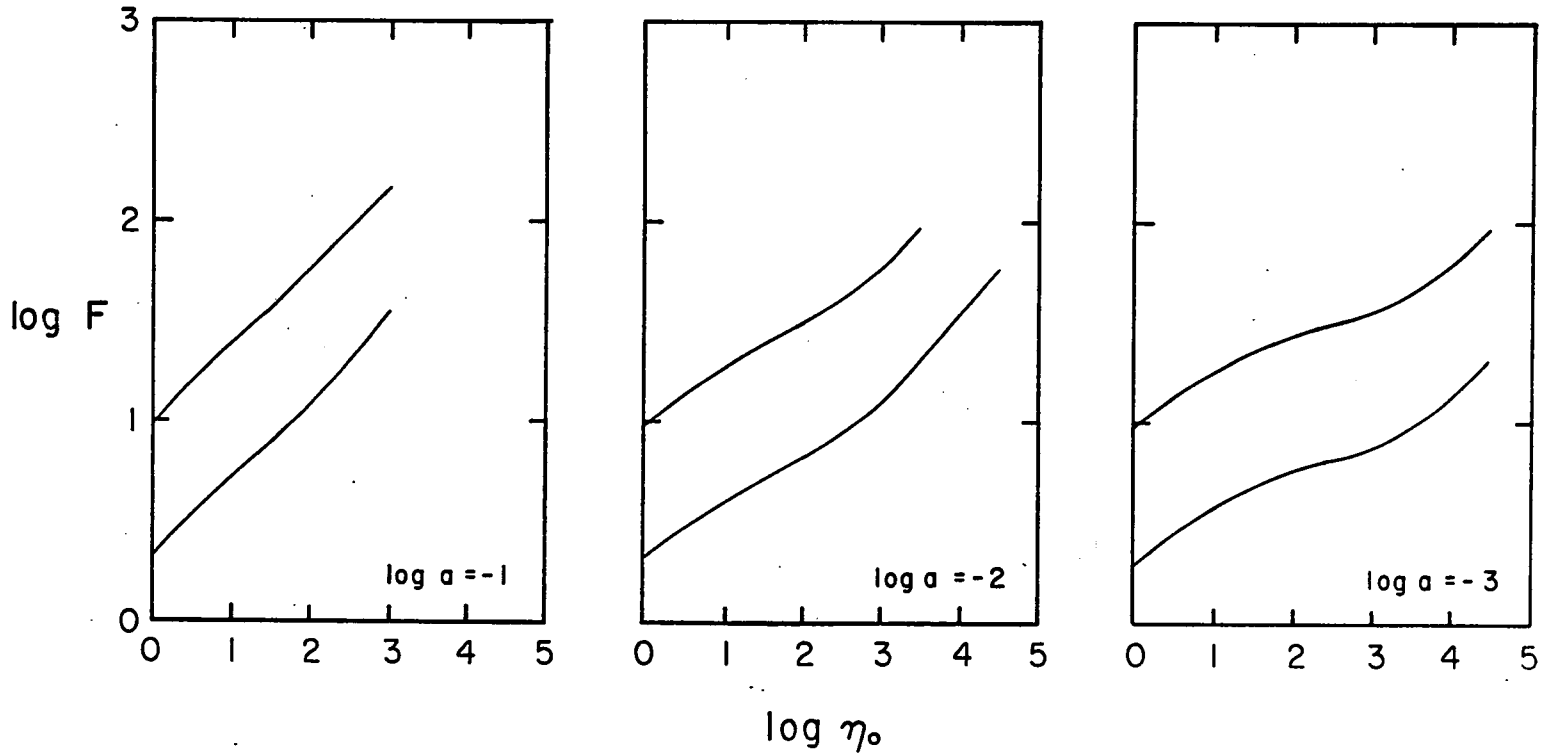

Fig. 15. Curve of Growth for the $C^{12}O^{16}$ (3-1) Band Head with T = 4500 K

The upper curve is for ξ_t = 10 km/s, the lower curve is for ξ_t = 0 km/s.

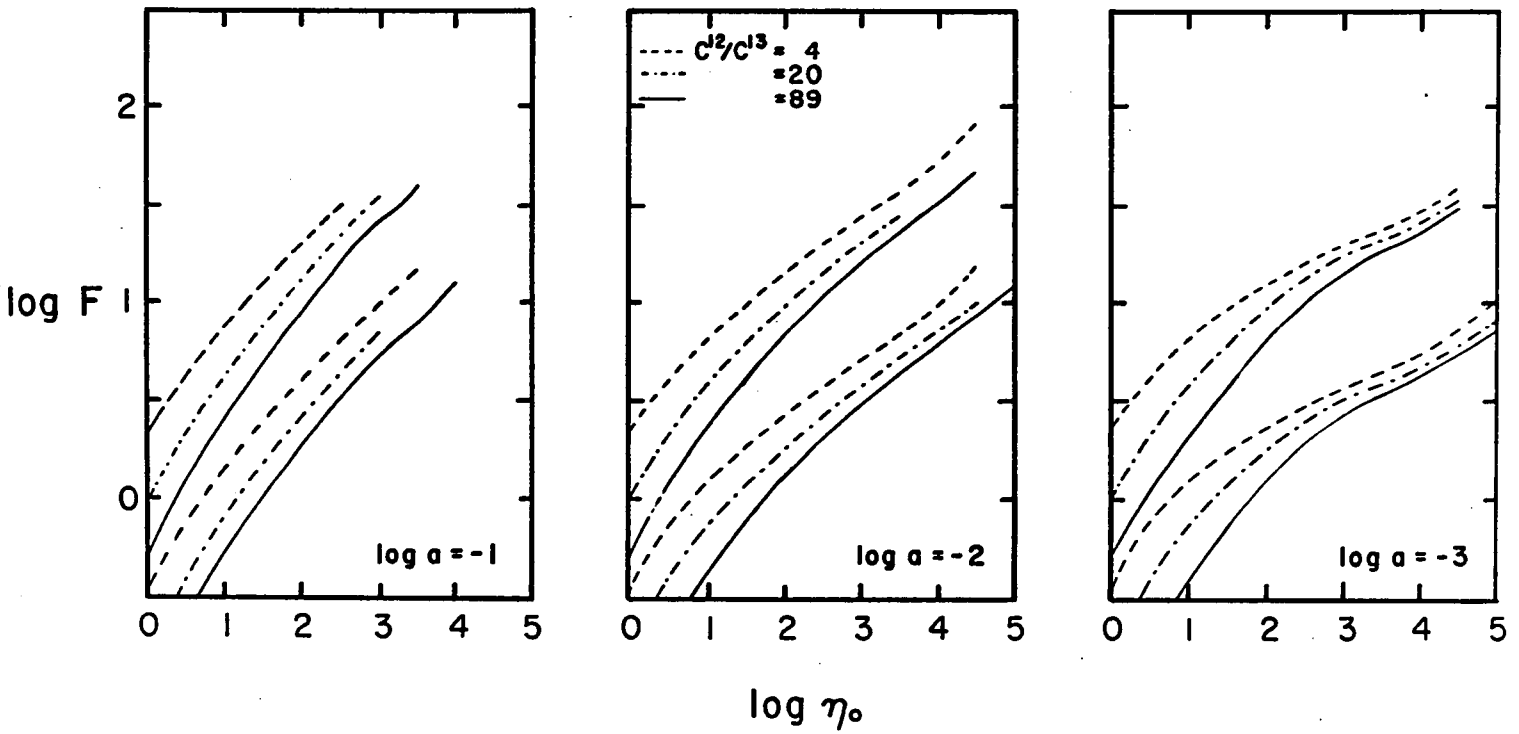

Fig. 16. Curve of Growth for the $C^{13}O^{16}$ (2-0) Band Head with T = 2500 K

The upper curve is for ξ_t = 10 km/s, the lower curve is for ξ_t = 0 km/s.

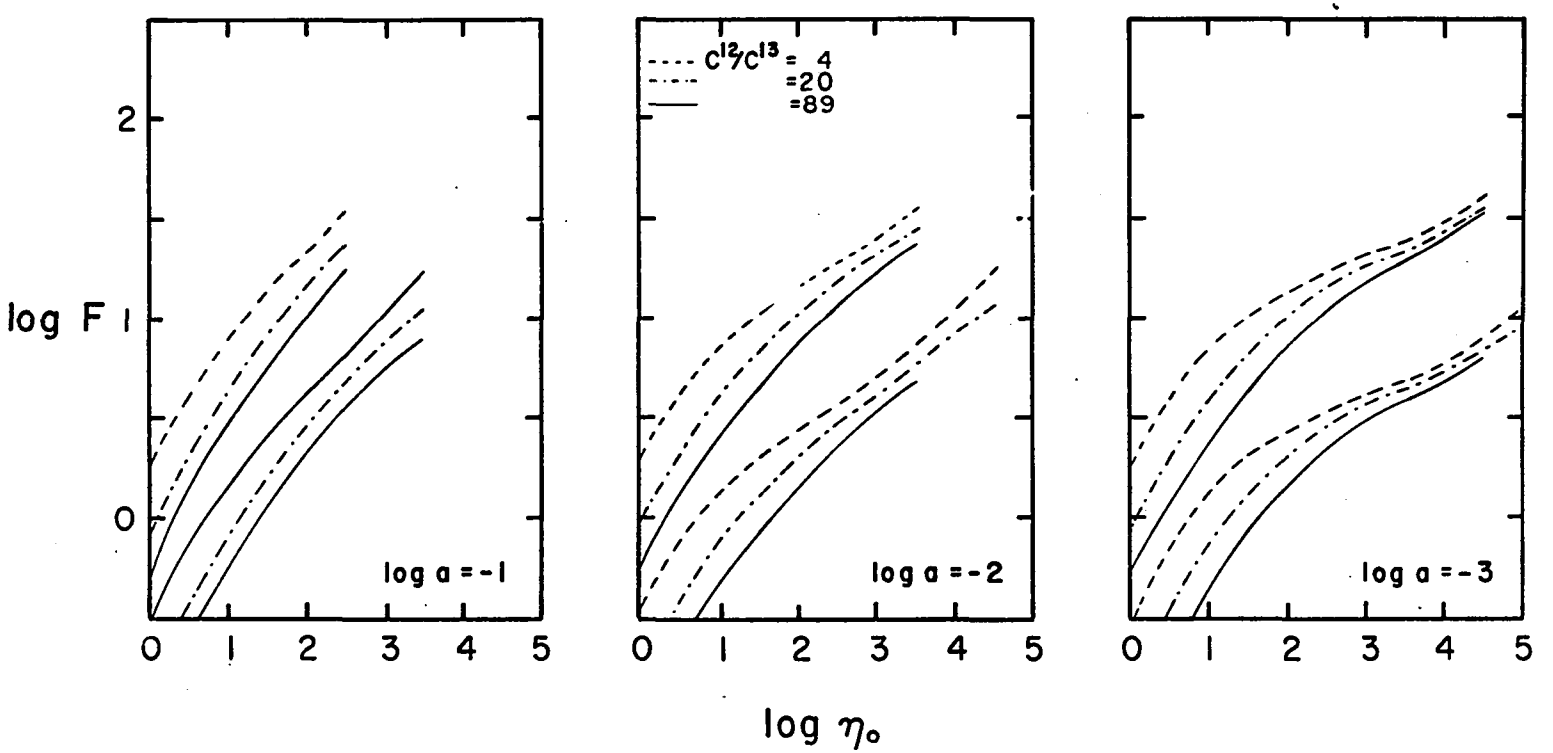

Fig. 17. Curve of Growth for the $C^{13}O^{16}$ (2-0) Band Head with T = 3500 K

The upper curve is for ξ_t = 10 km/s, the lower curve is for ξ_t = 0 km/s.

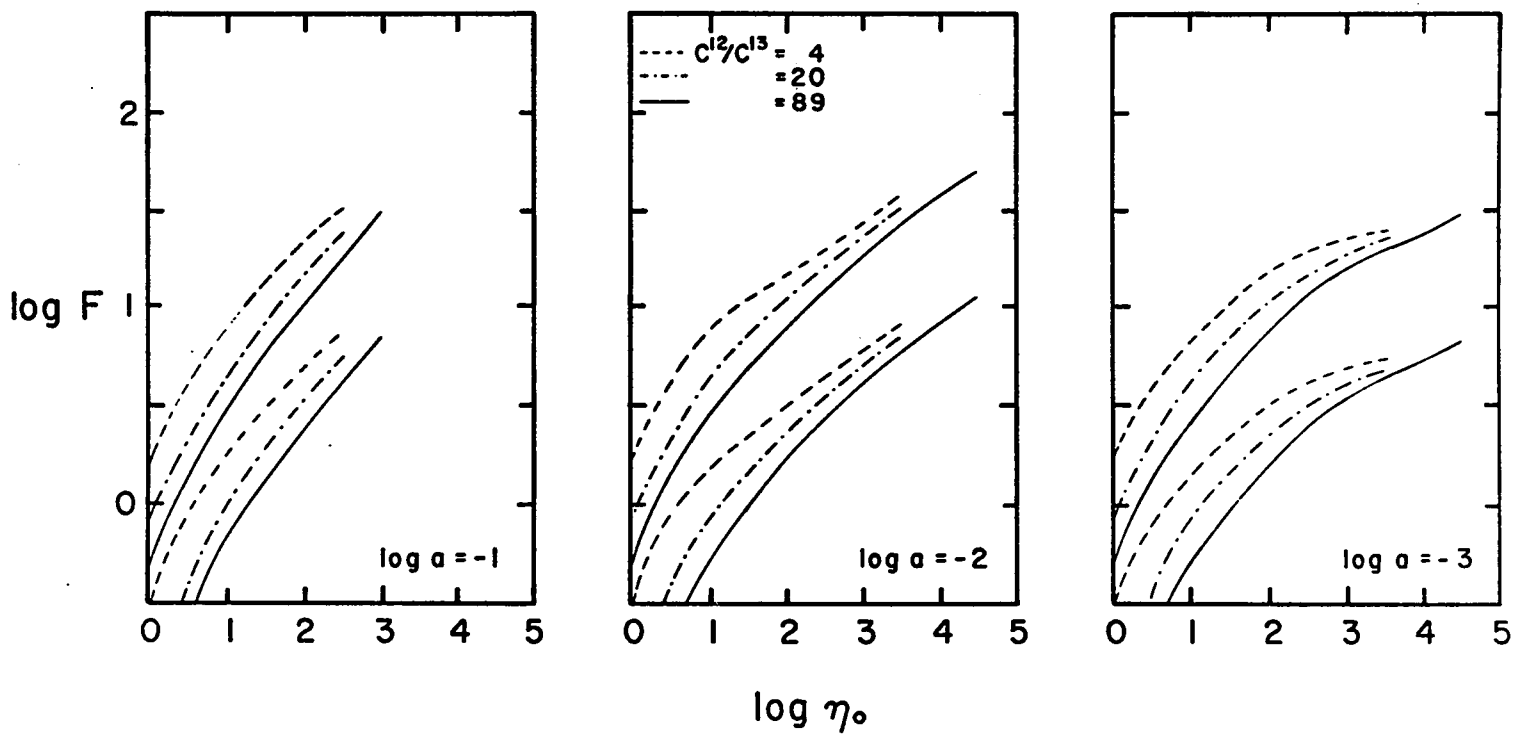

Fig. 18. Curve of Growth for the $C^{13}O^{16}$ (2-0) Band Head with T = 4500 K

The upper curve is for ξ_t = 10 km/s, the lower curve is for ξ_t = 0 km/s.

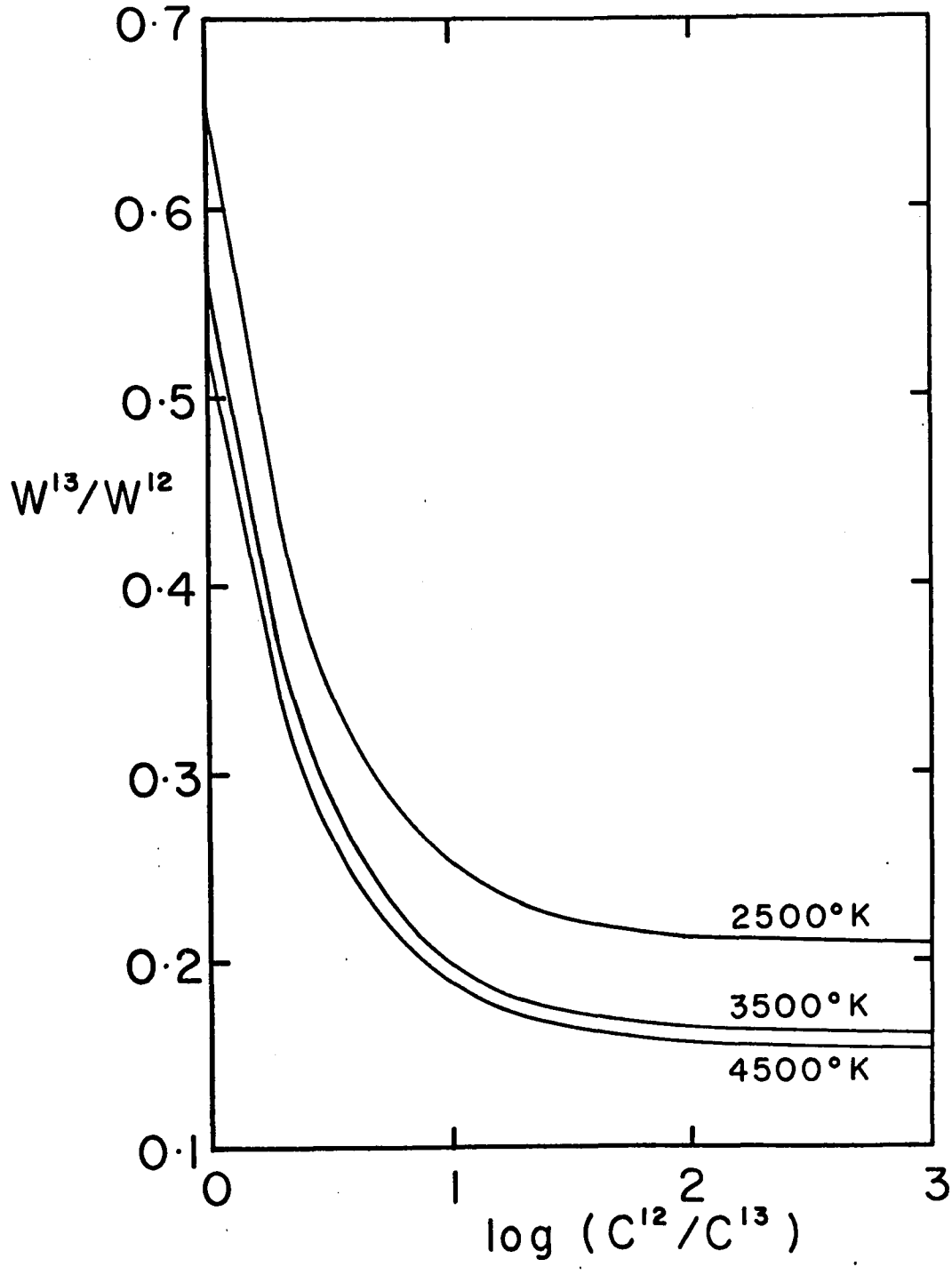

Fig. 19. W^{13}/W^{12} - C^{12}/C^{13} for a Linear Curve of Growth

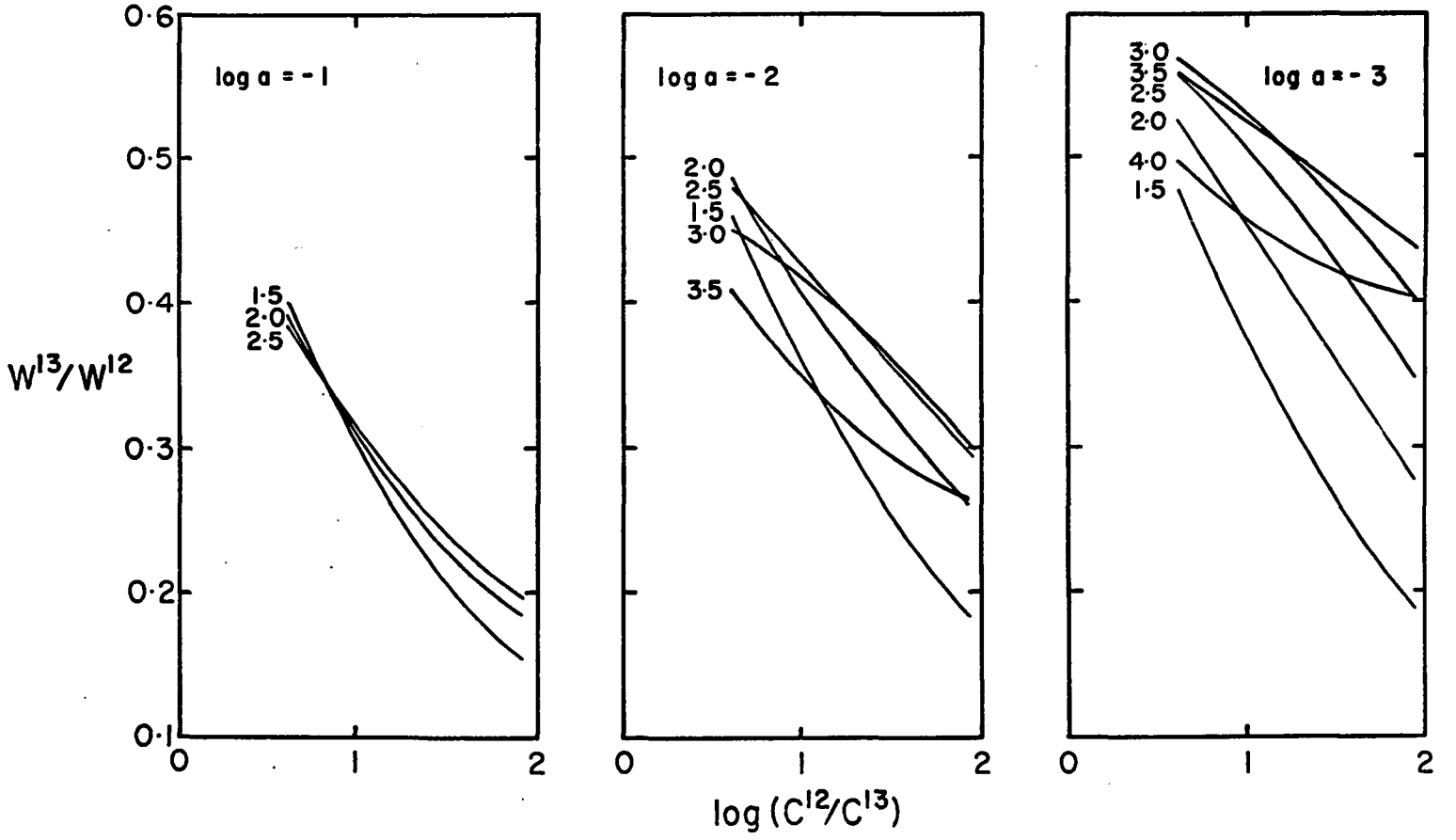

Fig. 20. W^{13}/W^{12} - C^{12}/C^{13} for T = 2500 K

The curves are labeled with log η.

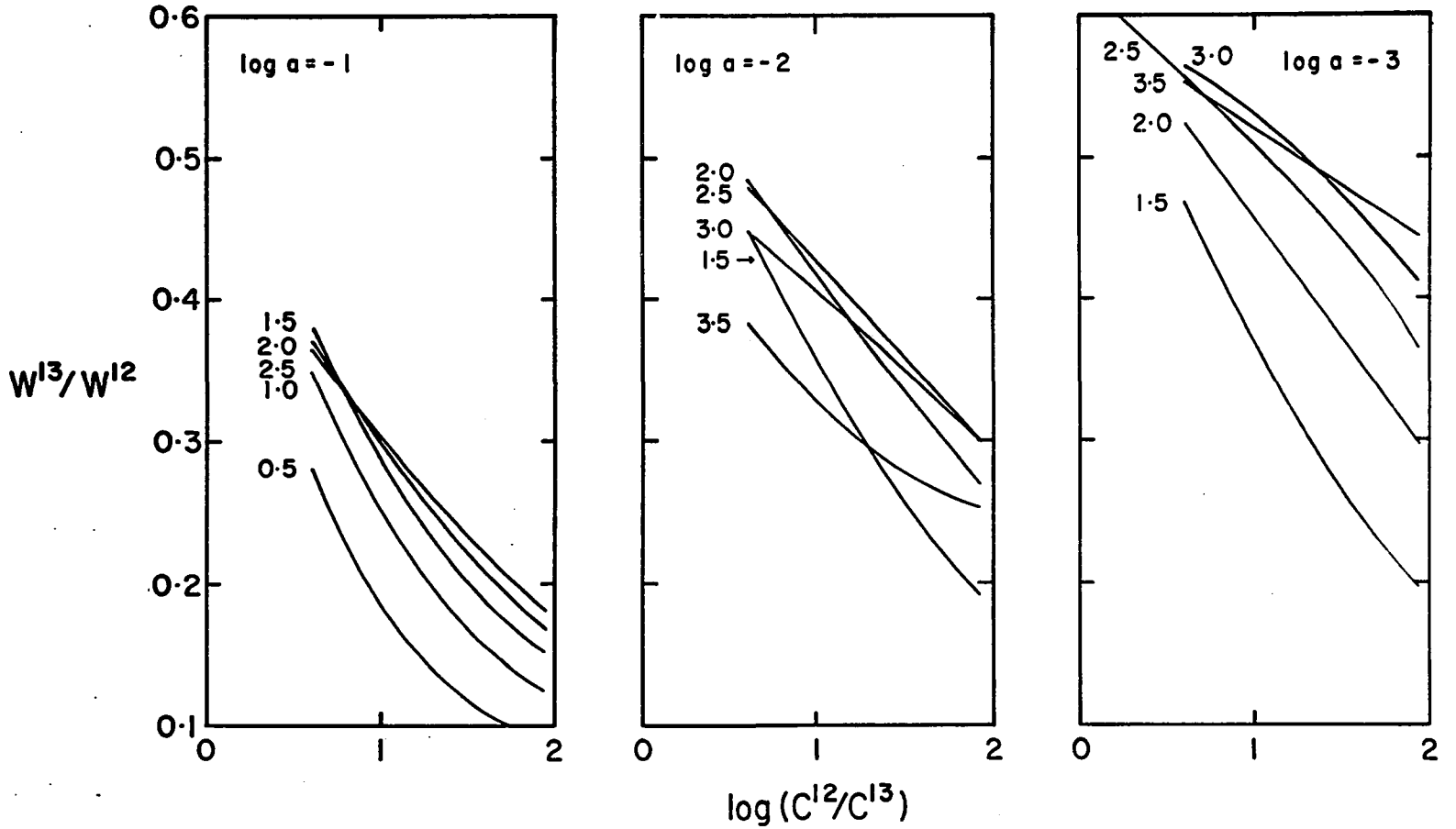

Fig. 21. $W^{13}/W^{12} - C^{12}/C^{13}$ for T = 3500 K

The curves are labeled with log η .

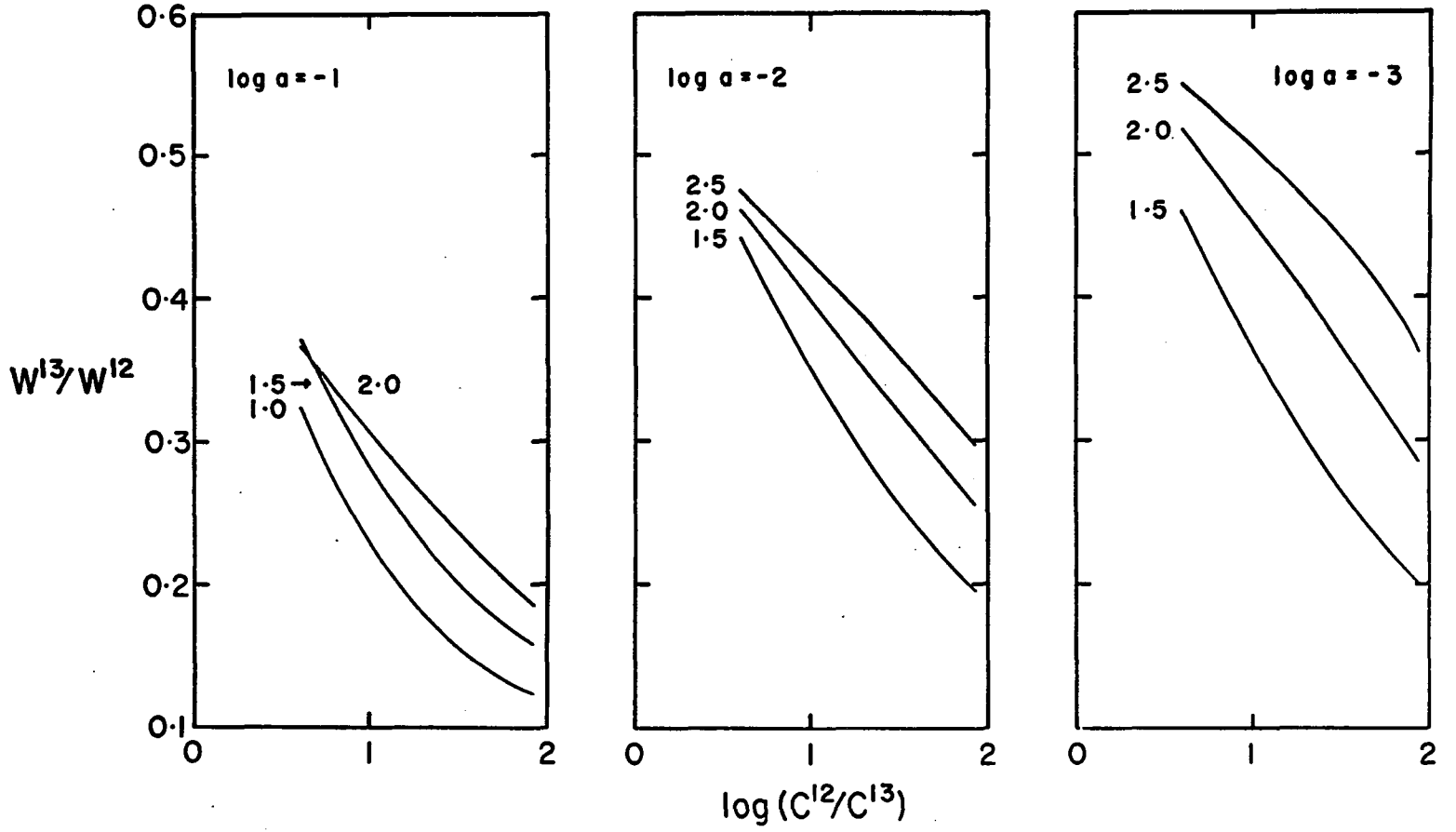

Fig. 22. $W^{13}/W^{12} - C^{12}/C^{13}$ for T = 4500 K

The curves are labeled with log.n .

THE STELLAR SPECTRA

The stellar spectra used for this investigation were obtained by Johnson and co-workers (Johnson et al. 1968, Johnson and Mendez 1970) using a Mertz type, rapid scanning Michaelson interferometer at the Catalina Station of the Lunar and Planetary Laboratory and are corrected for atmospheric extinction to zero air mass. Details of the instrumentation, observing procedure and atmospheric extinction correction are given by Johnson and Mendez (1970). The spectra cover the wavenumber region 2400-8200 cm^{-1} or 3900-8200 cm^{-1} depending on whether they were obtained with refrigerated or un-refrigerated detectors. The resolution is 8 cm^{-1}. There are 23 spectra of 15 K and M giants and supergiants. The spectra used are listed in Table 2 with their spectral types.

The individual spectra will be discussed below with the results of the investigation, but a few general remarks should be made here. The CO $\Delta v = 2$ vibration-rotation band sequence is the strongest feature in the spectra of these stars, extending from 4360 cm^{-1} to 3900 cm^{-1} at which point the terrestrial water vapor absorption blocks ground based observations. The $\Delta v = 3$ band sequence extending to lower wavenumbers from 6418 cm^{-1} is also visible although considerably weaker in most

Table 2. Spectra Used in this Investigation

Star	Spectral Type	Reference (Johnson & Mendez 1970)
Alpha Bootis	K2 IIIp	Fig. 2b
Gamma Draconis	K5 III	Fig. 2c
Alpha Tauri	K5 III	Fig. 3a, b
Delta Ophiuchi	MO.5 III	Fig. 3c
Beta Pegasi	M2-3 II-III	Fig. 4a, b
Eta Geminorum	M3 III	Fig. 4c
Mu Geminorum	M3 III	Fig. 5a
Rho Persei	M3 II-III	Fig. 5b
R Lyrae	M5 III SR	Fig. 5c, 6a, b
EU Delphini	M6 III SR	Fig. 6c
Alpha Orionis	M1-2 Iab	Fig. 9b, c
Alpha Scorpii	M1-2 Iab	Fig. 10a
Mu Cephei	M2 Ia	Fig. 10b, c, 11a
Delta^2 Lyrae	M4 II	Fig. 11b
Alpha Herculis	M5 Ib-II	Fig. 11c, 12a

stars. The fundamental ($\Delta v = 1$) vibration-rotation band sequence begins just beyond the long wavelength cut-off of these spectra at 2328 cm^{-1}.

Sources of Error

There are three sources of error to be considered; noise in the spectra, superimposed absorption features and errors in the placement of the continuum. These are discussed separately below.

Noise

The signal to noise ratio can not be accurately determined from the spectra, but a rough estimate of the noise level can be obtained by looking at the regions where the continuum intensity is low. The noise level should be approximately constant throughout the spectrum before correction for the terrestrial atmospheric absorption. This means that the signal to noise ratio is lowest where the intensity is low and the atmospheric correction is large.

The complete quantitative treatment of the transfer of noise from the observed interferogram, through the Fourier transform, to the spectrum is a complex problem. The assumption of White noise, made above, is sufficient for the purpose of estimating the quality of the spectra. For a more detailed discussion of noise see Connes (1961).

Other Absorptions

Terrestrial water vapor absorption completely blocks observation between 3500-3900 cm^{-1} and also usually blocks the region 5100-5500 cm^{-1}. Stellar water vapor, if it exists, will have strong absorption over significantly wider bands than the terrestrial water, due to the higher excitation temperature in the stars. This is easily visible in the published spectra of Mira variables. Stellar water vapor absorption seriously overlaps the CO $\Delta v = 2$ sequence and less seriously overlaps the $\Delta = 3$ sequence. This complicates analyses of the CO bands, since, even if the H_2O is considered as a separate, continuous, opacity source, the position of the continuum depends on the H_2O absorption and is strongly variable with frequency. If H_2O is not treated as a continuous opacity source it is necessary to treat it line by line, simultaneously with the CO. The model atmospheres calculated by Auman (1969) including H_2O predict a high abundance of H_2O and strong absorption across the CO bands. Auman's models however, only fit the H_2O spectrum of Mira variables. There is no evidence of H_2O absorption in non-variable K and M giants or supergiants in the spectra used for this investigation.

Other molecules also have absorption bands in the region of the CO first overtone sequence, but none are expected to be significant sources of interference. Spinrad et al. (1971) have identified HF in high resolution spectra of Alpha Orionis. Johnson and Mendez (1970)

claimed to have detected the CH (2-0) band head at 4112 cm^{-1} in K giants. These are both weak absorption features, however, and should not interfere significantly with the analysis of the CO bands. Both electronic and vibrational transitions of CN produce absorption within the CO bands. Band heads due to the $\Delta v = -2$ electronic transitions of the CN red system ($A\,^2\pi_i - X^2\Sigma^+$) have been detected in carbon stars by Thompson and Schnopper (1970), but have not been found in oxygen stars. The transition probability of vibrational transitions is much lower than that of electronic transitions, therefore the vibration-rotation bands are not expected to be detectable. There are some atomic lines in this region, but most are high excitation lines and are not expected to be strong enough or numerous enough to significantly affect the results. The exception to this is the analysis of the C^{12}/C^{13} ratio using very narrow sections of spectrum. A strong atomic line (or molecular band head) could contribute significantly to the equivalent width over a very narrow region. This effect is minimized by only measuring those regions where the CO absorption is strongest, therefore the percentage error due to a superimposed absorption line is smallest.

Placement of the Continuum

The placement of the continuum level for the CO first overtone bands is somewhat uncertain. The continuum level at the high wavenumber end of the sequence at 4360 cm^{-1} is well determined since the

$C^{12}O^{16}$ (2-0) band head produces a sharp break in the spectrum at this point. Between 4360 cm^{-1} and 3900 cm^{-1}, however, there is no place where the continuum is visible at this resolution. Beyond 3900 cm^{-1}, the terrestrial atmosphere blocks observations completely. Since only one continuum point is available, the continuum at larger wavenumbers must be used as a guide to extrapolate across the CO bands. This means that the position of the continuum becomes more uncertain for the higher level transitions in the sequence. This extrapolation can be carried out with sufficient accuracy for the present investigation, but it should be kept in mind that this is the largest source of error in the equivalent widths. The measured equivalent widths are probably accurate to about 10%.

In this respect, the second overtone CO bands would probably be easier to analyze. The continuum level can be more accurately determined because the bands are weaker and the continuum is usually visible between the band heads. However, interference from superimposed absorption lines is more severe, both because there are more and stronger absorptions and because the weaker CO bands are more susceptable to interference. Also, there are more band heads visible than are expected from the appearance of the first overtone sequence and the relative strengths of the band heads is not obviously explainable on the basis of a simple model.

Both of these effects can be explained if, as predicted by the models by Gingerich et al. (1967) and Carbon and Gingerich (1969), H^- is the dominant opacity source. The H^- opacity is lower in the region of the second overtone bands than in the region of the first overtone bands, and there is a minimum in the H^- opacity at 6060 cm^{-1}. The lower opacity accounts for the stronger bands and the variation of the opacity over the band sequence affects the relative strengths of the band heads. This will be discussed further in Chapter 4.

The Method of Analysis

As was pointed out in Chapter 2, there are four variables to be determined before unique values of C^{12}/C^{13} and CO abundance can be determined; T, B_0/B_1, ξ_t and log a. The results for each star are presented as a series of curves. Log (C^{12}/C^{13}) is plotted versus abundance (log η), with T, ξ_t and log a as parameters, in Figures 23 through 36. Log η is plotted versus B_0/B_1 in Figures 37 through 40.

The value of B_0/B_1 only affects the conversion of equivalent width to log η . For a given value of log η , a wide range of equivalent widths can be produced by varying B_0/B_1 without changing the band profile. Therefore it is only possible to determine B_0/B_1 indirectly. Log η does affect the band profile, however, as do T, ξ_t and log a. Therefore, log η , T, ξ_t and log a can be directly determined from the spectrum. These four parameters, with the measured equivalent width, then determine the value of B_0/B_1.

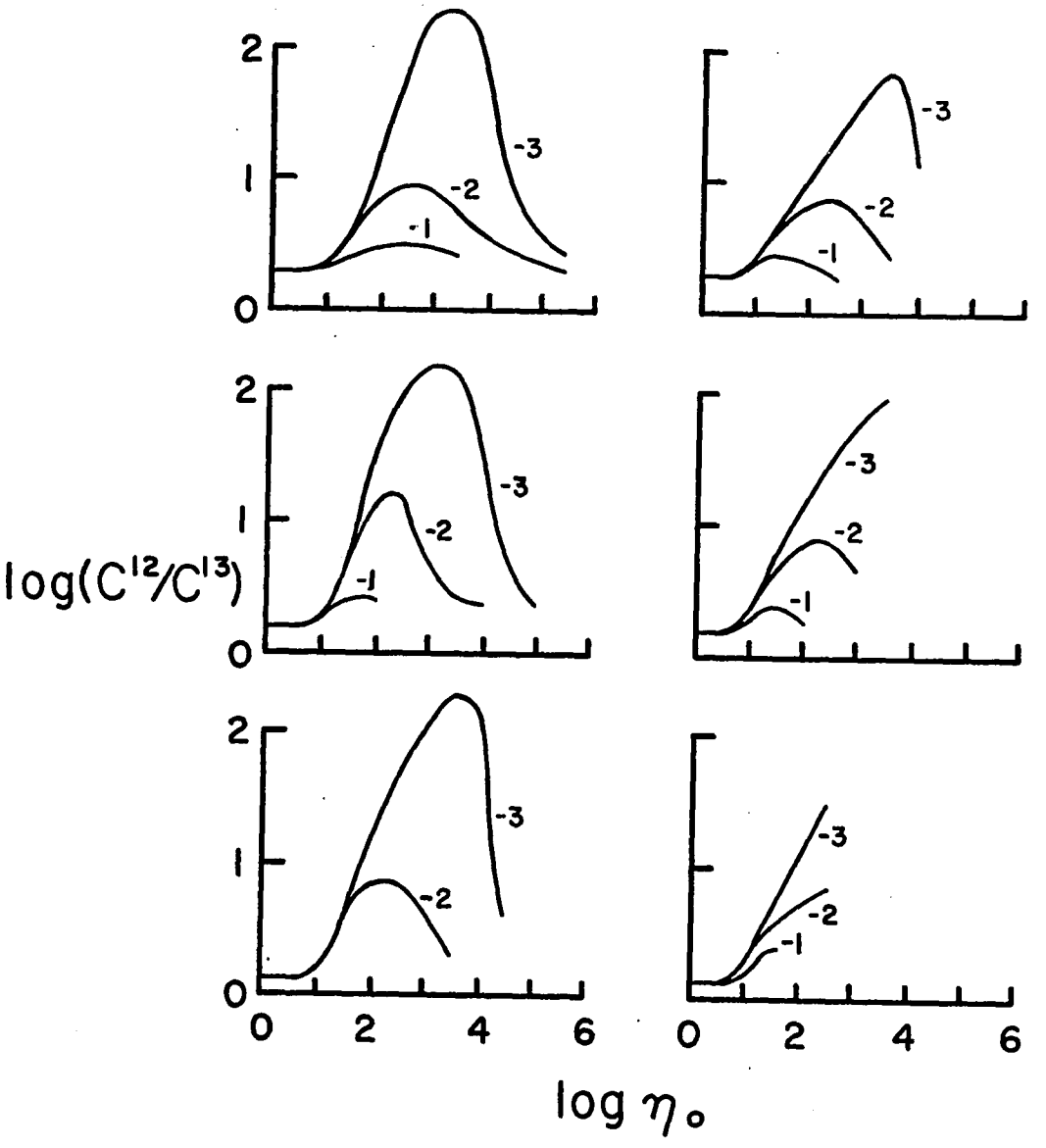

Fig. 23. C^{12}/C^{13} - Log η ; Alpha Bootis.

The curves are labeled with log a. The left column is ξ_t = 0 km/s, the right column is ξ_t = 10 km/s. The top row is T = 2500 K, the middle row is T = 3500 K, the bottom row is T = 4500 K.

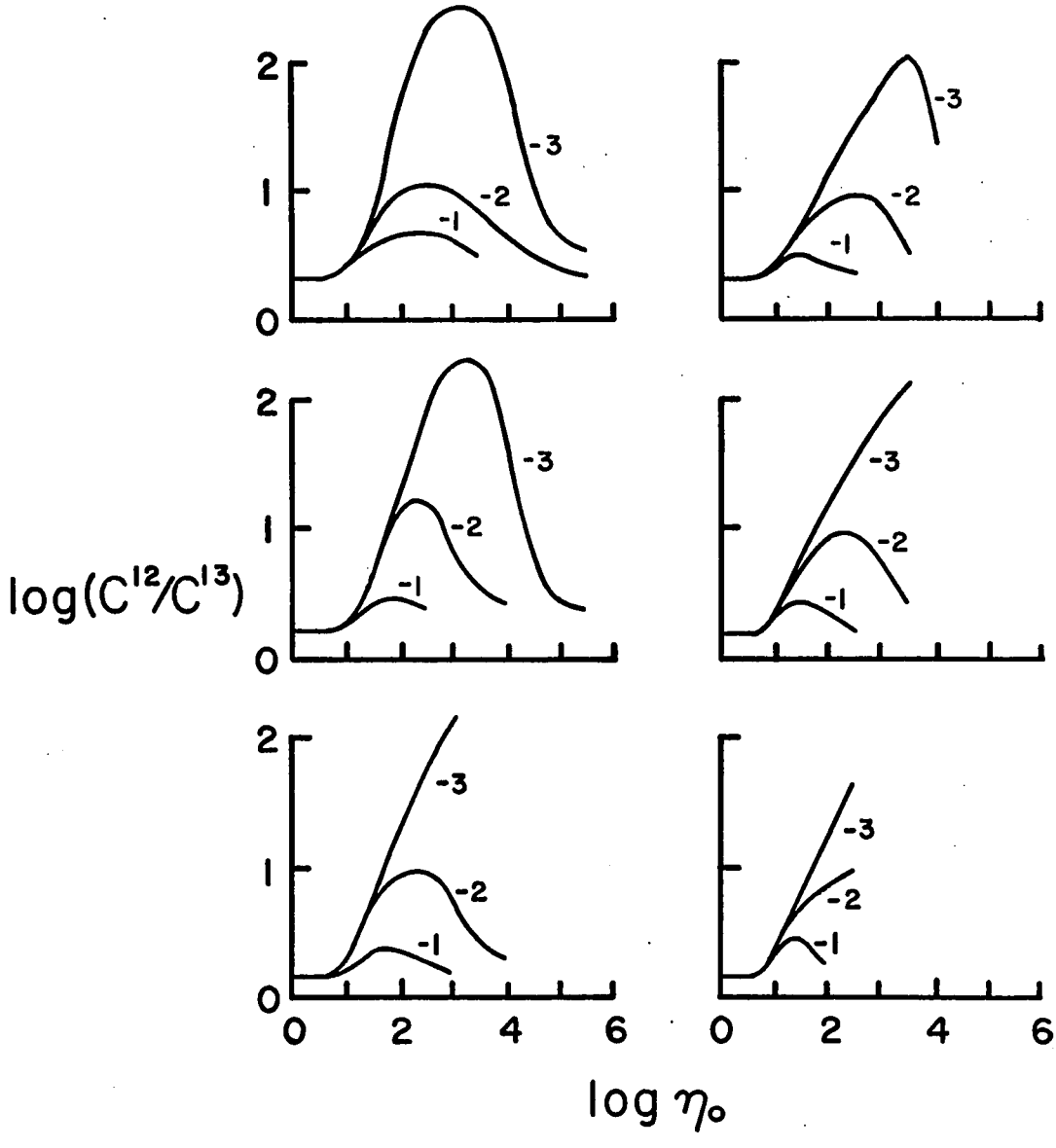

Fig. 24. C^{12}/C^{13} - Log η ; Gamma Draconis and Alpha Scorpii.

See Fig. 23 for explanation of arrangement.

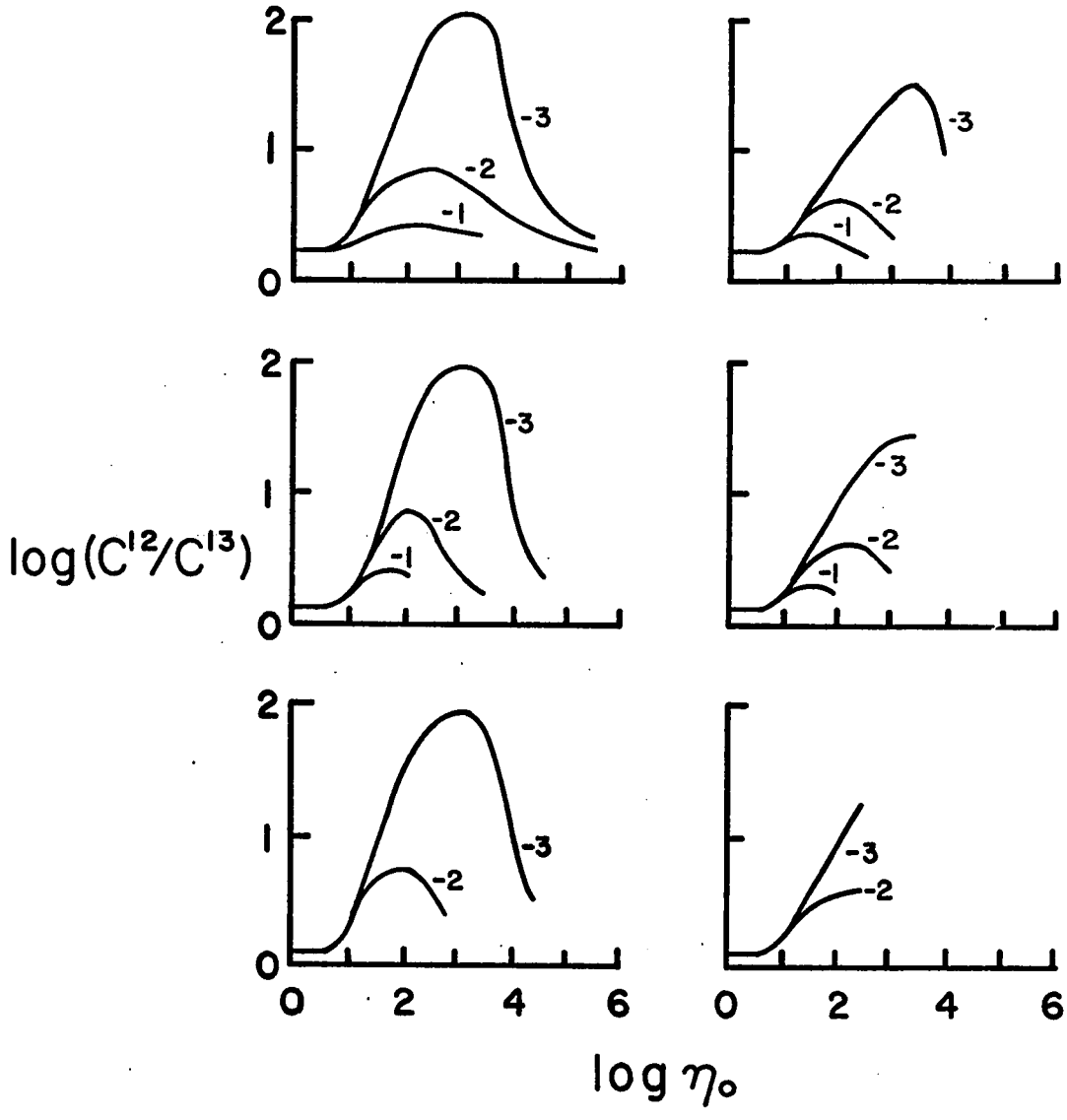

Fig. 25. C^{12}/C^{13} - Log η ; Alpha Tauri

See Fig. 23 for explanation of arrangement.

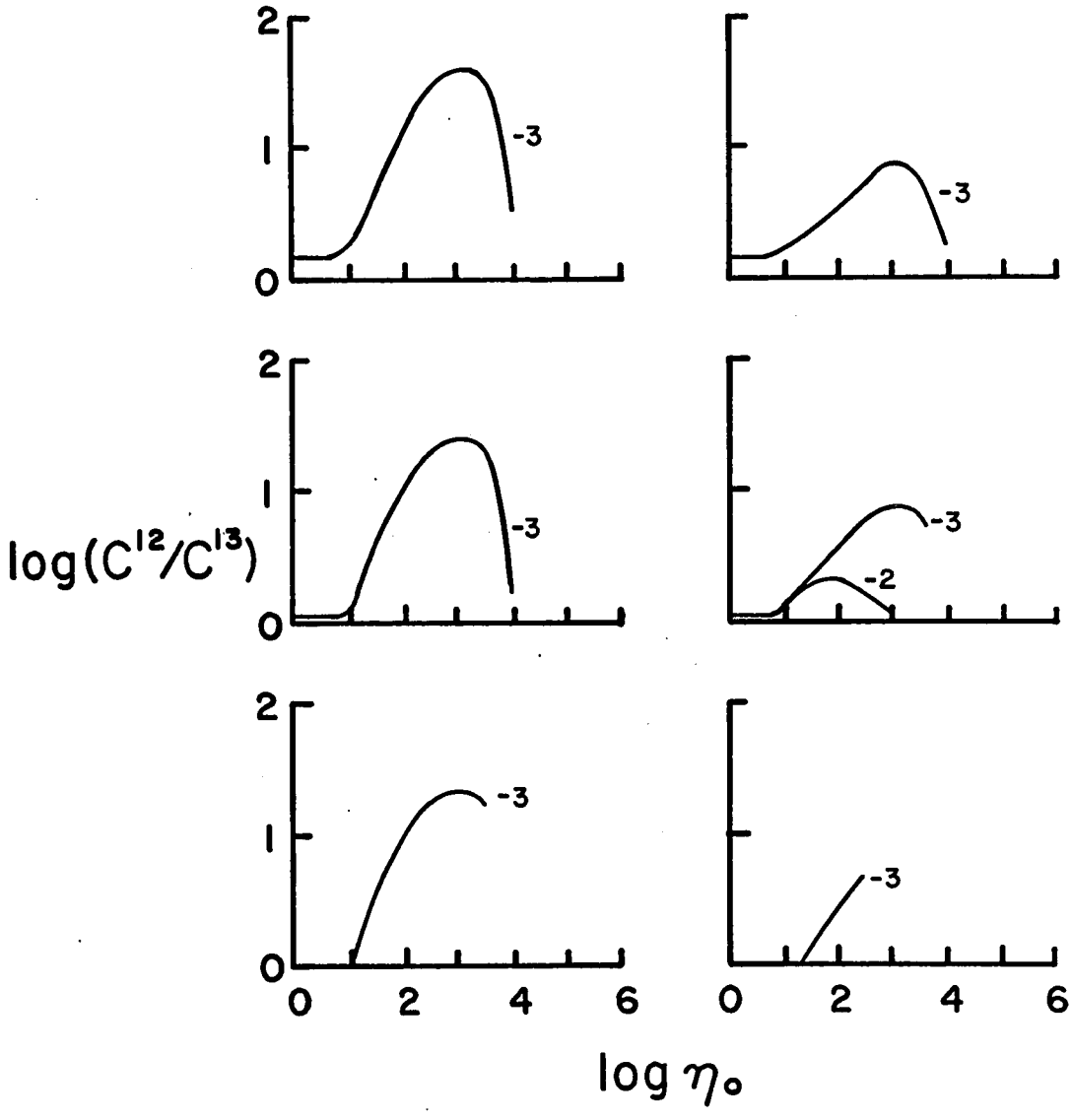

Fig.26. C^{12}/C^{13} - Log η ; Delta Ophiuchi

See Fig. 23 for explanation of arrangement.

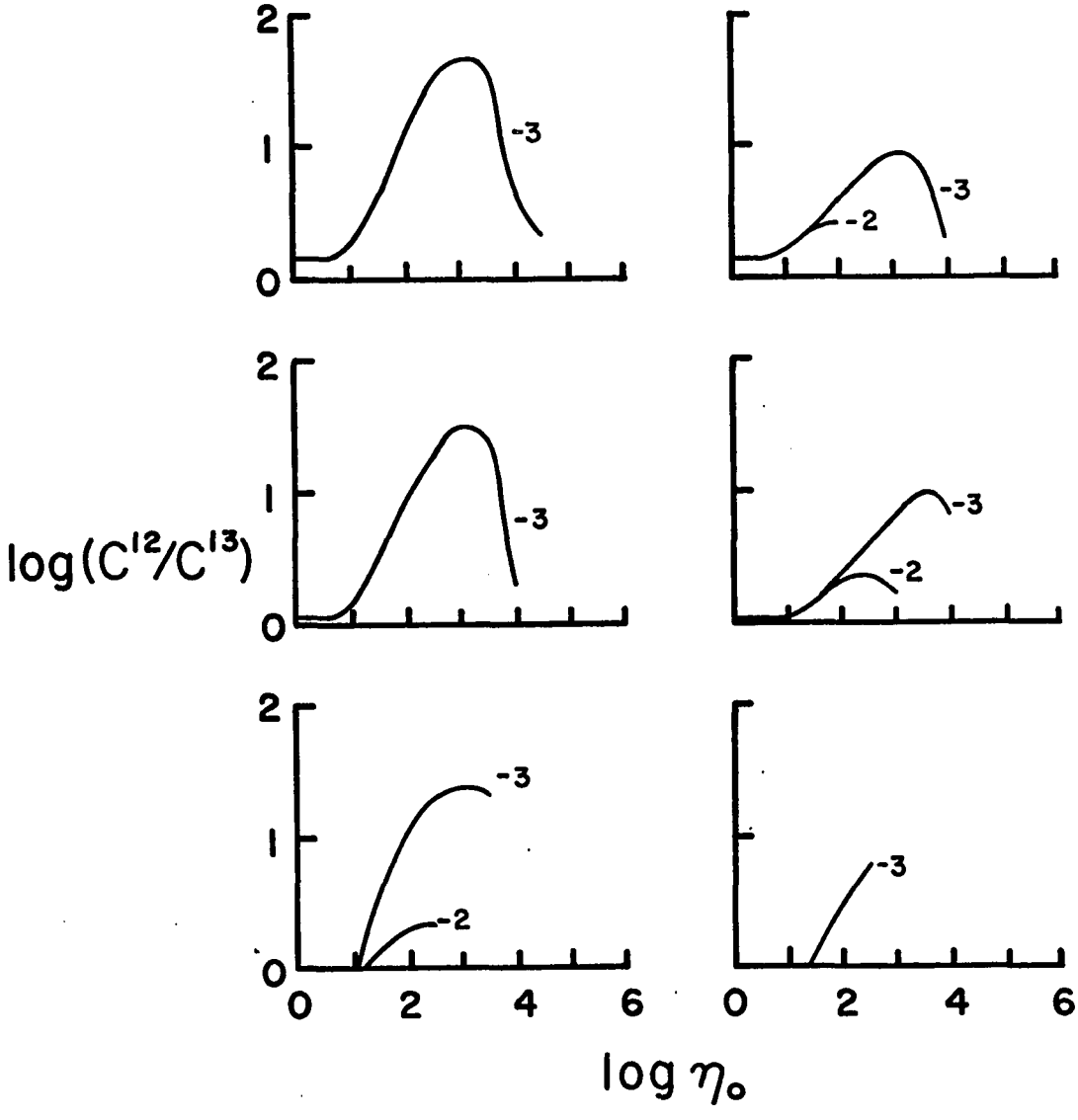

Fig. 27. C^{12}/C^{13} - Log η ; Beta Pegasi.

See Fig. 23 for explanation of arrangement.

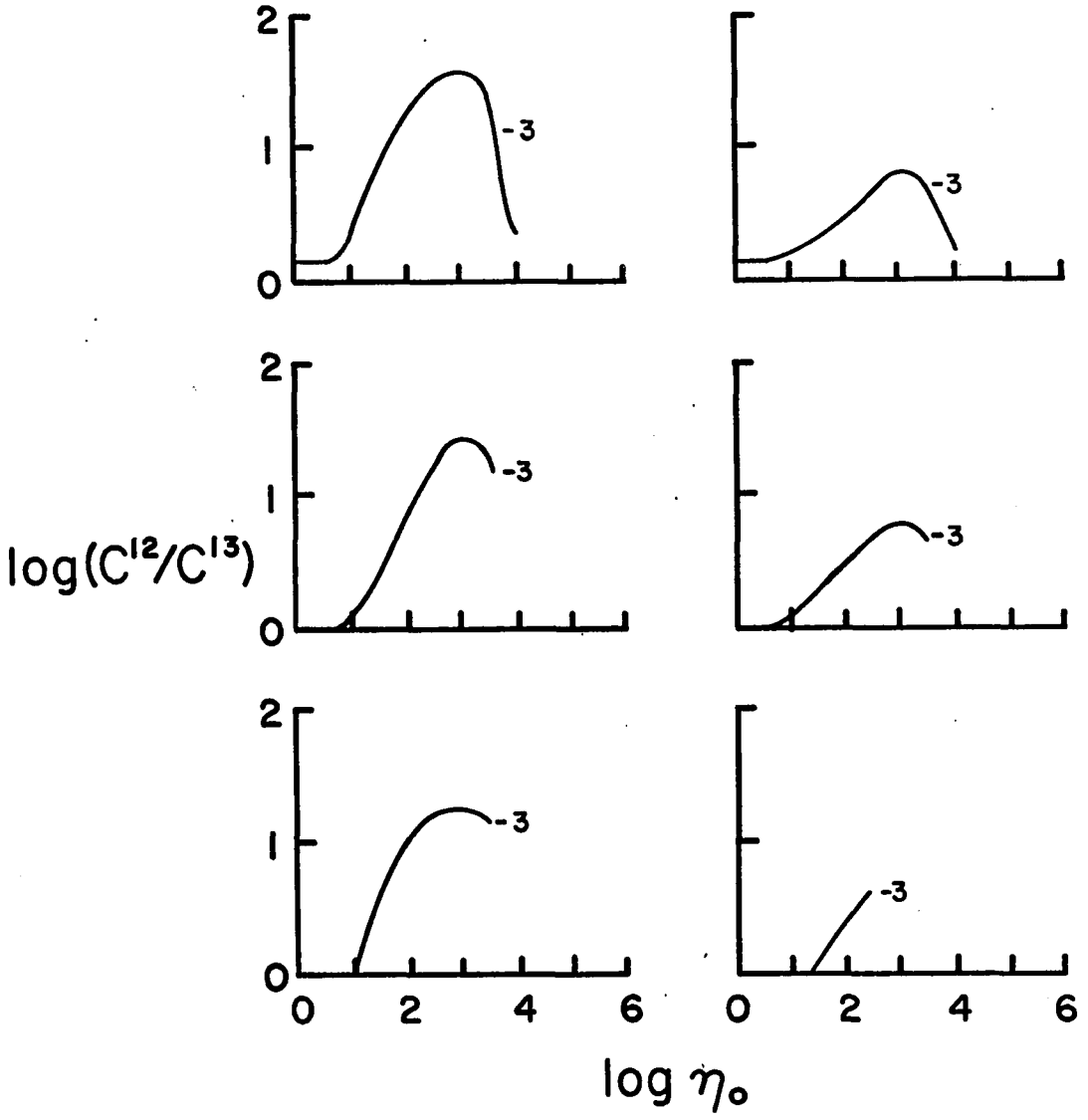

Fig. 28. C^{12}/C^{13} - Log η ; Eta Geminorum

See Fig. 23 for explanation of arrangement.

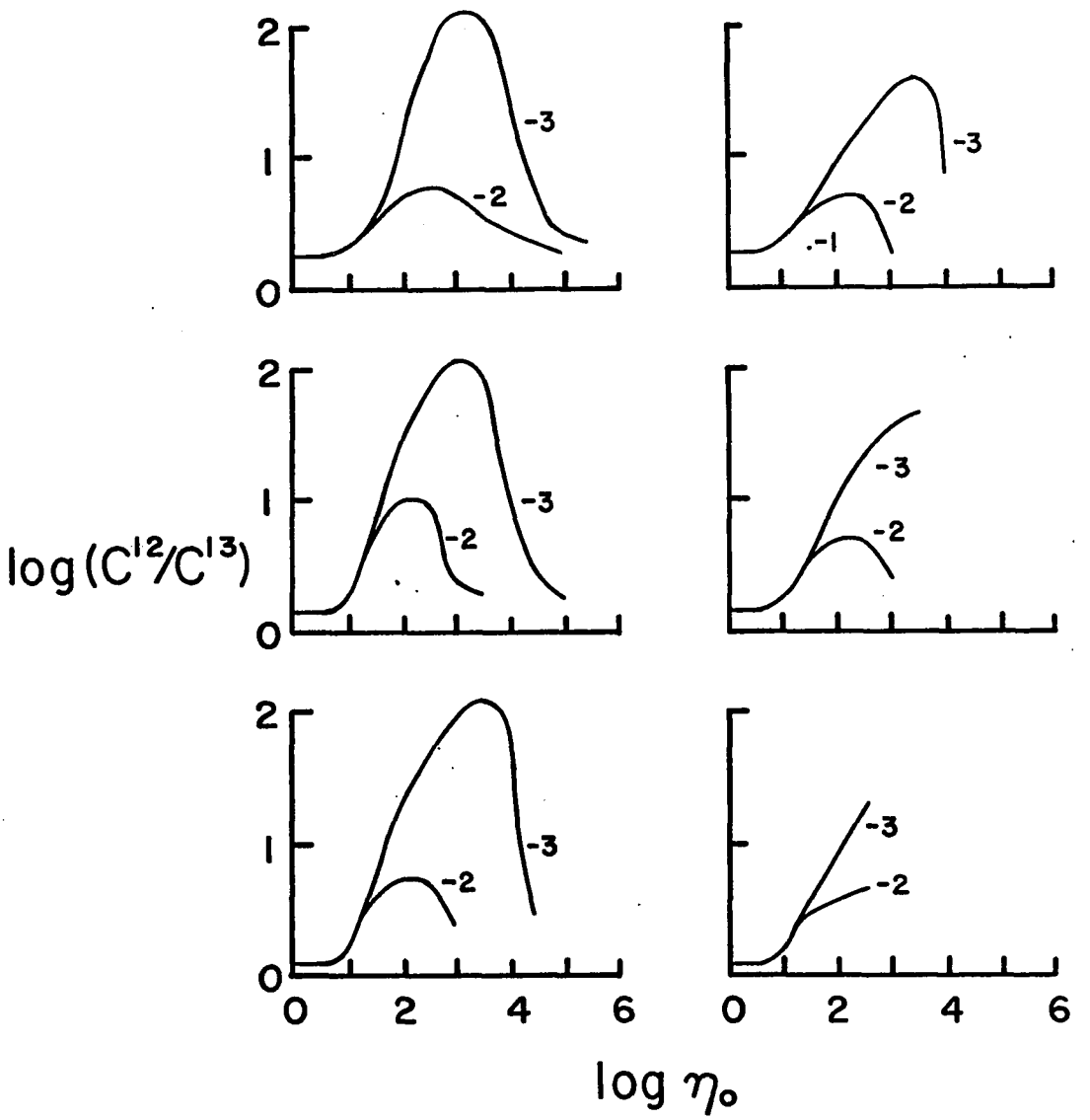

Fig. 29. C^{12}/C^{13} - Log η ; Mu Geminorum

See Fig. 23 for explanation of arrangement.

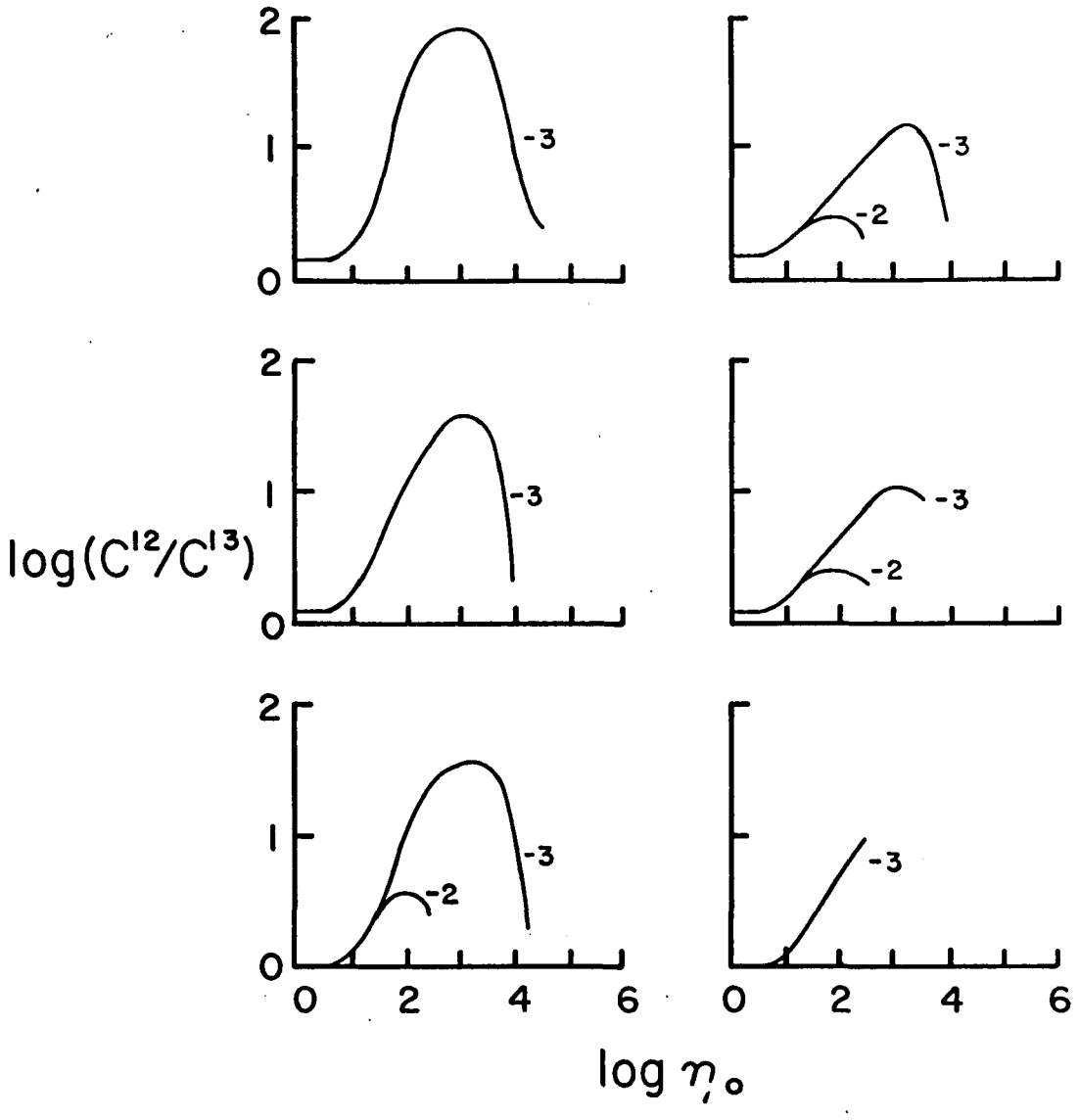

Fig. 30. C^{12}/C^{13} - Log η ; Rho Persei

See Fig. 23 for explanation of arrangement.

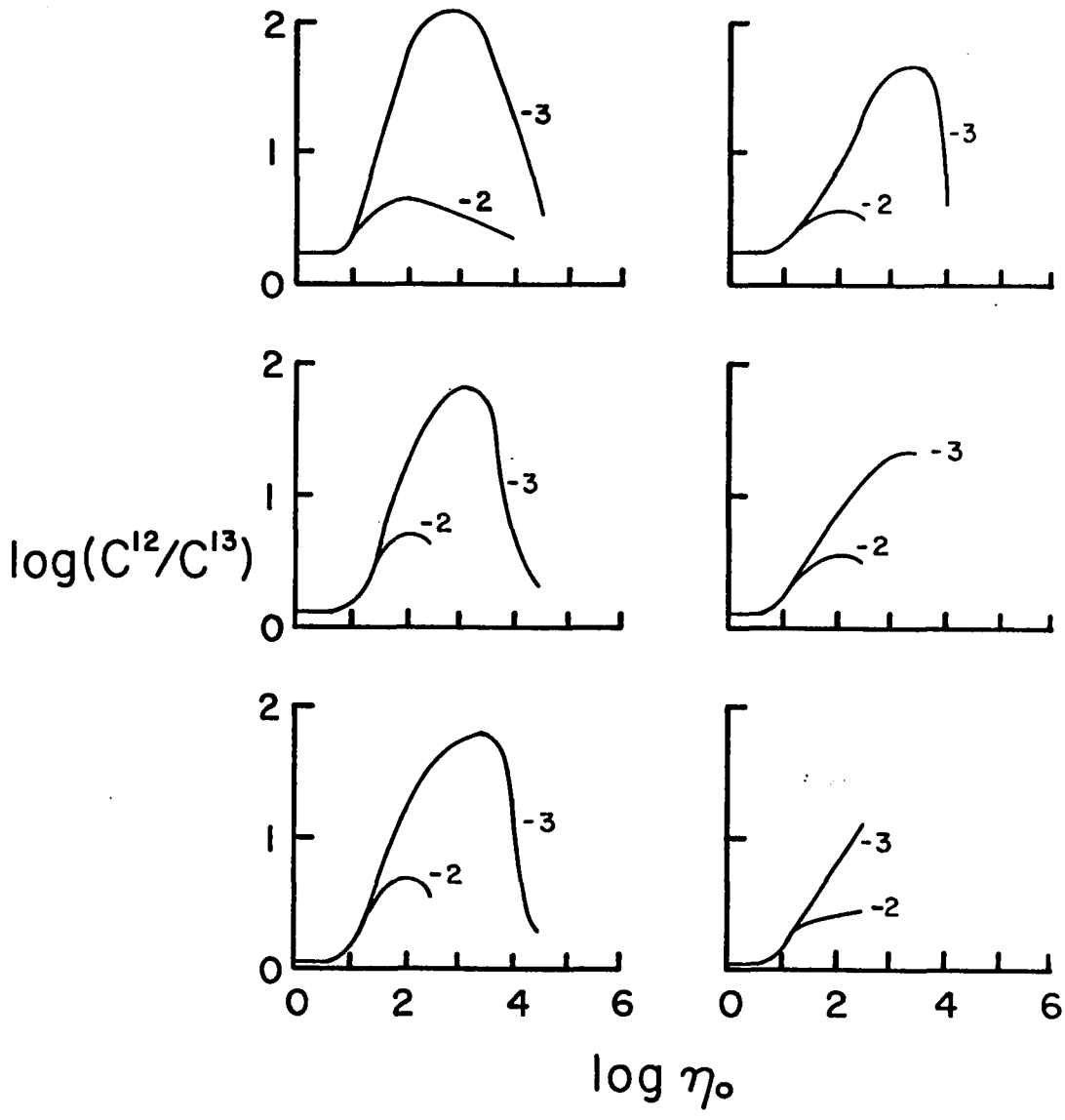

Fig. 31. C^{12}/C^{13} - log η ; R Lyrae

See Fig. 23 for explanation of arrangement.

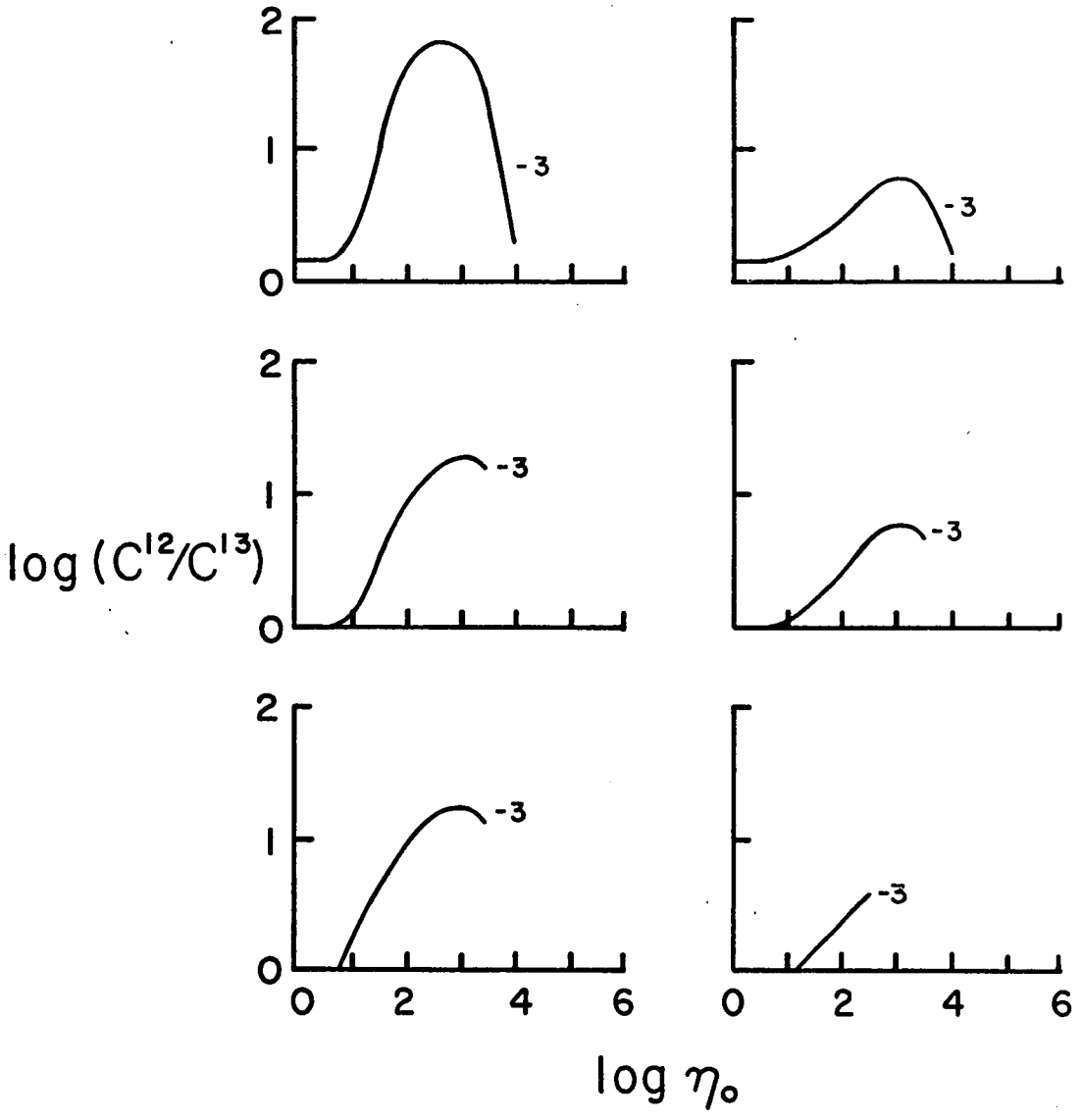

Fig. 32. C^{12}/C^{13} - Log η ; EU Delphini.

See Fig. 23 for explanation of arrangement.

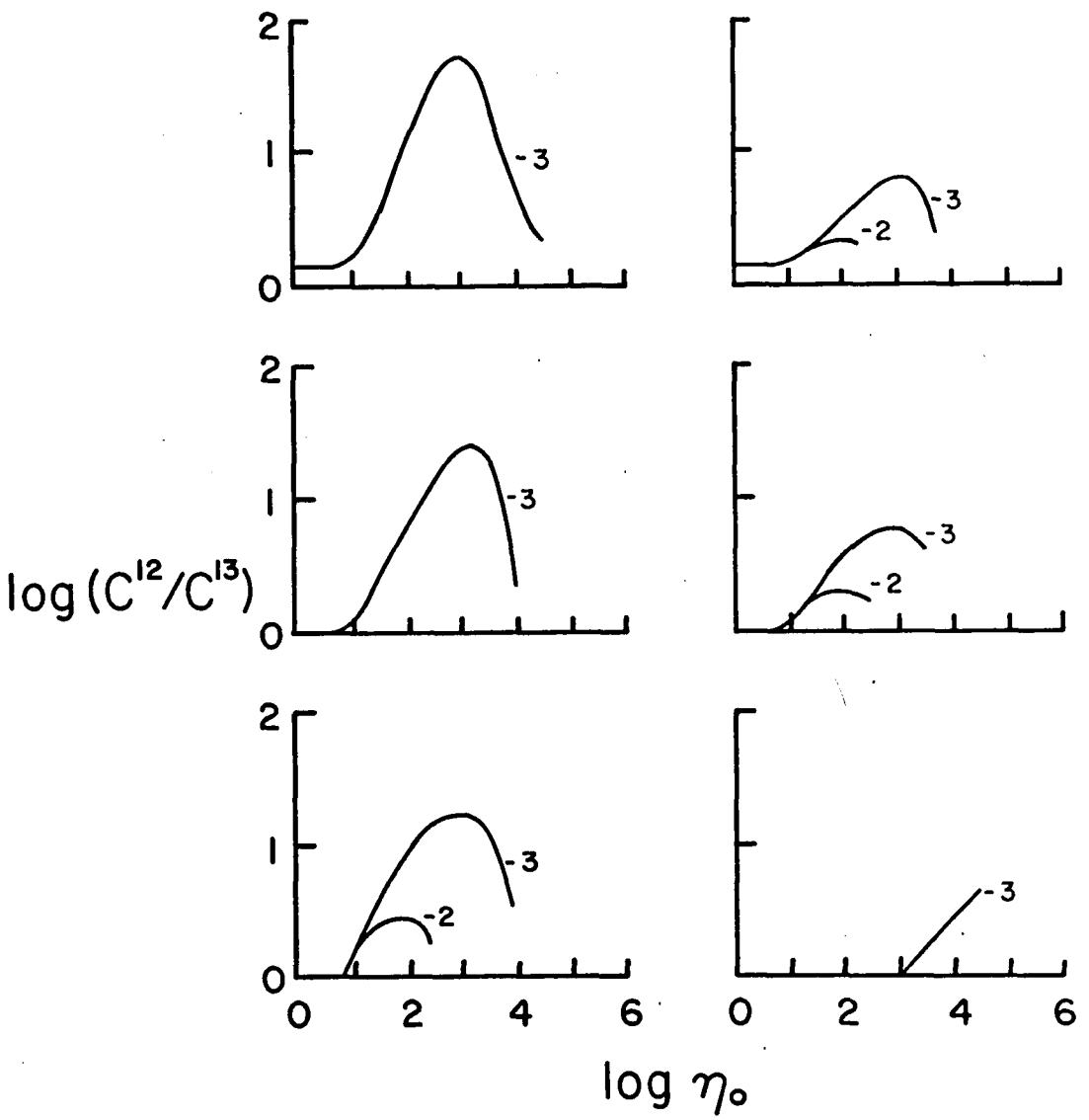

Fig. 33. C^{12}/C^{13} - Log η ; Alpha Orionis

See Fig. 23 for explanation of arrangement.

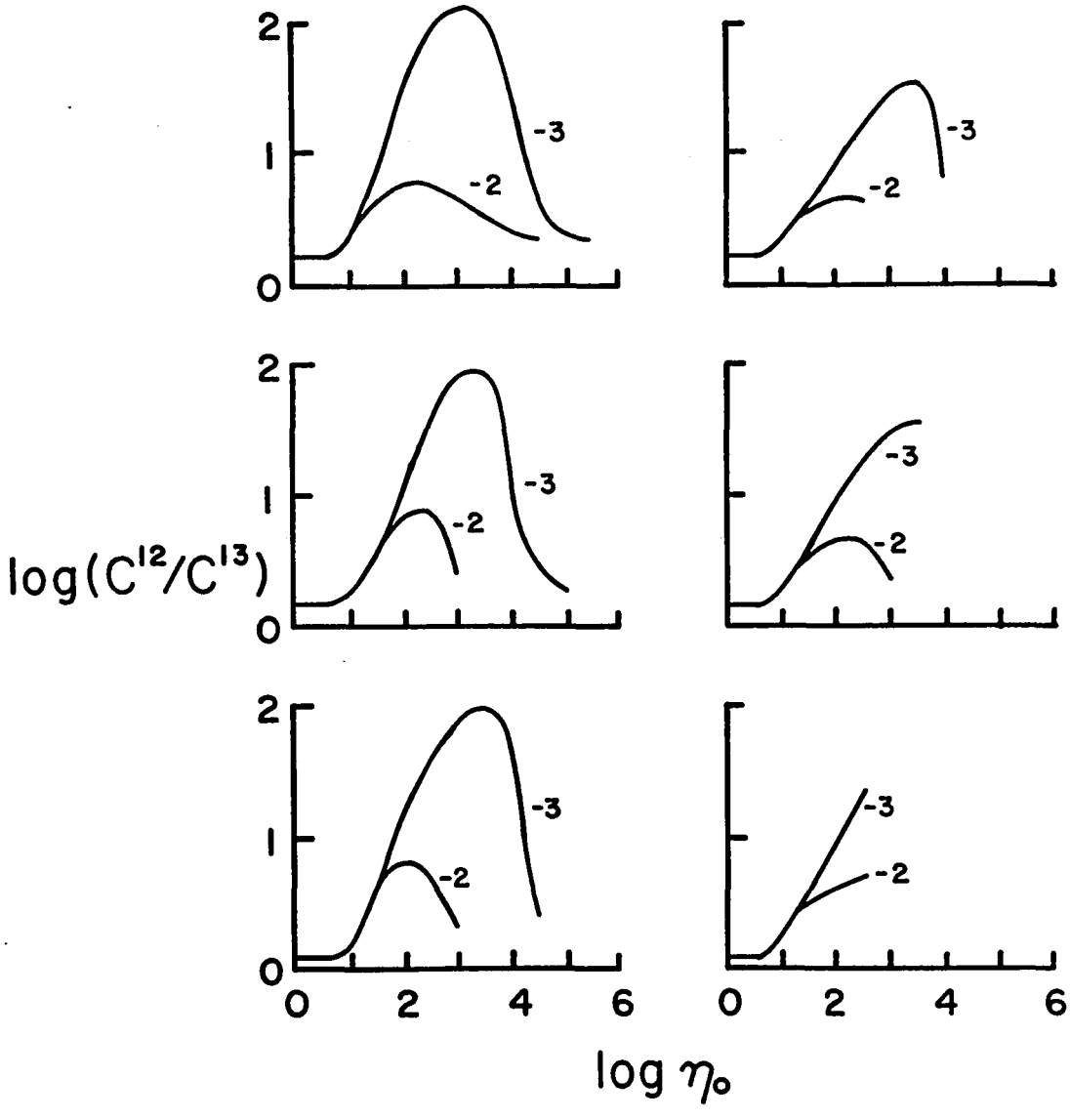

Fig. 34. C^{12}/C^{13} - Log η ; Mu Cephei

See Fig. 23 for explanation of arrangement.

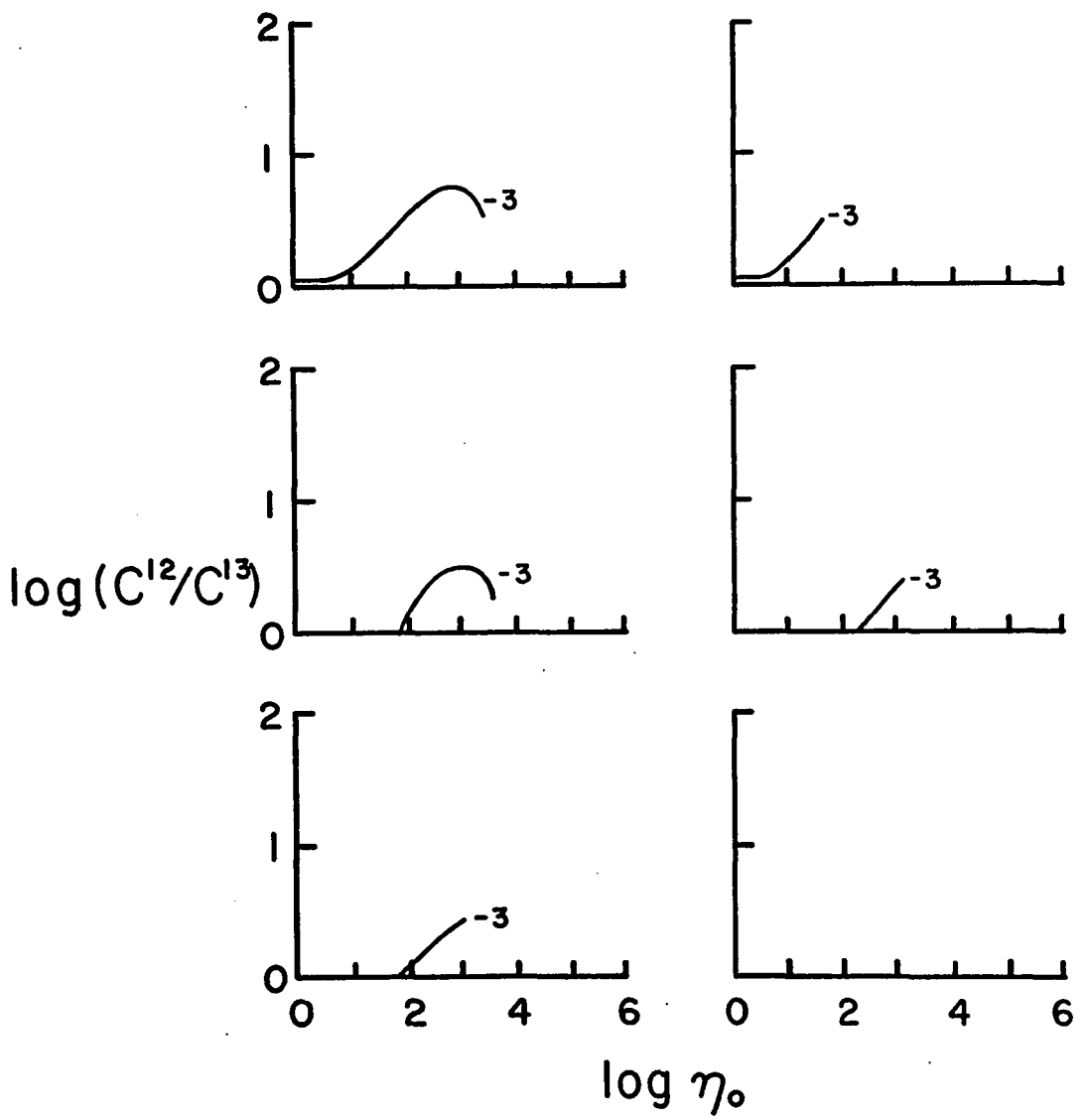

Fig. 35. C^{12}/C^{13} - Log η ; Delta^2 Lyrae

See Fig. 23 for explanation of arrangement.

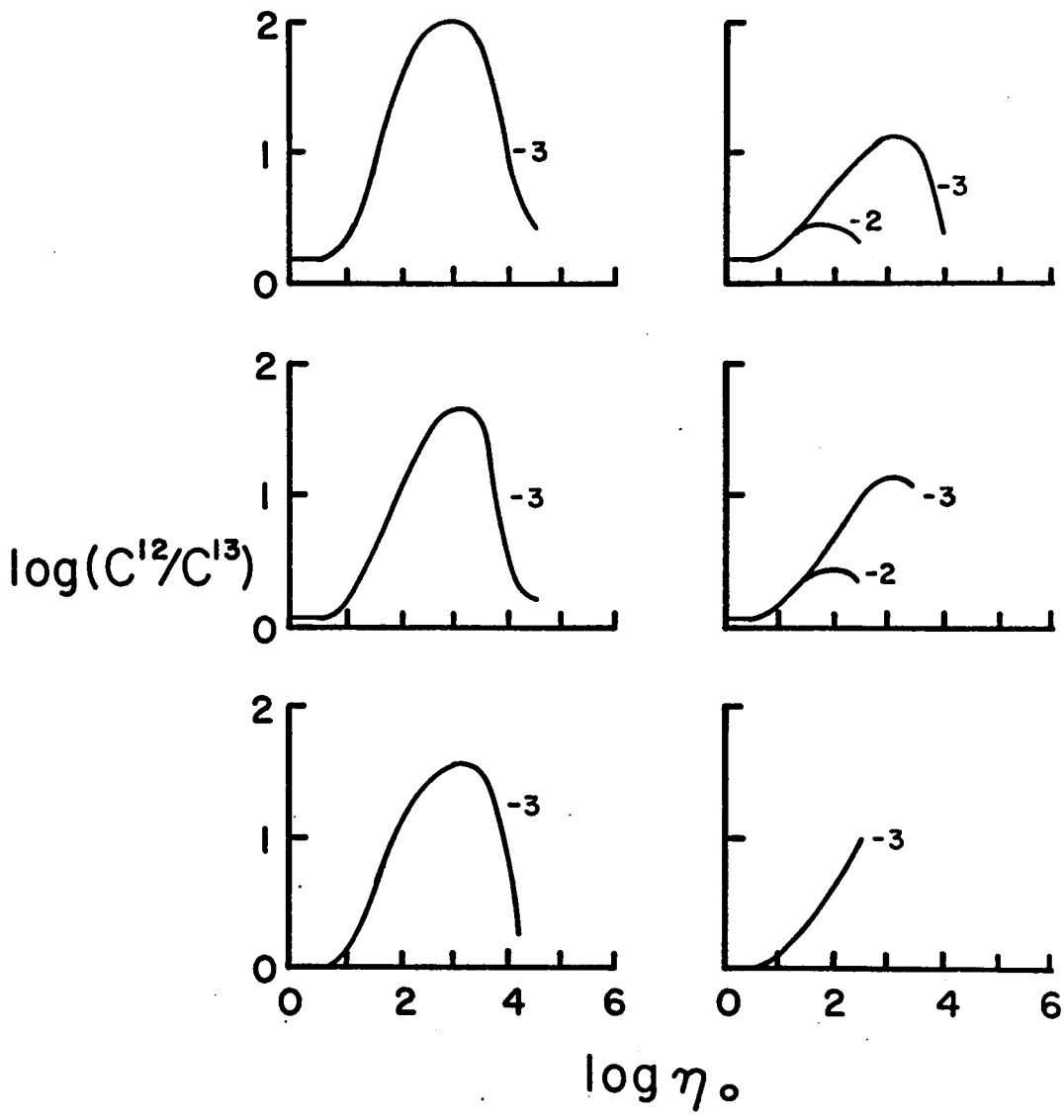

Fig. 36. C^{12}/C^{13} - Log η ; Alpha Herculis.

See Fig. 23 for explanation of arrangement.

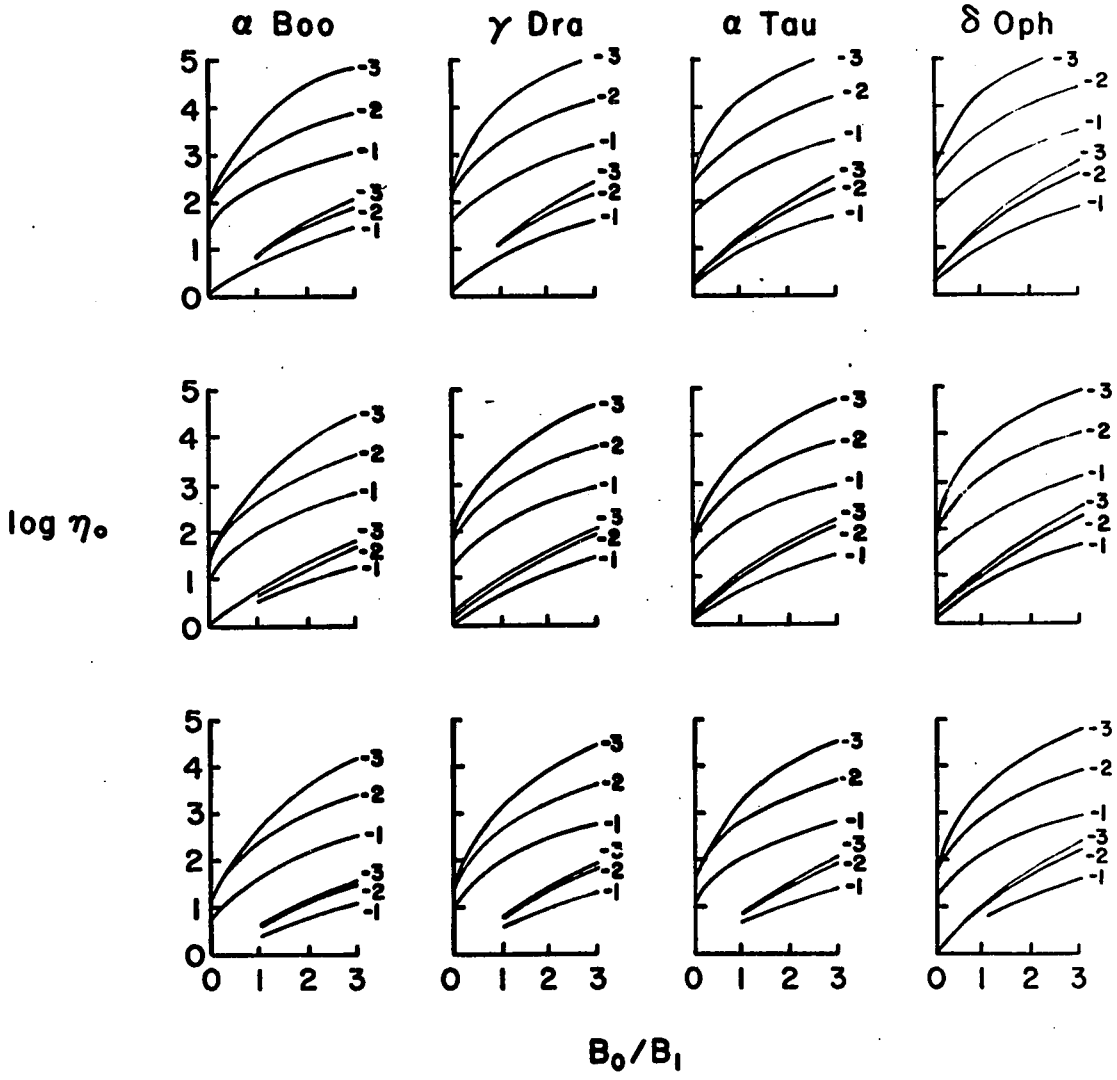

Fig. 37. Log η - B_0/B_1; Alpha Bootis, Gamma Draconis, Alpha Tauri and Delta Ophiuchi

The curves are labeled with log a. The top group of three curves within each frame is $\xi_t = 10$ km/s, the bottom group is $\xi_t = 10$ km/s. The top row is T = 2500 K, the middle row is T = 3500 K, the bottom row is T = 4500 K.

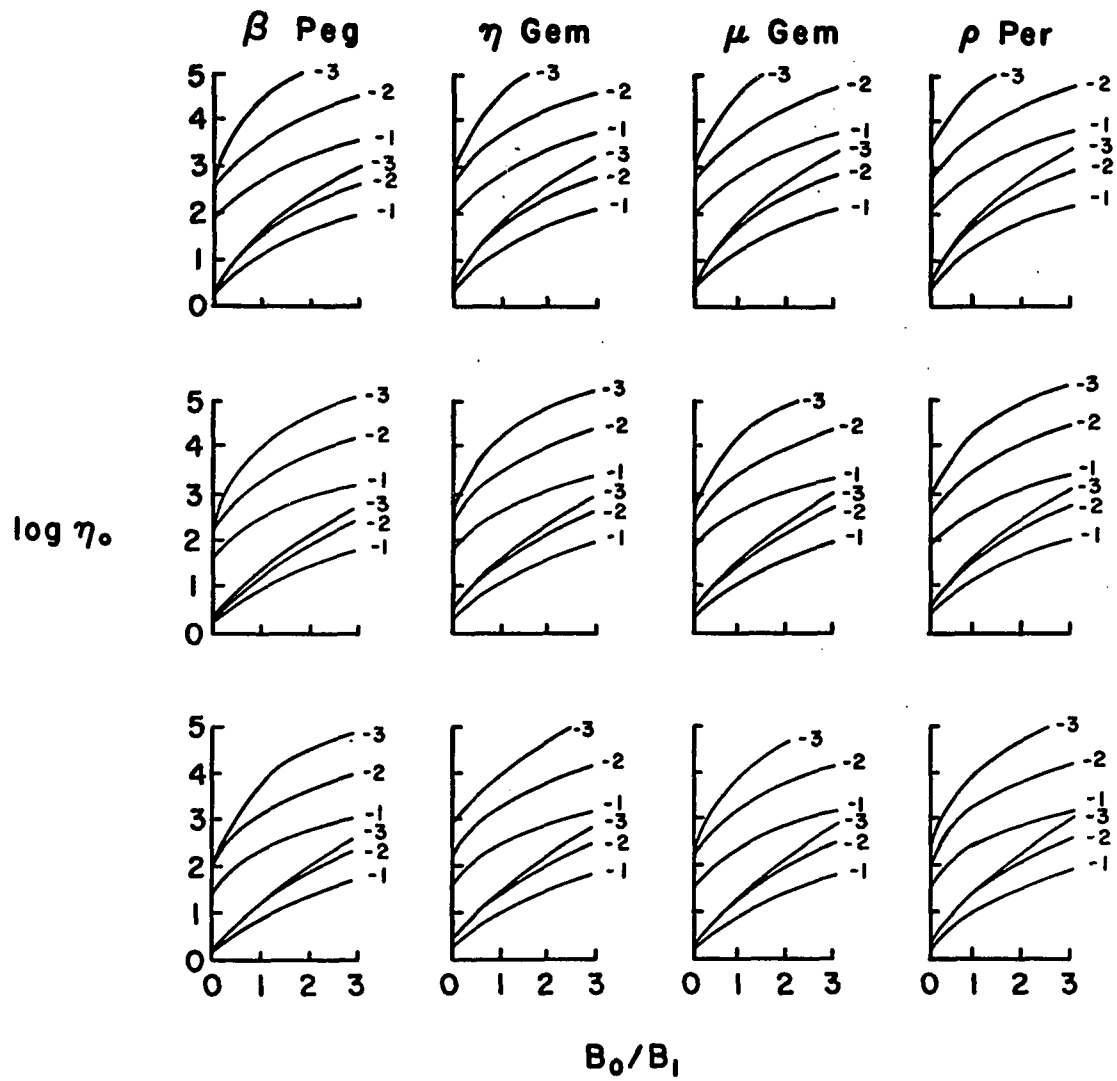

Fig. 38. Log η - B_0/B_1; Beta Pegasi, Eta Geminorum, Mu Geminorum and Rho Persei

See Fig. 37 for explanation of arrangement.

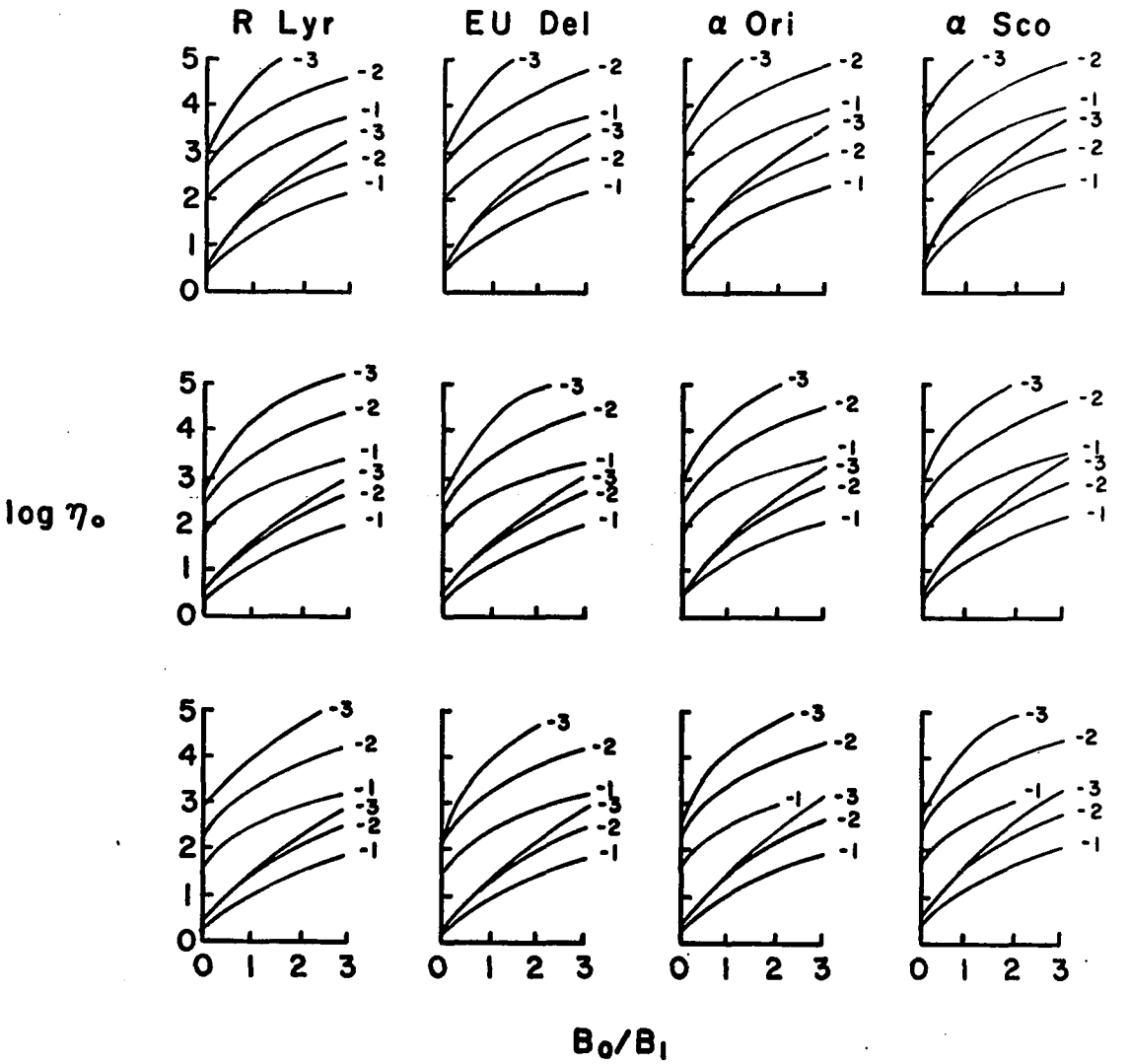

Fig. 39. Log η - B_0/B_1; R Lyrae, EU Delphini, Alpha Orionis and Alpha Scorpii

See Fig. 37 for explanation of arrangement.

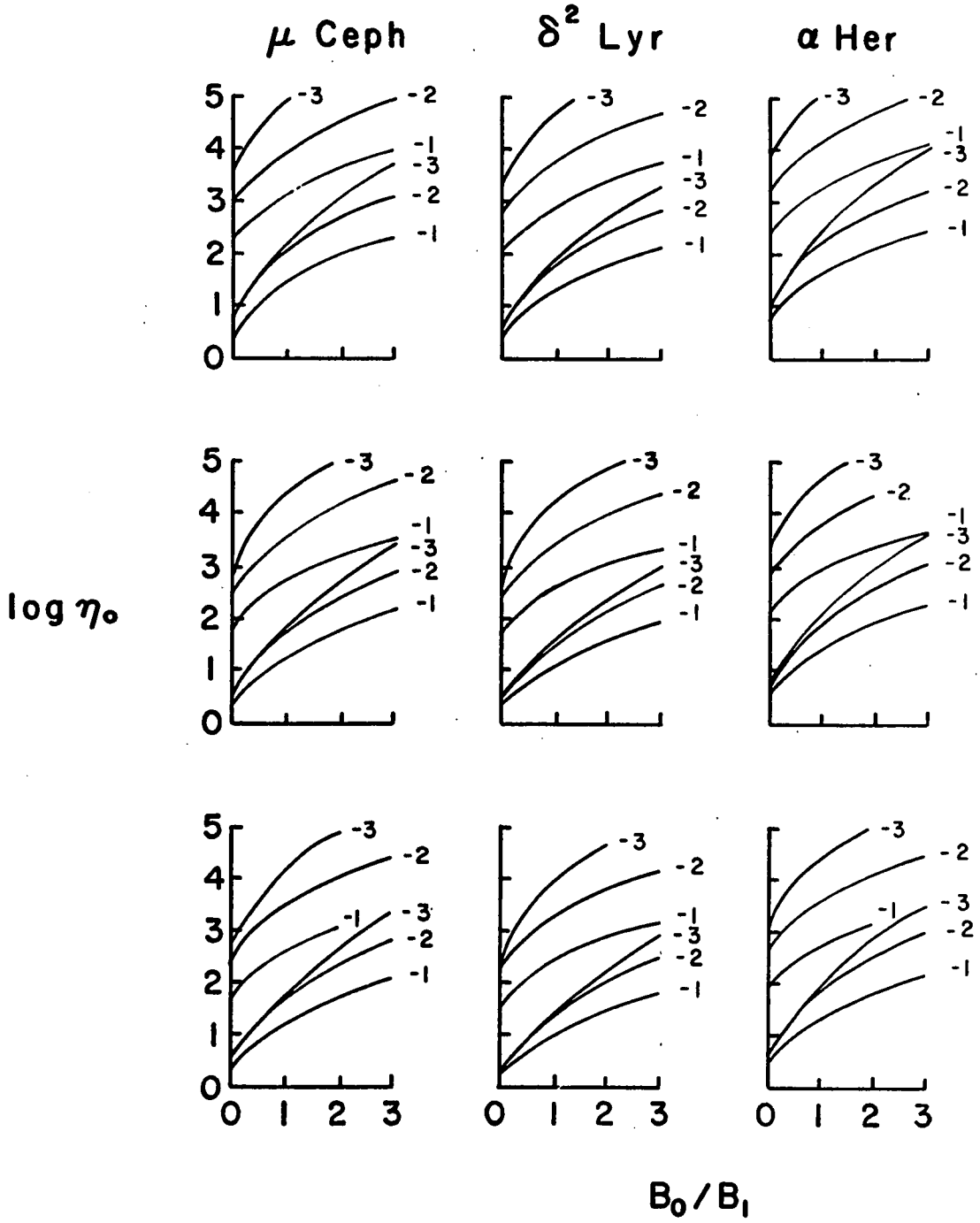

Fig. 40. Log η_0 - B_0/B_1; Mu Cephei, Delta^2 Lyrae and Alpha Herculis

See Fig. 37 for explanation of arrangement.

In principle, B_0/B_1 can be obtained from the temperature structure of a model atmosphere. This approach leaves only three adjustable parameters, T, ξ_t and log a. One problem with this approach is that the temperature must be known as a function of the optical depth at the observed frequency. The temperatures are published as a function of the optical depth at some standard frequency, which is not the observed frequency. When six to ten opacity sources must be included, the conversion is difficult without recalculating the entire model atmosphere. In practice, therefore, better results are obtained by allowing log η to also be determined by the band profile and only using B_0/B_1 to check the consistency of the results with the models.

The models used in this investigation are those published by Auman (1969). These models are not necessarily better than those published by Gingerich et al. (1967) and Carbon and Gingerich (1969); the water vapor opacity included by Auman in his models is certainly overestimated for the stars investigated here. However, the temperature structure of the model is the only information needed to determine B_0/B_1. This does not differ appreciably between the models by Auman and those by Gingerich and co-workers. Also, Auman's models cover the spectral type and luminosity range of interest. The published models by Gingerich and co-workers do not include any between 4000 K and 2500 K. For consistency, Auman's models are used throughout this investigation.

The Isotope Ratio Analysis

Determination of the C^{12}/C^{13} ratio requires measurement of the equivalent widths of two spectral features; one which is sensitive to $C^{13}O^{16}$ abundance and one which is only sensitive to $C^{12}O^{16}$ abundance. The features measured are the $C^{13}O^{16}$ (2-0) band head and the $C^{12}O^{16}$ (3-0) band head. The reasons for this choice were discussed in Chapter 2. The ratio of the measured equivalent widths (W^{13}/W^{12}) is listed in Table 3.

The C^{12}/C^{13} ratio depends strongly on the two parameters log n and log a. It is a much weaker function of T and ξ_t. The values of T, ξ_t, log a and log n listed in Table 4 were used to determine the C^{13}/C^{12} ratio.

Results

The analyses of individual stars are described below with a discussion of the reasons for the final choice of parameters and of the range of parameters that will produce an acceptable fit to the stellar band profiles. The final results are presented in Table 4.

The effective temperatures given in Table 4 are taken from Mendoza (1969) or Johnson (1966). Johnson gives a table of spectral type versus effective temperature which was used to obtain effective temperatures for those stars for which direct determinations have not been obtained.

Table 3. Measured Equivalent Widths of CO $\Delta v = 2$ Band Sequence and the Ratio of the $C^{13}O^{16}$ and $C^{12}O^{16}$ Band Heads

Star	W_ν (cm^{-1})	W^{13}/W^{12}
Alpha Bootis	39	0.45
Gamma Draconis	47	.43
Alpha Tauri	51	.51
Alpha Tauri	54	.45
Delta Ophiuchi	62	.54
Beta Pegasi	70	.65
Beta Pegasi	66	.54
Eta Geminorum	74	.55
Mu Geminorum	77	.47
Rho Persei	81	.52
R Lyrae	68	.49
R Lyrae	69	.50
R Lyrae	74	.53
EU Delphini	78	.55
Alpha Orionis	87	.57
Alpha Orionis	112	.52
Alpha Scorpii	95	.43
Mu Cephei	112	.49
Mu Cephei	94	.48
Mu Cephei	94	.47
Delta^2 Lyrae	80	.62
Alpha Herculis	107	.52
Alpha Herculis	92	0.62

Table 4. Stellar Results

Star	T_{eff}	T	ξ_t	B_0/B_1	log a	log η	C^{12}/C^{13}	Spectral Type
α Boo	4250	4000	8	1.7	-2	1.8	5	K2 IIIp
ν Dra	3860	4000	10	2.1	<-3	2.0	14	K5 III
α Tau	3860	4000	8	1.7	-3	1.9	20	K5 III
δ Oph	3630	3500	6	1.3	-3	2.3	8	MO.5 III
β Peg	3130	3000	6	1.0	-3	2.5	8	M2-3 II-III
η Gem	3300	3200	8	1.1	-3	3.0	10	M3 III
μ Gem	3300	3200	6	1.0	-2.5	2.8	20	M3 III
ρ Per	3300	3200	6	1.0	-2.5	2.8	15	M3 II-III
R Lyr	2950	3000	9	1.3	-3	2.0	5.5	M5 III SR
EU Del	2800	3000	9	1.3	-3	2.0	3.5	M6 III SR
α Ori	3790	3500	10	1.5	-3	2.5	5.0	M1-2 Iab
α Sco	3520	3200	8	1.6	-2	2.5	10	M1-2 Iab
μ Ceph	3500	3200	8	1.3	-2.3	2.7	10	M2 Ia
δ^2 Dyr	3100	3000	6	1.5	-3	3.0	3.5	M4 II
α Her	3400	3500	6	1.2	-3	3.0	9	M5 Ib-II

Alpha Bootis

This is the earliest spectral type (K2 IIIp) as well as the only metal poor star included in this investigation. High resolution infra-red spectra of Arcturus have been obtained (Montgomery et al. 1969) and the CO bands analyzed (Greene 1970). Greene finds, using the infra-red CO $\Delta v = 2$ bands, $C^{12}/C^{13} \approx 4$, but using the CN red system electronic bands in the photographic infra-red yields $C^{12}/C^{13} \approx 10$.

Mendoza (1969) gives the effective temperature (T_{eff}) of α Boo as 4250 K. The surface gravity is given by Allen (1963) as log g = 2.3.

Figure 23 gives the C^{12}/C^{13} ratio as a function of abundance. Figure 37 shows abundance as a function of B_0/B_1. Four parameters affect the band profile; T, ξ_t, log a and log η . Temperatures less than 3500 K and log a = -1 can be eliminated immediately. In both of these cases, no satisfactory fit to the observed profile can be obtained. If T = 3500 K, the best match to the observed profile is obtained with $\xi_t \approx 6$-10 km/s, log η = 1.7, log a = -2. The difference between log a = -2 and -3 is small, but log a = -2 provides a slightly better match. If T = 4500 K, then ξ_t = 6-10 km/s, log η = 1.8 and log a = -2. Temperature does not affect the adopted values of ξ_t, log a and log η significantly. On the basis of the profile, the acceptable temperature range is $3700\ K \lesssim T \lesssim 4200\ K$. These parameters imply $C^{12}/C^{13} \approx 5$, almost independent of T and log η over the ranges specified above. For log η

a = -2, the extremes are $4.0 \lesssim C^{12}/C^{13} \lesssim 7$. If log a = -3 however, the best value changes to $C^{12}/C^{13} = 11$ with a range of 8 to 14.

$B_0/B_1 \approx 1.5 - 2.0$ from Figure 37. Auman's (1969) model with T = 3500 K, log g = 2.0 yields $B_0/B_1 = 1.9$. This is satisfactory agreement.

Gamma Draconis

This star and the next (αTau) both have the same spectral type, K5 III, but the structure of the CO bands differs in the two stars. There are five strong band heads visible in γ Dra then a sudden break occurs in the band head strengths. The sixth, seventh and eighth band heads are nearly invisible. The break occurs after the sixth band head in αTau and is not as pronounced as in γ Dra. The higher band heads are still visible. None of the synthetic spectra show a break in band head strength after only five strong band heads although a break after six band heads is a common feature of spectra with log η in the range 2.5-4.5 for temperatures of 2500 K, 3500 K, and 4500 K. Possibly a lower temperature would move the break to lower band heads but it seems unlikely since a range of 2000 K has no noticable affect on its position.

The C^{12}/C^{13} ratio and log η are shown as functions of all parameters in Figures 24 and 37 respectively. Two conflicting factors make the choice of the best fit parameters difficult; the small number of visible band heads and the small general depression of the continuum.

If the parameters are adjusted to produce the proper general depression, all band heads are strong. If the break in the band strengths is produced, the general depression is 2 or 3 times too strong. The three best compromises were

T = 2500 K	log a = -3	ξ_t = 8-10 km/s	log η = 2.0
3500 K	-3	8-10 km/s	2.0
4500 K	-3	8-10 km/s	2.0

The best fit to the profile is obtained with T = 2500 K, but this is considered unrealistic in view of the spectral type. The general depression is sensitive to the damping constant at this value of log η, so log a < -3 would improve the fit at the higher temperatures. A lower damping constant requires an increase in log η to provide the same equivalent width, but this change should not be very large since log η = 2.0 is still primarily on the flat portion of the curve of growth for log a = -3. The C^{12}/C^{13} ratio would probably not be affected at all, since the features used for its determination are even further down on the curve of growth.

The effective temperature has not been directly determined for ν Dra. The spectral type and colors are similar to α Tau, however, so we will adopt T_{eff} = 3860 K. Surface gravity of a K5 giant is given by Allen (1963) as log g = 2.1.

The C^{12}/C^{13} ratio is nearly independent of temperature over the range 3500 K-4500 K, changing from 14 at 3500 K to 15 at 4500 K. On

the basis of the effective temperature, $C^{12}/C^{13} = 14$ and log a ≤ -3 were adopted.

From Figure 37, $B_0/B_1 \approx 1.8 - 2.3$ which is somewhat higher than the value 1.9 obtained from Auman's (1969) model with T = 3500 K, log g = 2.0, but is still reasonable.

Alpha Tauri

Two independent spectra of α Tau (K5 III) are available, one taken with a refrigerated detector, the second with an unrefrigerated detector. The second spectrum is slightly noisier than the first, but both are satisfactory for analysis of the CO bands. Mendoza (1969) lists the effective temperature as 3860 K. Allen (1963) gives the surface gravity of a K5 giant as log g = 2.1. The C^{12}/C^{13} ratio and log η are shown as a function of all parameters in Figures 25 and 37 respectively.

The best fit to the profile is obtained with

$T \approx 4000$ K, $\xi_t = 6$-10 km/s, log η = 1.9, log a = -3

At 4500 K, either log a = -2 or -3 provide equally good profiles, but at 3500 K, log a = -3 definitely provides a better fit. From Figure 37, these values give $B_0/B_1 \approx 1.5$-2.0. This is satisfactory agreement with Auman's (1969) model with T = 3500 K, log g = 2.0.

Each spectrum was analyzed separately and the results combined into an average in Table 4. The first spectrum indicated $C^{12}/C^{13} = 48$. The second spectrum gave $C^{12}/C^{13} = 10$.

Delta Ophiuchi

The effective temperature of an MO.5 III star, as obtained from Johnson (1966) is 3630 K. The surface gravity is given by Allen (1963) as log g = 1.7. The C^{12}/C^{13} ratio and log η are shown in Figures 26 and 37 respectively, as a function of all parmaters.

The best fit to the profile is obtained with

T = 3500 K, log a = -3, ξ_t = 3-6 km/s, log η = 2.3

This leads to $C^{12}/C^{13} = 8$, $B_0/B_1 = 1.4$. Compared to Auman's (1969) T = 3500 K, log g = 1.5 model, B_0/B_1 is satisfactory. Auman's model gives $B_0/B_1 = 1.5$.

The profile is not very sensitive to changes in the damping constant over the range log a = -2 to -3. We can, however, eliminate log a = -2. Intermediate values as large as log a = -2.5 can not be eliminated.

Temperatures from 3200 K to 3600 K produce a satisfactory fit to the profile. The C^{12}/C^{13} ratio is almost constant over this range of temperatures, varying from 7.9 to 8.5.

The range of the C^{12}/C^{13} ratio is from 4 to 10. The abundance is between log η = 2.0 and log η = 2.5.

Beta Pegasi

Two spectra of βPeg are available. These were analyzed separately and the results combined to produce the average parameters

discussed below. The effective temperature of β Peg is given by Mendoza as 3130 K. The C^{12}/C^{13} ratio and log η are shown as functions of all parameters in Figures 27 and 38.

The best fit to the band profile is obtained with

$T = 3000$ K, $\xi_t = 5$ km/s, log $a = -3$, log $\eta = 2.5$

These values lead to $C^{12}/C^{13} = 8$, $B_0/B_1 = 1.0$

Auman's (1969) $T = 3000$ K, log $g = 1.0$ model gives $B_0/B_1 = 1.1$. This is satisfactory agreement.

Both β Peg spectra are good quality and the profiles are reproduced very well by the parameters listed above. Therefore, the values are not likely to be in error by a significant amount. The possible range of C^{12}/C^{13} is from 5 to 12.

Eta Geminorum

The spectrum of ηGem is noisier than those previously discussed. Johnson (1966) gives the effective temperature of an M3 giant as 3300 K. The C^{12}/C^{13} ratio and log η are shown in Figures 28 and 38 as functions of all parameters.

The best fit to the profile is obtained with

$T = 3200$ K, $\xi_t = 8$ km/s, log $a = -3$, log $\eta = 3.0$

These lead to $C^{12}/C^{13} = 10$ and $B_0/B_1 = 1.1$. Auman's (1969) $T = 3000$ K, log $g = 1.0$ model gives $B_0/B_1 = 1.1$ which agrees perfectly with the value we derive.

Because of the noise in this spectrum, all of these values are uncertain. The temperature could be in error by 500 K. The turbulent velocity could be anywhere in the range 4 to 12 km/s. The damping parameter seems to be fairly well determined although log a = -2 might be possible. Log η could vary by $\pm$ 0.4. The C^{12}/C^{13} ratio is between 5 and 20.

Mu Geminorum

The spectral type of μ Gem is the same as that of η Gem, M3 III. The effective temperature is assumed to be 3300 K. The noise is noticable in this spectrum but is not as bad as in the spectrum of η Gem. Figures 29 and 38 show the C^{12}/C^{13} ratio and log η as functions of all parameters.

The values of the parameters that provide the best match to the observed profile are

T = 3200 K, ξ_t = 6 km/s, log a = -2 or 3, log η = 2.8

The best value of log a seems to be between -2 and -3. These values lead to

log a = -2	C^{12}/C^{13} = 3	B_0/B_1 = 1.3
log a = -3	C^{12}/C^{13} = 38	B_0/B_1 = 0.8

The adopted values are

log a = -2.5	C^{12}/C^{13} = 20	B_0/B_1 = 1.0

Either value of B_0/B_1 is in good agreement with Auman's (1969) T = 3000 K

log g = 1 model. Both log a = -2 or log a = -3 reproduces the observed profile reasonably well. The C^{12}/C^{13} ratio could be as low as 2 or as high as 50 although we believe it is probably in the range 10 to 35.

Rho Persei

This spectrum is noisier than most, but is still satisfactory for analysis. The spectral type is M3, the same as the preceding two stars, but the luminosity may be higher (II-III). According to Johnson (1966) this does not change the effective temperature which is still 3000 K. The C^{12}/C^{13} ratio and log η are shown as functions of all parameters in Figures 30 and 38.

The band profile does not differ significantly from that of μ Gem except for the strength of the $C^{13}O^{16}$ band heads. See the discussion of μ Gem for details of the band profile analysis.

The best value of C^{12}/C^{13} is 15 with a range from 3 to 40 possible. The value is probably between 6 and 25.

R Lyrae

There are three spectra of R Lyrae (M5 III) available. The first and the third are independent. The second was included in the third, therefore is not independent.

This is one of two semi-regular variables included in the investigation. Each spectrum was analyzed separately. The possibility of spectral changes over the three month interval between observations

was considered, but no differences larger than the errors of measurement were found. We will, therefore discuss all three spectra together.

The effective temperature is given by Johnson (1966) as 2950 K. The C^{12}/C^{13} ratio and log η for each spectrum are shown as functions of all parameters in Figures 31 and 39.

The best match to the stellar band profile is obtained with

$$T = 3000 \text{ K}, \ \xi_t = 9 \text{ km/s}, \ \log a = -3, \ \log \eta = 2.0$$

These lead to $C^{12}/C^{13} = 5.5$ and $B_0/B_1 = 1.3$. These values are all very well determined. The probable ranges are

$$5.0 \leq C^{12}/C^{13} \leq 6.0$$
$$1.8 \leq \log \leq 2.2$$

The value of $B_0 B_1$ agrees well with Auman's (1969) T = 3000 K, log g = 1.0 model.

EU Delphini

EU Deophini is the second semi-regular variable included in this investigation. The spectral type is M6 III, for which Johnson (1966) gives the effective temperature as 2800 K. The C^{12}/C^{13} ratio and log η are shown as functions of all parameters in Figures 32 and 39.

The band profile does not differ significantly from that of R Lyr. See the discussion of R Lyr for details of the band analysis.

The best value of C^{12}/C^{13} is 3.5 with a range from 3 to 4.5 possible.

Alpha Orionis

Two independent spectra of α Ori (M1-2 Iab) are available; the first obtained with a refrigerated detector, the second used an unrefrigerated detector. The first spectrum is the noisiest included in the current investigation.

The effective temperature of α Ori is given by Mendoza (1969) as 3790 K. The C^{12}/C^{13} ratio and log η are shown as functions of all parameters in Figures 33 and 39.

The best match to the observed band profile is obtained with

$$T = 3500\ K,\ \xi_t = 10\ km/s,\ \log a = -3,\ \log \eta = 2.5$$

These lead to $C^{12}/C^{13} = 5.0$, $B_0/B_1 = 1.5$

The value of B_0/B_1 agrees satisfactorily with the values obtained from Auman's (1969) models. The T = 3500 K, log g = 0.5 model gives $B_0/B_1 = 1.6$ and the T = 4000 K, log g = 1.0 model gives $B_0/B_1 = 2.0$.

The possible range of log η is from 2.3 to 2.8. This leads to a possible range of C^{12}/C^{13} from 4.0 to 6.0.

Alpha Scorpii

The spectral type of α Sco is the same as that of α Ori (M1-2 Iab), but the effective temperature is given by Mendoza as 3520 K. The C^{12}/C^{13} ratio and log η are shown as functions of all parameters in Figures 24 and 39.

The best match to the observed profile is obtained with

$T = 3200$ K, $\xi_t = 8$ km/s, $\log 2 = -2$, $\log \eta = 2.5$

These lead to $C^{12}/C^{13} = 10$, $B_0/B_1 = 1.6$.

The temperature is lower than that of α Ori even though the spectral types are the same. This temperature difference is well determined, being based on the different appearance of the CO depression in the two stars, and is also indicated by their effective temperatures.

The value of B_0/B_1 is in satisfactory agreement with Auman's (1969) $T = 3000$ K, $\log g = 1.0$ model.

The possible range of C^{12}/C^{13} is from 8 to 14. That of $\log \eta$ is from 2.3 to 2.7.

Mu Cephei

Three spectra of μ Ceph (M2 Ia) are available. The first and third are independent. The second was included in the third and is noisier than the other two. All three were analyzed separately. No differences were found that could not be attributed to measurement errors, therefore the three results were combined and the average results discussed below.

The effective temperature is given by Johnson (1966) as 3500 K for an M2 supergiant. The C^{12}/C^{13} ratio and $\log \eta$ are shown as functions of all parameters in Figures 34 and 40.

The damping parameter is probably between log a = -2 and log a = -3. For log a = -2 the best fit is obtained with

$$T = 3200\ K,\ \xi_t = 8\ km/s,\ \log a = -2,\ \log \eta = 2.6$$

which leads to

$$C^{12}/C^{13} = 3.7,\ B_0/B_1 = 1.3$$

For log a = -3, the best values for the parameters are

$$T = 3200\ K,\ \xi_t = 8\ km/s,\ \log a = -3,\ \log \eta = 2.8$$

which leads to

$$C^{12}/C^{13} = 10,\ B_0/B_1 = 1.4$$

The damping constant is probably closer to log a = -2 than to log a = -3, so log a = -2.3 was adopted, which leads to

$$C^{12}/C^{13} = 10,\ B_0/B_1 = 1.3,\ \log \eta = 2.7$$

Either value of B_0/B_1 agrees well with Auman's (1969) models for T = 3000 K, log = 1.0 and T = 3500 K, log g = 0.5.

The most likely range for C^{12}/C^{13} is from 3 to about 20; that of log η from 2.5 to 3.0.

Delta^2 Lyrae

The spectrum of δ^2 Lyr is noisier than most spectra included in this investigation, but is still satisfactory for analysis. Johnson (1966) gives the effective temperature of an M4 II star as 3100 K. The C^{12}/C^{13} ratio and log η are shown as functions of all parameters in Figures 35 and 40.

The value of the parameters that best reproduce the observed band profile are

$$T = 3000 \text{ K}, \xi_t = 6 \text{ km/s}, \log a = -3, \log \eta = 3.0$$

which leads to

$$C^{12}/C^{13} = 3.5, B_0/B_1 = 1.5$$

This value of B_0/B_1 agrees reasonably well with the value 1.1 obtained from Auman's (1969) model with T = 3000 K, log g = 1.0.

All parameters are poorly determined because of the noise in this spectrum. Temperature could be in error by ± 500 K; ξ_t by ± 5 km/s; log η by ± 0.5. The damping constant could be log a = -2. On this basis, the possible range of C^{12}/C^{13} is from 2 to 6.

Alpha Herculis

Two independent spectra of α Her (M5 Ib-II) are available; both are very good quality. Mendoza lists the effective temperature of α Her as 3400 K. The C^{12}/C^{13} ratio and log η are shown in Figures 36 and 40 as functions of all parameters.

The best match to the observed profiles was obtained with

$$T = 3500 \text{ K}, \xi_t = 6 \text{ km/s}, \log a = -3, \log \eta = 3.0$$

These lead to

$$C^{12}/C^{13} = 9, B_0/B_1 = 1.2$$

The parameters are well determined although the temperature may be somewhat lower than 3500 K. It is probably not as low as 3000 K.

The possible range of C^{12}/C^{13} is from 4 to 25; that of log n from 2.7 to 3.2.

SUMMARY AND CONCLUSIONS

In the preceding chapter, the analysis of 15 late type giants and supergiants has been presented. The C^{12}/C^{13} abundance ratio and the ratio of CO line opacity to continuous opacity have been determined for each star. This chapter is devoted to a discussion of carbon monoxide and the carbon isotopes in the late type giants and supergiants as a class, how these properties vary with spectral type and luminosity and the implications of these properties for the theoretical models of these stars.

The Carbon Isotope Ratio

The C^{12}/C^{13} ratios determined for the 15 stars included in this investigation are listed in Table 4 (Chapter 3) and plotted versus spectral type in Figure 41. Schopp (1954) determined carbon isotope ratios for 20 KO through K5 giants. The only star the two investigations have in common is Alpha Tauri (K5 III). Schopp determined a lower limit of C^{12}/C^{13} for α Tau equal to 0.6. The value determined in Chapter 3 is $C^{12}/C^{13} = 20$.

There is no easily discernable trend in Figure 41. The M stars may have lower C^{12}/C^{13} ratios than the K stars. Alpha Bootis, the only known metal deficient star included in this investigation, may be

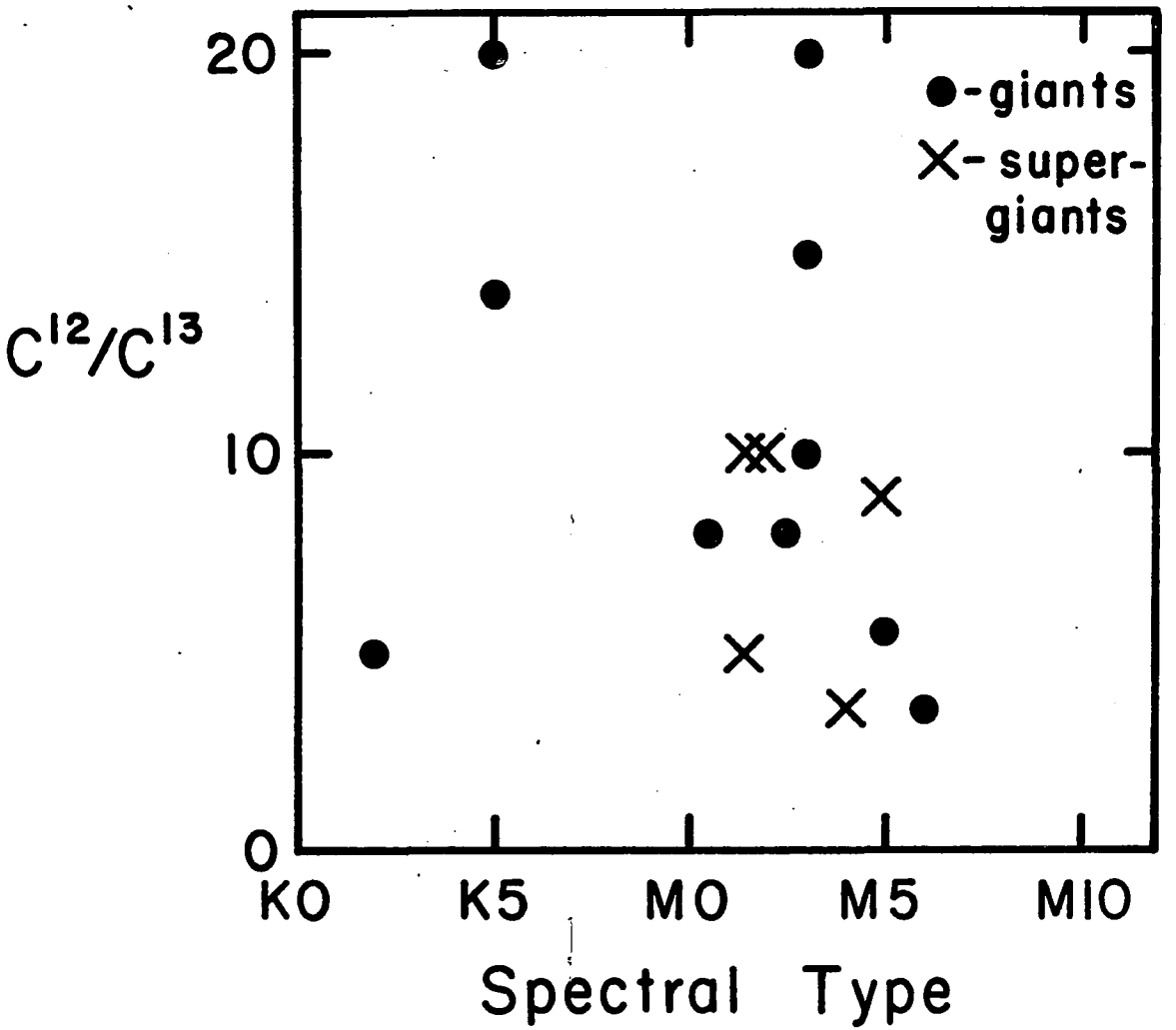

Fig. 41. Carbon Isotope Ratios in Stars

abnormal in the sense that it has a lower C^{12}/C^{13} ratio than is typical for early K stars. However, until the discrepancy between the C^{12}/C^{13} ratio determined from the CN bands and that determined from the CO bands (Greene 1970) is resolved, even this point is not clear.

The only well determined feature of Figure 41 is that all the stars included in this investigation have $C^{12}/C^{13} \lesssim 20$. Although the number of stars analyzed is small, this seems to be a general characteristic, at least of those stars of spectral type K5 or later. This is significantly lower than the terrestrial (89) or solar ($\gtrsim$100) ratio.

The Carbon Monoxide Abundance

The ratio of line to continuous opacity (η) in the CO bands was determined for each of the 15 stars included in this investigation. The results are listed in Table 4 (Chapter 3). The accuracy of the individual determinations was discussed in Chapter 3. In most cases, the η values are only expected to be accurate within a factor of 3.

The Assumption of Local Thermodynamic Equilibrium

The η values obtained in Chapter 3 were based on a comparison of theoretical band profiles with the observed stellar profiles. The theoretical profiles were calculated assuming LTE. Spinrad et al. (1971) have suggested that the relative strengths of the CO lines in Alpha Orionis differ systematically from those expected on the basis of LTE. This does not necessarily imply that LTE is not a good

approximation to the energy level populations of CO. The effect can be produced by failure of the single layer, isothermal atmospheric model used for the curve of growth analysis. If this is a general property of CO absorption in late type stars, the n values determined in Chapter 3 are systematically wrong.

A few theoretical spectra were calculated treating the vibrational and rotational excitation separately, as described in Appendix A, in order to determine whether or not the effect described by Spinrad et al. (1971) could be recognized in spectra of this resolution. Differences in the band profile were detectable between the LTE and non-LTE models, but the non-LTE models were not unambiguously distinguishable from LTE models with a different choice of log n , T and log a. The C^{12}/C^{13} ratios are not very sensitive to the changes in parameter values required by the non-LTE models. The scatter in Figure 41 is much larger than the changes due to non-LTE effects. Because non-LTE effects can not yet be quantitatively predicted for late type stars, nor can they be recognized observationally at this resolution, only LTE models were used to obtain the results of Chapter 3.

The Continuous Opacity

The sources of continuous opacity in cool stars are not well known. There are two reasons for this. The formation of molecules strongly influences the importance of individual opacity sources by

depleting atomic species and forming new, molecular opacity sources. Elemental abundances in the atmospheres of cool giants and supergiants are uncertain, which makes the importance of opacity sources such as He^- uncertain and also modifies the abundances of molecules.

Some molecular abundances are extremely sensitive to small changes in the elemental abundances. For example, the abundance of free oxygen is sensitive to the O/C ratio because carbon monoxide dominates the molecular equilibrium. The H_2O abundance is, in turn, sensitive to the abundance of available oxygen, therefore it is sensitive to both the oxygen abundance and the O/C ratio. Auman's models (1969) predict that for a solar composition, H_2O is the dominant infra-red opacity source in these stars. However, there is no evidence for H_2O absorption in these spectra therefore H_2O opacity is not considered in the discussion to follow. The lack of H_2O can be explained by an O/C ratio that is closer to unity than the solar value.

The strongest sources of continuous infra-red opacity for solar compositions are negative ions such as H^-, He^- and H_2^-. The abundance of these species is proportional to the electron pressure in the atmosphere. The sources of free electrons are the light, easily ionized metals, therefore the abundances of these negative ions is related to the metal abundance in the atmosphere. Model atmospheres by Gingerich et al. (1967) show that with metal abundances that are reduced by a factor of 100 from the solar values, Rayleigh scattering from atomic and

molecular hydrogen approaches the negative ions in importance as an opacity source.

Accurate elemental abundances in cool giant and supergiant stars are not known. Calculations of model atmospheres and molecular equilibria have been based on solar abundances or on solar abundances with the metals decreased by an arbitrary factor. The presence of low C^{12}/C^{13} ratios in these stars, however, indicates that the abundances have been modified by nuclear burning in the stellar interior.

Results

Because of the uncertainties discussed above, no attempt has been made to interpret the η values determined in Chapter 3 as carbon monoxide abundances. All that can be said is that, using only H^- opacity with the electron pressures determined from model atmospheres of solar composition, the CO/H abundance ratio is higher than would be expected for solar composition.

Relation to Theoretical Models

There are two ways in which a low C^{12}/C^{13} ratio can be obtained in the observable surface layers of a star; by forming the star from gas which has a low C^{12}/C^{13} ratio initially, or by mixing material, that has been processed through the CNO bi-cycle, from the interior to the surface of the star.

If the low C^{12}/C^{13} ratio was a characteristic of the initial composition of the star it can tell us nothing about the history of the star itself. The problem then is to explain the source of a low interstellar C^{12}/C^{13} ratio and why the sun has a high C^{12}/C^{13} ratio. The C^{13} would, presumably, come from an earlier generation of evolved stars that had produced it and then returned it to the interstellar medium. The mechanisms by which material is cycled from the interstellar medium, through stars, and returned to the interstellar medium are not all understood. However, the C^{12}/C^{13} ratio should depend on age and place of formation of the star. The consistently low C^{12}/C^{13} ratio observed in late type stars would have to be regarded as a chance result of only observing a small number of stars. Although the possibility can not be eliminated, it is unlikely that the low C^{12}/C^{13} ratio reflects the initial composition of the stars. This possibility will not be discussed further.

The low C^{12}/C^{13} ratio can not be produced by a star contracting onto the main sequence because C^{13} is not produced until the CNO bi-cycle becomes operative. Therefore, the stars with low C^{12}/C^{13} ratio must have evolved off the main sequence into the red giant region. Also, in order to see C^{13}, a significant amount of material must have been mixed from their interior to their surface.

Nucleosynthesis

The mechanism of nucleosynthesis that is of interest here is the CNO bi-cycle. Clayton (1968) discusses energy generation and nucleosynthesis by the CNO bi-cycle in great detail. Only those points relevant to the present discussion will be reviewed here.

The CNO bi-cycle is given in Table 5. This, as its name implies, is actually two interlocking cycles; a CN cycle and an ON cycle. The CN cycle reaches equilibrium very quickly. This converts the nuclei involved predominantly (~98%) into N^{14} and establishes the C^{12}/C^{13} ratio.

The ON cycle reaches equilibrium very slowly because it is only weakly coupled to the CN cycle. The ON cycle determines the oxygen abundance, and through its relation to the CN cycle, the O/C ratio.

The equilibrium abundances of the CNO nuclei, with the exception of N^{14}, are very temperature sensitive. The fractional abundances at equilibrium are shown in Figure 42 which is taken from Caughlan and Fowler (1962). The equilibrium C^{12}/C^{13} ratio is almost independent of temperature but the abundance ratios of most other nuclei are temperature sensitive. Figure 43 (also from Cauglan and Fowler 1962) shows the abundance ratios of the CNO nuclei at equilibrium. In particular, note the strong temperature dependence of the O/C ratio.

Table 5. The CNO Bi-cycle

$$C^{12} + H^{1} \longrightarrow N^{13} + \gamma$$

$$N^{13} \longrightarrow C^{13} + e^{+} + \nu$$

$$C^{13} + H^{1} \longrightarrow N^{14} + \gamma$$

$$N^{14} + H^{1} \longrightarrow O^{15} + \gamma$$

$$O^{15} \longrightarrow N^{15} + e^{+} + \nu$$

$$N^{15} + H^{1} \longrightarrow C^{12} + He^{4}$$

or

$$N^{15} + H^{1} \longrightarrow O^{16} + \gamma$$

$$O^{16} + H^{1} \longrightarrow F^{17} + \gamma$$

$$F^{17} \longrightarrow O^{17} + e^{+} + \nu$$

$$O^{17} + H^{1} \longrightarrow N^{14} + He^{4}$$

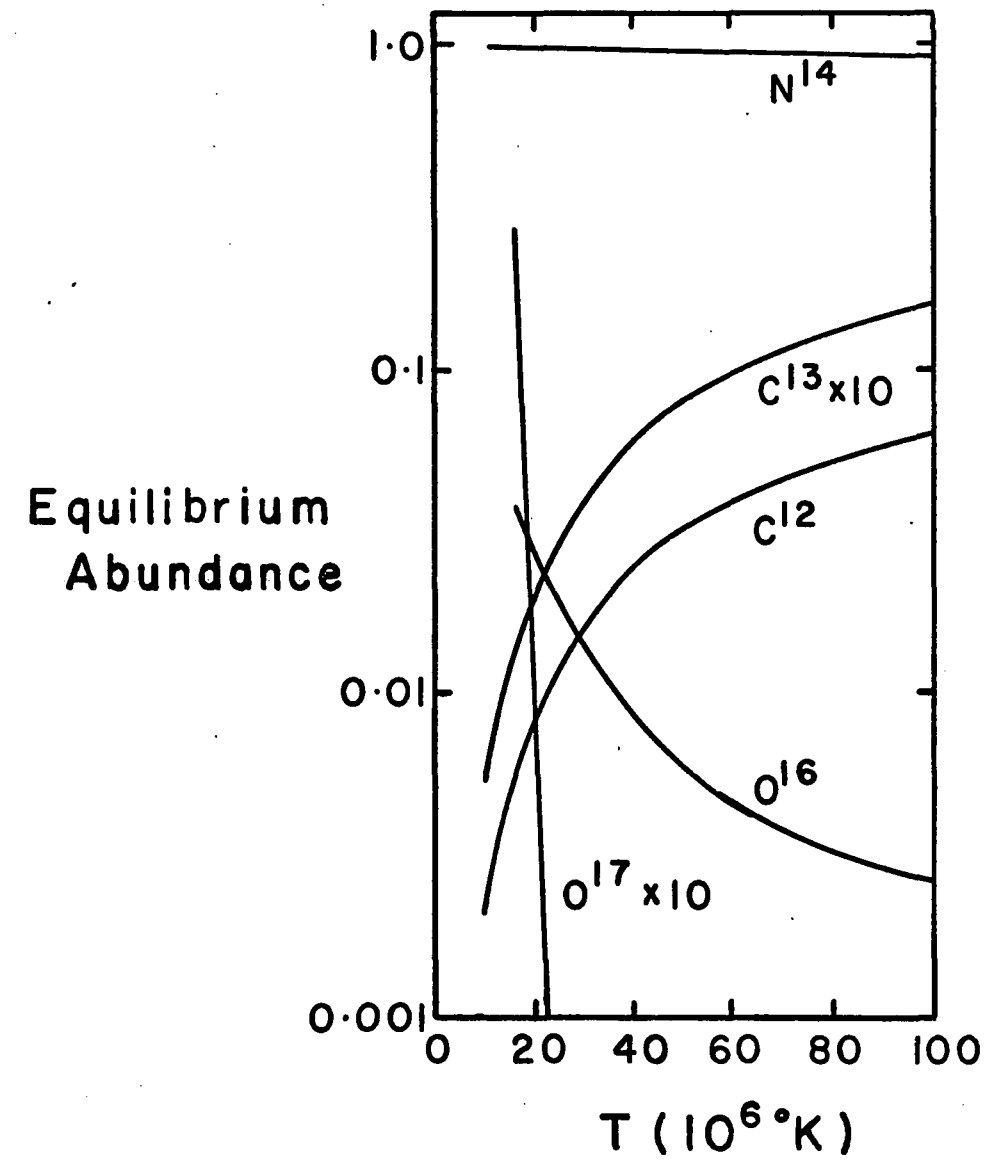

Fig. 42. Fractional Equilibrium Abundances of CNO Nuclei

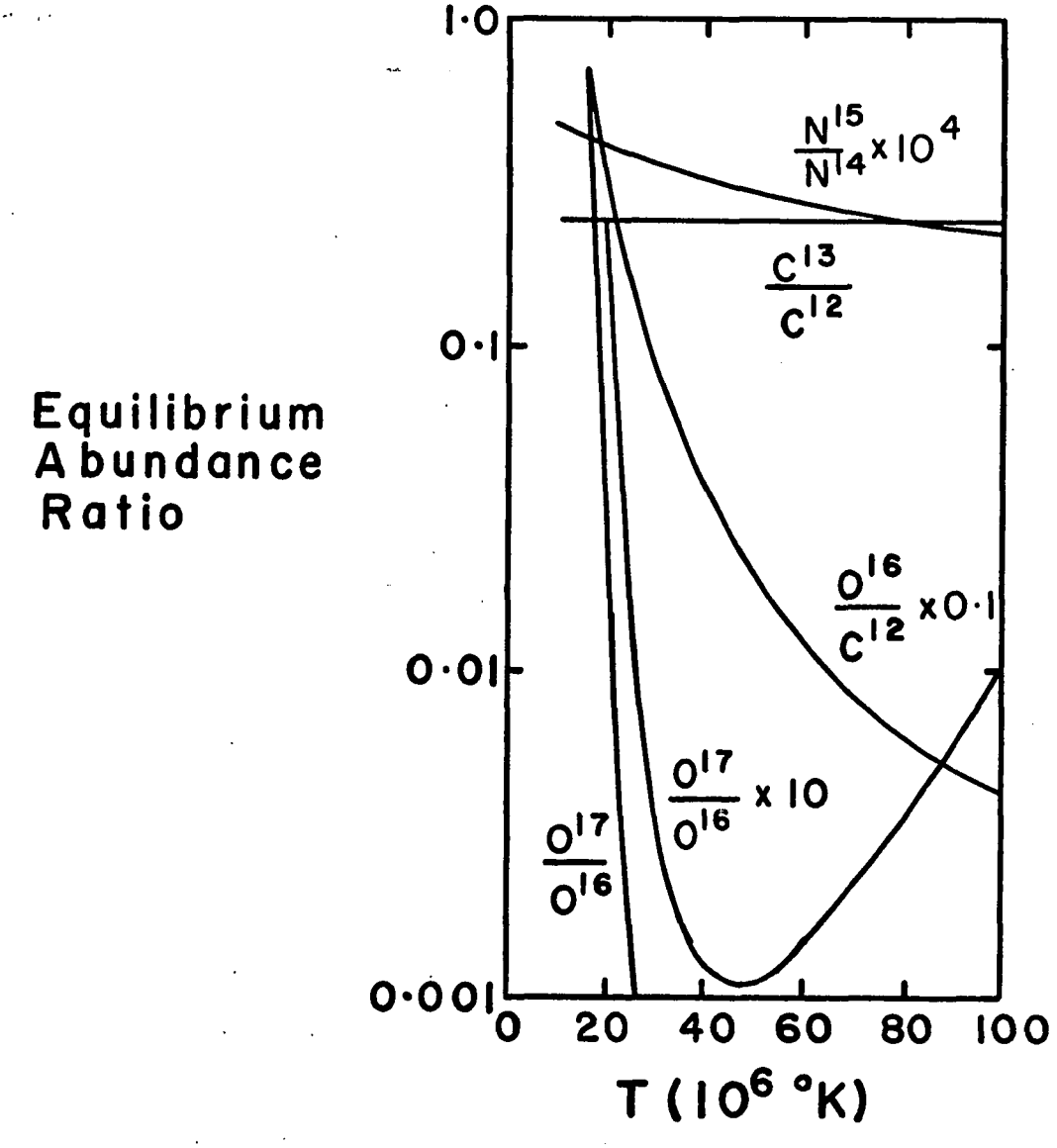

Fig. 43. Equilibrium Isotope Ratios of CNO Nuclei

The relative abundances of the CNO nuclei are shown as a function of the number of protons consumed per initial nucleus in Figure 44 which is taken from Cauglan (1965). The number of protons consumed per initial nucleus is related to time through the reaction rates which depend on temperature, density and hydrogen abundance. The rapid approach to C^{12}/C^{13} equilibrium and the much slower approach to oxygen equilibrium is evident in Figure 44.

The abundance of hydrogen decreases as hydrogen is converted into helium. The H/He ratio depends on the length of time the CNO bi-cycle has been operating and on the temperature in the energy generating region.

Convection

From the discussion above, it is evident that if the CNO bi-cycle is operative in stars, the C^{12}/C^{13} ratio can safely be expected to have its equilibrium value of about 3 or 4 in the stellar interior. In order to detect the C^{13} spectroscopically, it must be convectively transported from the unobservable interior to the observable surface layers.

According to Iben (1967) a convective zone extends from the surface to the energy generating regions of red giants. This brings material from the interior, where the CNO bi-cycle is operating, to the surface and carries surface material to the interior, where it can be

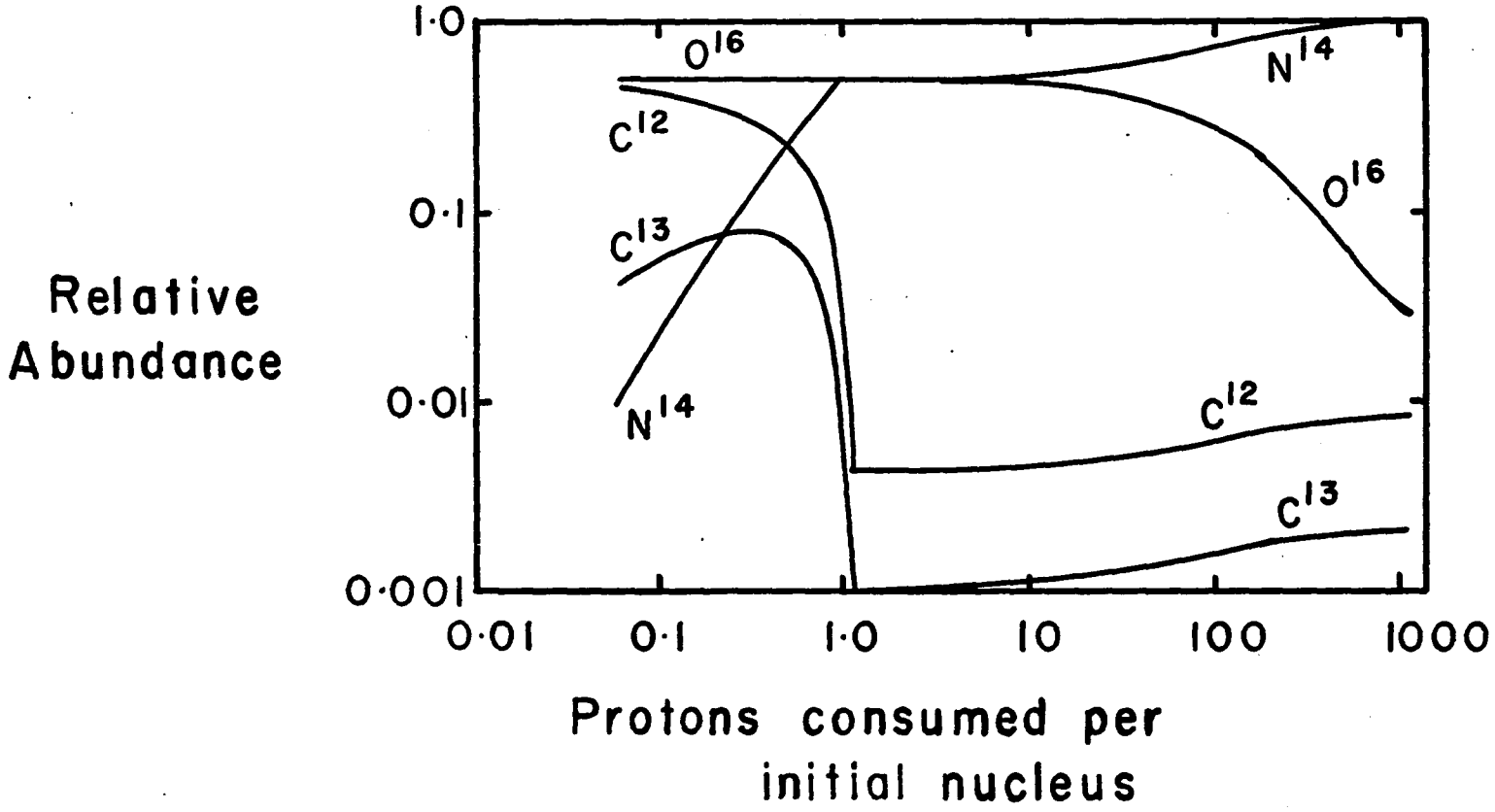

Fig. 44. Fractional Abundances of CNO Nuclei During the Approach to Equilibrium

processed by the CNO bi-cycle. This results in changes of the surface abundances towards the CNO bi-cycle equilibrium abundances. The carbon abundance and the C^{12}/C^{13} ratio decrease. The nitrogen abundance increases. The hydrogen and oxygen abundances may also decrease if the CNO bi-cycle has significantly depleted the hydrogen in the energy generating region.

The C^{12}/C^{13} ratio in the stellar atmosphere depends on the amount of mixing that has occurred between the interior and the atmosphere, the ratio of the abundances of C^{12} in the atmosphere to that in the interior and the ratio of the abundance of C^{13} in the atmosphere to that in the interior. If mixing continues until an equilibrium is attained, the surface abundances will be the same as those in the CNO burning region.

Complete mixing of the atmosphere with the region of CNO burning does not imply a homogeneous star, which would move back to the vicinity of the main sequence. The CNO bi-cycle in red giants is operating in a shell source around a hydrogen depleted core. This core region produces the giant structure of the star.

Results

The stellar C^{12}/C^{13} ratios, which are lower than the terrestrial ratio but not as low as the CNO bi-cycle equilibrium ratio, indicate that mixing has occurred between the surface and the region where the

CNO bi-cycle is operating. This mixing has not been extensive enough to produce a homogeneous region from the CNO shell source to the surface.

Summary and Suggestions for Further Research

A grid of synthetic spectra was calculated for the carbon monoxide first overtone ($\Delta v = 2$) vibration-rotation bands between 3900 cm^{-1} and 4360 cm^{-1}. The grid was used to determine C^{12}/C^{13} abundance ratios for fifteen K and M giant and supergiant stars for which infra-red spectra have been published by Johnson and co-workers.

The results were as follows:

1. $3.5 \leq C^{12}/C^{13} \lesssim 20$ for all stars analyzed.
2. No definite variation of C^{12}/C^{13} with spectral type or luminosity class could be established over the range K2 to M6.
3. The low C^{12}/C^{13} ratio indicates that mixing has occurred between the interior and the surface of the stars.
4. No reliable carbon monoxide abundance was determined.
5. It is not necessary to drop the assumption of LTE to satisfactorily reproduce the stellar band profiles, but the possibility of non-LTE effects can not be eliminated.
6. The carbon monoxide first and second overtone band sequences are qualitatively consistent with the assumption that H^- is a significant source of continuous opacity.

Much can still be accomplished with spectra of this resolution, particularly in the nature of survey work; looking for interesting objects. Quantitative analysis of medium resolution spectra can be accomplished but it is difficult because there are many interacting parameters. High resolution infr-red spectra have been obtained by Pierre Connes of three late type stars. It is now feasible to obtain infra-red spectra of all the stars included in this investigation, at a resolution that will resolve the rotational structure of the CO bands. Detailed analyses of more stars at high resolution will help to suggest reasonable ranges of parameters for the analyses of moderate resolution spectra.

The problem of obtaining different C^{12}/C^{13} ratios from different spectral regions of the same star needs to be solved before the C^{12}/C^{13} ratios obtained can be trusted. Perhaps, if convection has not distributed CNO products throughout the entire atmosphere, the variation of continuous opacity from one spectral region to another allows the spectrum to be formed in regions of different C^{12}/C^{13} ratio. The H^- opacity in the region of the CN red system bands in the photographic infra-red is about an order of magnitude larger than the H^- opacity in the CO first overtone bands for a temperature of 3500 K, but this ratio is sensitive to temperature.

Isotopic abundances need to be obtained for as many different elements as possible, particularly nitrogen and oxygen, so that they can be compared to the predictions of nucleosynthesis. Isotope ratios for

the elements involved in building up the heavy elements can only be obtained through molecular spectra.

Elemental abundances should be determined for late type stars. This will involve using high resolution spectra to determine both atomic and molecular abundances. The H, C, N and O abundances are important due to their relation to the CNO bi-cycle. The light metals with low ionization potentials (e.g., Na, Mg, Si, Ca) provide free electrons that strongly influence the continuous opacity.

Most diatomic molecules have fundamental vibration-rotation bands that occur in the 3 - 10 μ region. Some molecules have no electronic transitions in accessible spectral regions, therefore spectra in this range might allow detection of molecules that are otherwise unobservable.

APPENDIX A

CALCULATION OF S^m AT ARBITRARY TEMPERATURES AND C^{12}/C^{13}, O^{16}/O^{18} RATIOS

We define optical depth in the usual way as

(1) $d\tau = k^m(\nu)\, ds$

The line strength is then defined as

(2) $S^m (cm/gm) = \int_{-\infty}^{\infty} k^m(\nu) d\nu$

Kunde (1968) shows that

(3) $S^m(T) = K \exp(-E_1/kT) \left[1 - \exp(-hc\,\nu_{1a}/kT)\right] /Q$

where

K = a constant for each line

E_1 = excitation energy of the lower level of the transition

$\nu_{1\mu}$ = frequency of the line (cm^{-1})

Q = partition function

and the other symbols have their usual meanings

The partition function is given by

(4) $Q = \sum_{v=0}^{\infty} \sum_{J=0}^{\infty} (2J+1) \exp(-E_{vJ}/kT)$

where

E_{vJ} = the excitation energy of the energy level corresponding to quantum numbers v & J

For a temperature of 4500 K, the first excited electronic state affects the partition function less than 0.01%. At lower temperatures the excited electronic states have less effect. Therefore Equation (4) ignores electronic states.

It is possible to use the data presented by Kunde (1967) to determine the constant K in Equation (3) for each rotational line. Equations (3) and (4) can then be used with any value of T to determine $S^m(T)$.

The isotopic abundance ratios enter S^m only as a weighting factor. To change the C^{12}/C^{13} ratio from Kunde's value of 89, we simply multiply S^m for the C^{13}/O^{16} lines by $89/(C^{12}/C^{13})$. The extension to the O^{16}/O^{18} ratio is obvious. Kunde's calculations assume $O^{16}/O^{18} = 493$.

It is possible, at least formally, to separate the excitation energy of any energy level into a vibrational and a rotational contribution

$$E_{v,J} = E_v + E_J$$

If this is done, a quasi-non-LTE form of S^m can be calculated from Equations (3) and (4) by allowing different values of excitation temperature for the vibrational and rotational energy levels. This can be viewed as two independent cases of LTE in the vibrational and rotational levels separately. The justification for doing this is that the higher

vibrational levels seem to be under populated with respect to the lower levels and the rotational population distribution (Spinrad et al. 1971).

The partition functions calculated from Equation (4) including 25 vibrational levels and 300 rotational levels in each vibrational level are given in Appendix B.

APPENDIX B

PARTITION FUNCTIONS FOR CARBON MONOXIDE

T_{rot}	T_{vib}	$C^{12}O^{16}$	$C^{13}O^{16}$	$C^{12}O^{18}$
4500	4500	3378.0	3589.7	3606.8
	4000	3107.3	3299.6	3315.2
	3500	2842.1	3015.2	3029.2
4000	4000	2758.5	2929.2	2943.0
	3500	2523.0	2676.7	2689.2
	3000	2293.6	2430.6	2441.6
3500	3500	2204.7	2339.1	2350.0
	3000	2004.3	2124.0	2133.7
	2500	1811.1	1916.4	1924.9
3000	3000	1715.7	1818.2	1826.4
	2500	1550.3	1640.5	1647.8
	2000	1394.3	1472.5	1478.8

T_{rot}	T_{vib}	$C^{12}O^{16}$	$C^{13}O^{16}$	$C^{12}O^{18}$
2500	2500	1290.2	1365.3	1371.3
	2000	1160.4	1225.5	1230.7
	1500	1043.8	1099.4	1103.8
2000	2000	927.01	979.02	983.19
	1500	833.86	878.30	881.84
	1000	760.96	798.72	801.71
1500	1500	624.45	657.74	660.39
	1000	569.87	598.16	600.39
	500	544.64	569.90	571.88
1000	1000	379.22	398.06	399.55
	500	362.44	379.26	380.58
	250	361.67	378.35	379.65
500	500	180.67	189.08	189.73
	250	180.29	188.62	189.27

APPENDIX C

BAND ORIGINS AND BAND HEADS FOR THE FIRST AND SECOND OVERTONE VIBRATION-ROTATION BAND OF $C^{12}O^{16}$, $C^{13}O^{16}$ AND $C^{12}O^{18}$

Isotope	Vibrational Transition	Band Origin (cm^{-1})	R Branch Band Head (cm^{-1})
$C^{12}O^{16}$	2-0	4260.06	4360.04
	3-1	4207.14	4305.37
	4-2	4154.37	4250.84
	5-3	4101.73	4196.47
	6-4	4049.24	4142.25
	7-5	3996.88	4088.18
	8-6	3944.65	4034.27
	9-7	3892.57	3980.50
	10-8	3840.62	3926.91
	11-9	3788.82	3873.45
	12-10	3737.15	3820.15
	3-0	6350.42	6417.77
	4-1	6271.15	6337.30
	5-2	6192.10	6257.04
	6-3	6113.24	6177.01
	7-4	6034.60	6097.20

Isotope	Vibrational Transition	Band Origin (cm^{-1})	R Branch Band Head (cm^{-1})
	8-5	5956.16	6017.59
	9-6	5877.94	5938.21
	10-7	5799.91	5859.05
	11-8	5722.10	5780.10
	12-9	5644.49	5701.36
	13-10	5567.09	5622.87
$C^{13}O^{16}$	2-0	4166.82	4264.64
	3-1	4116.23	4212.36
	4-2	4065.77	4160.23
	5-3	4015.44	4108.23
	6-4	3965.24	4056.39
	7-5	3915.17	4004.68
	8-6	3865.22	3953.12
	9-7	3815.41	3901.70
	10-8	3765.72	3850.42
	11-9	3716.16	3799.29
	12-10	3666.73	3748.29
	3-0	6212.30	6278.16
	4-1	6136.52	6201.27

Isotope	Vibrational Transition	Band Origin (cm^{-1})	R Branch Band Head (cm^{-1})
	5-2	6060.93	6124.53
	6-3	5985.53	6048.01
	7-4	5910.32	5971.68
	8-5	5835.31	5895.54
	9-6	5760.49	5819.62
	10-7	5685.86	5743.90
	11-8	5611.42	5668.38
	12-9	5537.18	5593.06
	13-10	5463.13	5517.95
$C^{12}O^{18}$	2-0	4159.02	4256.73
	3-1	4108.63	4204.65
	4-2	4058.37	4152.73
	5-3	4008.23	4100.93

REFERENCES

Allen, C. W. 1963 Astrophysical Quantities 2nd ed. (London: Athlone Press, Univ. of London).

Aller, Lawrence H. 1960 Stellar Atmospheres ed. J. Greenstein (Chicago: University of Chicago Press), chapter 4.

_____. 1963. The Atmospheres of the Sun and Stars 2nd ed. (New York: Ronald Press).

Auman, Jason R. 1966 Colloquium on Late Type Stars ed. M. Hack (Trieste: Osservatorio Astronomico di Trieste), p. 313.

_____. 1969 Ap. J. 157, 799.

Boyce, Peter B. and William M. Sinton 1964 A. J. 69, 534.

_____. 1965 Sky & Telescope 29, 78.

Bouigue, R. 1954 Ann. d'Ap. 17, 35; Publ. Obs. Haute-Provence 3, #9.

_____. 1957 Mem. Soc. Roy. Sci. Liege 18, 346.

Carbon, Duane F. and Owen J. Gingerich. 1969 Theory and Observation of Normal Stellar Atmospheres, ed. O. Gingerich (Cambridge: The MIT Press), p. 377.

Caughlan, G. R. 1965 Ap. J. 141, 688.

Caughlan, G. R. and W. A. Fowler. 1962 Ap. J. 136, 453.

Clayton, Donald D. 1968 Principles of Stellar Evolution and Nucleosynthesis (New York: McGraw-Hill).

Climenhaga, J. L. 1960 Publ. Dom. Ap. Obs. 11, 307 (#16).

_____. 1966 Colloquium on Late Type Stars, ed. M. Hack (Trieste: Osservatorio Astronomico di Trieste), p. 54.

Cohen, J. G. and C. F. Grandalen. 1968 Ap. J. 151, 141.

Connes, J. 1961 Rev. d'Opt. 40, 45, 116, 171, 231 (English Translation: Navweps Report 8099, China Lake, 1963).

Connes, P., J. Connes, R. Bouigue, M. Querci, J. Chauville and F. Querci. 1968 Ann. d'Ap. 31, 485.

Danielson, R. E., N. J. Woolf, and J. E. Gaustad. 1965 Ap. J. 141, 116.

Daudin, A. and C. Fehrenbach. 1946 C. R. 222, 1083.

Fujita, Y. 1935 Jap. Journ. Astr. and Geophys. 13, 21.

_____. 1939 Jap. Journ. Astr. and Geophys. 17, 17.

_____. 1940 Jap. Journ. Astr. and Geophys. 18, 45.

_____. 1941 Jap. Journ. Astr. and Geophys. 18, 177.

_____. 1950 P.A.S.J. 1, 171.

_____. 1970 Interpretation of Spectra and Atmospheric Structure in Cool Stars (Baltimore: University Park Press).

Gingerich, Owen J. 1967 SAO Spec. Rep. #240.

Gingerich, Owen J. and Shiv S. Kumar. 1964 A. J. 69, 139.

Gingerich, Owen J., David W. Latham, Jeffrey L. Linsky and Shiv S. Kumar. 1967 SAO Spec. Rep. #240.

Greene, Thomas F. 1970 Ap. J. 161, 365.

Greenstein, Jesse L. 1970 Spectroscopic Astrophysics, ed. G. Herbig (Berkeley: University of California Press), chapter 3.

Griffin, R. F. 1968 A Photometric Atlas of the Spectrum of Arcturus (Great Britain: Cambridge Philosophical Society).

Herzberg, G. 1946 A. J. 52, 149.

Hirai, M. 1969 P.A.S.J. 21, 91.

Iben, Icko. 1967 Ann. Rev. Astr. and Ap. 5, 571.

de Jager, C. and L. Neven. 1957 Mem. Soc. Roy. Sci. Liege 18, 357.

Johnson, H. L. 1966 Ann. Rev. Astr. and Ap. 4, 193.

Johnson, H. L., I. Coleman, R. I. Mitchell and D. Steinmetz. 1968 Comm. L.P.L. 7, 83.

Johnson, H. L. and M. E. Mendez. 1970 A. J. 75, 785.

Kuiper, G. P. 1962 Comm. L.P.L. 1, 1.

_____. 1964a Mem. Soc. Roy. Sci. Liege 5th Ser. 9, 365.

_____. 1964b Sky & Telescope 27, 88.

Kumar, Shiv S. 1964 Mem. Soc. Roy. Sci. Liege 5th Ser. 9, 476.

Kunde, Virgil G. 1967 NASA Goddard Space Flight Center, Document X-622-67-248.

_____. 1968 Ap. J. 153, 435; NASA Tech. Note TN D-4798.

Krupenie, Paul H. 1966 National Bureau of Standards NSRDS-NBS 5.

Menzel, D. H. 1930 P.A.S.P. 42, 34.

Mertz, L. 1965 A.J. 70, 548.

Mihalas, D. 1967 Methods in Computational Physics Vol. 7 (New York: Academic Press).

Montgomery, Earl F., Pierre Connes, Janine Connes, and Frank N. Edmonds, Jr. 1969 Ap. J. Suppl. 19, 1 (#167).

Mendoza, E. E. V. 1969 Theory and Observation of Normal Stellar Atmospheres, ed. O. Gingerich (Cambridge: The MIT Press), p. 27.

Moroz, V. I. 1966 Soviet Astron.-A. J. 10, 47.

McCammon, D., G. Munch, and G. Neugebauer. 1967 Ap. J. 147, 575.

McKellar, Andrew. 1936 P.A.S.P. 48, 216.

_____. 1948 Publ. Dom. Astroph. Obs. 7, 395.

McKellar, Andrew. 1949a P.A.S.P. 61, 34.

_____. 1949b P.A.S.P. 61, 199.

Phillips, John G. 1957 Ap. J. 125, 153.

_____. 1966 Appl. Opt. 5, 549.

Querci, M. and F. Querci. 1970 Astron. and Astroph. 9, 1.

Russell, H. N. 1934 Ap. J. 79, 317.

Sanford, R. F. 1929 P.A.S.P. 41, 271.

_____. 1932 P.A.S.P. 44, 248.

_____. 1940 P.A.S.P. 52, 203.

Schopp, John D. 1954 Ap. J. 120, 305.

Shajn, G. 1942 Observatory 64, 255; Bull. Abastumani Ap. Obs. 6, 1.

Shajn, G. and V. Gaze. 1948 Publ. Crimian Ap. Obs. 2, 131.

_____. 1950 Publ. Crimian Ap. Obs. 5, 24.

_____. 1954 Mem. Soc. Roy. Sci. Liege 4th Ser. 14, 397.

Sinton, William M. 1962 Appl. Opt. 1, 105.

_____. 1966 A. J. 71, 398.

Sinton, William M. and Peter B. Boyce. Lowell Obs. Bull. (in press).

Spinrad, Hyron and Robert F. Wing. 1969 Ann. Rev. Astr. and Ap. 7 249.

Spinrad, Hyron, Lewis D. Kaplan, Pierre Connes, Janine Connes and Virgil G. Kunde. 1971 Proceedings of the Conference on Late Type Stars. Kitt Peak National Observatory Contribution #554.

Strom, S. E. and R. L. Kurucz. 1966 J.Q.S.R.T. 6, 591.

Swihart, Thomas L. and David R. Brown. 1967 Ann. d'Ap. 30, 659.

Thompson, Rodger I. and Herbert W. Schnopper. 1970 Ap. J., 160, 697.

Thompson, Rodger I., Herbert W. Schnopper and William K. Rose. 1971 Ap. J. 163, 533.

Thompson, Rodger I., Herbert W. Schnopper, Richard I. Mitchell and Harold L. Johnson. 1969 Ap. J. 158, L117.

Tsuji, Takashi. 1964 Ann. Tokyo Astr. Obs. 2nd Ser. 9, 1.

_____. 1966 Colloquium on Late Type Stars, ed. M. Hack (Trieste: Osservatorio Astronomico di Trieste), p. 260.

Utsumai, K. 1963 P.A.S.J. 15, 482.

_____. 1967 P.A.S.J. 19, 342.

Woolf, N. J., M. Schwarzschild and W. K. Rose. 1964 Ap. J. 140, 833.

Wrubel, Marshall H. 1949 Ap. J. 109, 66.

_____. 1950 Ap. J. 111, 157.

_____. 1954 Ap. J. 119, 51.

Wurm, K. 1932 Z_s. f. Ap. 5, 260.

Wyller, A. A. 1957 Ap. J. 125, 177.

_____. 1959 A. J. 64, 57.

_____. 1960 Ap. Norveg. 7, 13.

_____. 1966 Ap. J. 143, 828.